Enclosure II to ET 07-0043

Westinghouse Electric Company LLC LTR-CDME-07-198 NP-Attachment, "Response to NRC Request for Additional Information Relating to LTR-CDME-07-72 P-Attachment and LTR-CDME-05-209-P of the Wolf Creek Generating Station (WCGS) Permanent B* License Amendment Request."
(NON-PROPRIETARY)

LTR-CDME-07-198 NP-Attachment

Wolf Creek Nuclear Operating Corporation

Response to NRC Request for Additional Information Relating to LTR-CDME-07-72 P-Attachment and LTR-CDME-05-209-P of the Wolf Creek Generating Station (WCGS) Permanent B* License Amendment Request

September 24, 2007

Westinghouse Electric Company LLC
P.O. Box 158
Madison, PA 15663

Wolf Creek Generating Station (WCGS) Permanent B* Responses to NRC Request for Additional Information

Steam Generator Tube Alternate Repair Criteria
for the Portion of the Tube Within the Tubesheet
at the Wolf Creek Generating Station
(LTR-CDME-05-209-P and LTR-CDME-07-72 P-Attachment)

Wolf Creek Nuclear Operating Corporation (WCNOC) submitted a license amendment request on February 21, 2005 (letter ET 06-0004), proposing changes to the Technical Specifications for WCGS. The proposed changes are to revise Technical Specification 5.5.9, "Steam Generator Program," to exclude portions of the steam generator tube below the top of the tubesheet in the steam generators from periodic tube inspections based on the application of structural analysis and leak rate evaluation results to re-define the primary-to-secondary pressure boundary. The NRC staff provided an initial Request for Additional Information (RAI) on June 27, 2006. Subsequently, a second NRC staff RAI was received by WCNOC via electronic mail on June 22, 2007. The purpose of this letter report is to provide responses to the NRC staff's second RAI (Questions 1 through 29). Throughout the response, reference is made to LTR-CDME-05-0209-P and LTR-CDME-07-72 P-Attachment. Enclosure 1 to WCNOC letter ET 06-0004 provided LTR-CDME-05-209-P which is the technical justification of H*/B* for Wolf Creek. Enclosure I to WCNOC letter WO 07-0012 provided LTR-CDME-07-72 P-Attachment which is the responses to the first NRC staff RAI.

Provided below are responses to the second NRC staff RAI. Reference 1 and Reference 2 identified in the NRC questions are:

1. Wolf Creek Nuclear Operating Corporation (WCNOC) letter dated February 21, 2006 (ET 06-0004)

2. WCNOC letter dated May 3, 2007 (WO 07-0012)

REFERENCES

1. Wolf Creek Nuclear Operating Corporation (WCNOC) letter ET 06-0004 dated February 21, 2006.

2. LTR-CDME-07-72 P-Attachment, "Response to NRC Request for Additional Information on the Wolf Creek Generating Station (WCGS) Permanent B* License Amendment Request" (Enclosure I to WCNOC letter WO 07-0012).

3. LTR-CDME-05-209-P, "Steam Generator Tube Alternate Repair Criteria for the Portion of the Tube Within the Tubesheet at the Wolf Creek Generating Station" (Enclosure I to WCNOC letter ET 06-0004).

4. EPRI Report 1012987, "Steam Generator Integrity Assessment Guidelines," Rev. 2.

5. USNRC, Draft Regulatory Guide DG-1074, "Steam Generator Tube Integrity," December 1998.

6. NEI 97-06, "Steam Generator Program Guidelines," Rev. 2.

7. NCE-88-271, "Assessment of Tube-to-Tubesheet Joint Manufacturing Processes for Sizewell B Steam Generators Using Alloy 690 Tubing," November 1988.

8. WCAP-12522, "Inconel Alloy 600 Tubing-Material Burst and Strength Properties," January 1990.

9. WNEP-9725, "The Westinghouse Tube to Tubesheet Joint Hydraulic Expansion Process," July 1997.

10. Westinghouse Drawing 3458C85, "Steam Generator – Model F Tube Schedule."

11. PR27988-52336, Anter Laboratories, Inc.

12. EPRI Report 10104982, "Analysis of Primary Water Stress Corrosion Cracking and Mechanical Fatigue in the Alloy 600 Stub Runner to Divider Plate Weld Material."

13. LTR-SGDA-07-197, "Wolf Creek Model F Steam Generator Faulted Transient Delta-P Evaluation," August 31, 2007.

14. CN-SGDA-01-35, "Wolf Creek NSAL (Primary-to-Secondary) Delta P Evaluation for the Tubesheet, Tubes and Tube-to-Tubesheet Welds," April 19, 2001.

15. "Statistics, Probability and Reliability for Civil and Environmental Engineers," McGraw-Hill, © 1997.

16. LTR-CDME-07-201; Technical Support Letter and Spreadsheet Summary for LTR-SGDA-07-4, Rev. 1; Septmeber 14,2007.

1. *Reference 1, Enclosure 1, Table 6-4 - Are the listed F/L, force per length, values correct? If so, please describe in detail how they were calculated. If not correct, please provide all necessary revisions to the H* analysis results. [For Byron 2, Braidwood 2, and Seabrook, F/L is calculated as follows:*

F/L = (Pull Force/specimen length) x (net contact pressure/total contact pressure)

A consistent approach for Wolf Creek (based on allowing 0.25 inch slip) would yield F/L values on the order of 200 pounds per inch (lb/inch) rather than 563 lb/inch as shown in the Table.]

Response to RAI Number 1:

There have been two approaches to calculating the F/L value using the empirical test data. The first involves a basic calculation using first principles and the second involves a model based on the theory of elasticity. Although the equation for calculating F/L is not the same as noted in the question, the first principles method yields the same value.

The following response details the two methods that have been used for calculating the ratio F/L. Following the explanation of the methods, F/L is recalculated for Wolf Creek using the method that is consistent with that used for Byron 2, Braidwood 2, etc. The values provided in Reference 3 are believed to be correct based on application of the theory of elasticity; however, for consistency with prior submittals of H*/B*, the recalculation based on first principles was performed, and is now the basis for the technical justification of H*/B* for Wolf Creek.

The pullout force for the Model D5, Model 44F and Model 51F SGs used the following formula to calculate the contact pressure (P_c), based on the first principles approach:

a,c,e

(1)

Next, an average value minus one standard deviation value (-1σ) is determined for contact pressure based on the measured pullout force data. The F/L values, in units of lbf/in are calculated using the formula:

a,c,e

(2)

The theory of elasticity model was used to calculate the residual contact pressure and the pullout force for the Wolf Creek Model F steam generators, reflecting the advance in the state of this analysis compared to prior application such as Seabrook, Byron and Braidwood.

Using the theory of elasticity model:

- The listed value of 522.3 lb_f/in. is correct.
- The values are based on 0.25 inch slip pullout test data and contact pressures that were calculated using the theory of elasticity:

a,c,e

Where:

a,c,e

- [redacted] a,c,e

- [redacted] a,c,e (3)

Where:

[redacted] a,c,e

The theory of elasticity model was chosen because there is a decrease in the contact pressure between the tube and the tubesheet due to Poisson's contraction of the tube in response to the application of the axial end cap load. Conversely, an increase in the contact pressure would result from the application of an axial load tending to push on the tube; a push load arises from pressure on the crack flanks in operation. (Assuming a 360° throughwall crack.) The decrease in contact pressure results in a radial inward springback of the tubesheet and a radial outward springback of the tube outside radius. Resistance to pullout of the tube is manifested as a shear stress from the contact pressure between the tube and the tubesheet. The pullout resistance incrementally decreases along the interface as the axial load is applied. Not all of the axial load is transmitted downward into the tubesheet because of the resistance provided by the shear stress, thus the Poisson contraction is progressively less with distance into the tubesheet. The complex theory of elasticity model is required to properly describe the complicated relationship between the deformations of the tube and the tubesheet.

The load carrying capability of a joint, F, was calculated by considering a force equilibrium for a short cylindrical element of the tube to establish a differential equation involving axial stress and net contact pressure. Compatibility and force deformation relations were then used to express the contact pressure as a function of depth in the tubesheet resulting in a first order differential equation (DE). When the contact pressure is constant the DE is homogeneous. When the contact pressure is a function of depth into the tubesheet the DE is not homogeneous. By considering the initial contact pressure to be linear (i.e., a constant slope) through the tubesheet, a linear first order DE results.

The theory of elasticity method used to calculate the residual contact pressure and pullout force for the Wolf Creek Model F SGs is different from the calculation of the residual contact pressure and pullout forces in the Model D5 and Model 44F H*/B* submittals. In order to be consistent with prior H*/B* submittals, the following empirically based approach for determining residual contact pressure and joint pullout force is applied: This approach will be consistent with the calculations described in prior submittals for Model D5 and Model 44F (i.e., the first principles approach) and will bound the empirical data available.

Note that only room temperature data will be used to determine tube resistance to pullout so that temperature effects do not have to be subtracted out from the test data. This is conservative because the value of mean – 1 σ bounds essentially all of the data points as shown in Figures 1-1, 1-2 and 1-3, below.

The room temperature F/L values are calculated by taking the pullout force for each specimen test result and dividing it by the expansion length. The following data will be used to derive the Wolf Creek Model F steam generator tube joint resistance to pullout (F/L) and residual contact pressure values (Source: Test Numbers 1 through 8 of Table 6-3 of LTR-CDME-05-209-P):

a,c,e

Test No.	Specimen No.	Expansion Length (in.)	Pull Force (0.25 inch displacement)	Contact Pressure [1] (psi)	F/L (lbf/in) [2]

The resulting force per length number for the Wolf Creek Model F steam generators is the mean minus one standard deviation value for force per unit length and is [.]^{a,c,e} This number is conservative and remains below all of the room temperature pullout data. See Figure 1-1 below.

[a,c,e

]

Figure 1-1 Tube Pullout Force Plot – Model F SGs

A comparison of the pullout forces per length values for all Model D5, 44F, and F steam generators using this same methodology is provided in the table below:

[

Room Temperature Tube Pullout Force (F/L) Values		
Model Steam Generator	**Original Pullout Force Value (lbf/in)**	**Revised Pullout Force value (Lbf/in)**

1. Based on Theory of Elasticity model.
2. Based on first principles approach
3. Based on first principles approach and room temperature test data only

]a,c,e

The revised joint pullout force value of [ ]^{a,c,e} for the Wolf Creek steam generators will be factored into the response to NRC RAI question number 2. Similar plots of the room temperature pullout data are provided below for the Model D5 and 44F steam generators in Figures 1-2 and 1-3 for information only.

a,c,e

Figure 1-2 Tube Pullout Force Plot – Model D5 SGs

a,c,e

Figure 1-3 Tube Pullout Force Plot – Model 44F Data

It is important to note that the use of room temperature only data does not significantly change the previous values for pullout force used for the Model D5 and Model 44F for which both room temperature and elevated temperature data were considered.

2. *Reference 2, Enclosure 1, Response to RAI questions 1 and 2 - provides the sensitivity of contact pressure to many of the material and geometric parameters used in the analyses. The response provides only a qualitative assessment of these sensitivities to support the conclusion that the values assumed in the H* analyses support a conservative calculation of H*. For example, the sensitivity study showed that contact pressure is sensitive to the yield strength of the tubing. The response states that the yield strength of the tubing used in the pullout test specimens was higher than the documented mean yield strength for prototypical tubing material, but did not indicate to what extent the yield strength of the test material bounds the range of prototypic yield strength variability. Thus, the staff has no basis to agree or disagree with the conclusion that test specimen contact pressures are conservatively low. The steam generators contain up to 5620 tubes, and it needs to be demonstrated that the computed H* distances are conservative for all the tubes, not simply the average tubes or 95% of the tubes. Please provide a quantitative assessment demonstrating that the assumed values of the material and geometric parameters support a conservative H* analysis for all tubes. This assessment should consider thermal expansion coefficient (TEC) for the tube and tubesheet in addition to the parameters included in the Reference 2 response.*

Response to RAI No. 2:

The yield strength of the tubing for the pullout test data for specimen numbers 1 through 6 of Table 6-3, of LTR-CDME-05-209, ranges between [.]^{a,c,e} The average yield strength for the tubing for specimen number 7 through 14 is [ ]^{a,c,e} (per STD-DP-1997-8015, Rev. 6). Only specimens 9 through 14 were used to calculate the corresponding tube pullout strength for the Model F tubing using the theory of elasticity.

The following sources of potential variability were identified and the impact on H*/B* distances of varying these parameters has been quantified(Reference 16):

a,c,e

[ ]

Only six (6) of these must be addressed numerically in the uncertainty study for H*/B*, and only five (5) of these affect the residual contact pressure for hydraulic expansion. The remaining three variables (Hydraulic Expansion Pressure, Strain Hardening, Tube Outer Diameter) are inherently modeled in the analysis process and do not require independent variation and are discussed below. The greatest potential quantitative impacts on the H*/B* distances are the result of tolerances in [

.]^{a,c,e}

Analysis Approach

Three approaches were considered for combining the uncertainties associated with determining the H*/B* distances. The three approaches considered are defined in Reference 4, EPRI Report 1012987, Steam Generator Integrity Assessment Guidelines, Rev. 2 and they are:

- Arithmetic strategy
- Simplified statistical strategy
- Monte Carlo strategy

Only the arithmetic strategy and simplified statistical methods were used to combine the uncertainties for the sensitivity study discussed below. This is the case because the arithmetic approach to combining uncertainties is expected to provide conservative results relative to both the simplified statistical and the Monte Carlo approaches. Moreover, the simplified statistical and Monte Carlo results typically provide similar results when it is assumed that the independent variables are normally distributed (as is the case with the parameters discussed above).

The method discussed below is a modified arithmetic strategy were the parameters were combined using at least a mean plus/minus one standard deviation value, whichever results in the greatest increase in H* distance. The method for combining the uncertainties is defined as a "stacked model" because all of the identified uncertainties are superimposed in a conservative direction.

The simplified statistical method result for combining uncertainties is provided in the discussion below but the explanation of the method for combining the uncertainties is not because the method is entirely consistent with that described in Section 7.3.5.2 of Reference 4, EPRI Report 1012987, Steam Generator Integrity Assessment Guidelines, Rev. 2.

The sensitivity study is divided into two parts:

1. An evaluation of those variables which affect the residual contact pressure due to tube expansion. Only five (5) of the nine (9) listed parameters directly affect the residual contact pressure used in the analysis of the Model F tubesheet joint. The applicable parameters do not include the uncertainty in the tube TEC and tubesheet TEC, tube outer diameter and tubesheet hole size.

2. An evaluation of, those variables which affect the contact pressure developed between the tube and the tubesheet during all plant operating conditions.

The uncertainty in all of the parameters above is considered in a sensitivity study. The maximum contribution from hydraulic expansion to tube-to-tubesheet contact pressure is calculated to be [[1] .]^{a,c,e} This is the mean minus 1σ value based on the equation in the response to RAI No. 1. The contribution of residual contact pressure to tube pullout resistance is small compared to the contribution

[1] This value is derived from Figure 2 of Reference 2.

from differential thermal expansion between the tube and the tubesheet, internal pressure, and tubesheet bow (depending on tube radial location and elevation in the tubesheet).

The steam generator tube integrity acceptance criterion for the sensitivity study is cited on page 20 of the Draft Regulatory Guide DG-1074 (Ref. 5). The conditional probability noted in DG-1074 states that "burst of one or more tubes under postulated accident conditions shall be limited to 1.0E-2." The 1.0E-2 value is 40% of the limiting 0.025 value described in Draft Regulatory Guide DG-1074. This value is conservatively used as an acceptable probability for combining uncertainties for the critical parameters identified above to calculate H* and B* distances. For the calculation of the H*/B* distances, this value represents the probability that the performance criteria of NEI-97-06, Rev. 2 (Ref. 6) will not be met and, in this application, does not represent the probability of a steam generator tube rupture event. Tube burst is prevented by the constraint provided by the tubesheet, and the probability of tube pullout or excessive leakage during accident conditions will be considerably lower because the analysis for H*/B* already assumes a factor of 3 on the normal operating pressure differential. The calculation of a probability smaller than the acceptance criterion of 1.0E-2 supports the technical specification requirement that all tubes have adequate margin against burst (or tube pullout).

The empirical rule is used to assign a probability to each individual parameter, assuming a normally distributed population, given the mean and standard deviation of the data set. The empirical rule states that for a normal distribution:

- 68% of the data will fall within 1 standard deviation of the mean
- 95% of the data will fall within 2 standard deviations of the mean.
- Almost all (99.7%) of the data will fall within 3 standard deviations of the mean.

This translates into a probability of 0.16 of varying from the mean value by +/- one standard deviation. The probability of varying by +/- two standard deviations is 0.025. And, likewise, the probability of varying by 3 standard deviations is 0.0015.

A "stacked" model of the uncertainties is used to determine a limiting combination of H*/B* distances. The model is considered to be a "stacked" model because all of the uncertainties are superimposed simultaneously in a conservative direction (i.e., a direction that results in the greatest H*/B* distances). The combination of uncertainties on the variables that result in an acceptably low probability closest to the acceptance criterion of 0.01 is used. Each of the parameters evaluated are assumed to be independent of each other. This is a valid assumption because no functional relationship exists between component dimensions and material properties, nor among the individual material properties noted above. The probability (Φ) that the "stacked" model H* /B* distances will not meet the performance criteria of NEI 97-06, Rev. 2 is calculated using the equation:

a,c,e

a,c,e

[ ]

The parameters considered in the analysis that affect residual contact pressure are addressed below. Figure 2 of Reference 2 presents a normalized sensitivity analysis for various parameters based on an FEA study for hydraulic expansions performed at approximately 40 ksi. This sensitivity study is considered to also apply to the Wolf Creek SGs whose tube expansions were performed at pressures between 30 ksi and 33 ksi.

In the context of this sensitivity analysis, an increase in the H* or B* distance means that the required inspection depth into the tubesheet, relative to the top of the tubesheet, increases. A decrease in the H* or B* distance means that the required inspection depth into the tubesheet, relative to the top of the tubesheet, decreases. The discussion below describes the effect on the H* and B* analysis from a variation of each parameter. Table 2-1 summarizes the discussion and provides a view of relative sensitivities.

These results are based on more than 100 individual sensitivity studies to determine the most limiting parameters and trends in the sensitivity of the H* and B* criteria to variations in the input parameters.

The following lists the parameters in order of greatest to smallest effect on the H* distance.

a,c,e

[ ]

Similarly, the following lists the parameters in order of greatest to smallest effect on the B* distance.

a,c,e

[ ]

The magnitude of the variability of each parameter was altered based on its importance to the H* and B* criteria. The term "greatest effect" in this context means that a variation in that parameter caused a larger difference in the final value of H* or B* than the next lower ordered parameter. For example, varying the

[

]a,c,e

Variables Not Addressed Independently

As shown in Figure 2 in LTR-CDME-07-72 P-Attachment (Reference 2), three other variables can affect residual contact pressure. These are [

]^{a,c,e}

Impact of the Variability of [ ]^{a,c,e}

The uncertainty on [

]^{a,c,e}

[

]a,c,e

Impact of the Variation of [ ]a,c,e

Similarly, the variation in [

]a,c,e

Impact of [ ]a,c,e

Based on NCE-88-271, Reference 7, dimensional data for [

]a,c,e

[

]^{a,c,e}

Impact of [ ]^{a,c,e}

In solid mechanics, [

]^{a,c,e}

Impact of [ ]^{a,c,e}

A calculation was performed using the [

]^{a,c,e}

The values for the various parameters for the stacked model are included in the table below. The stacked model includes the variability of each parameter and the results of a series of sensitivity studies to determine the worst case, or maximum effect, on the H* and B* analysis. For example, the effect of varying the [

]^{a,c,e}

The probability (Φ) that the stacked model H*/B* distances will not meet the performance criteria of NEI 97-06, Rev. 2 is determined to be:

a,c,e

[

]

= 2.6E-6.

0.01 >> 2.6E-6

This probability compares favorably with the acceptance criterion of 1.0E-2 which is *conservatively* based on the conditional probability of tube burst for one or more tubes under accident conditions.

Table 2-1 Stacked Model Parameters and Corresponding Uncertainties

a,c,e

[

Parameter Varied	Definition of Uncertainty Used	Input Parameter Value	Probability of Occurrence

]

The revised values for H*/B* using the parameters from the stacked model analysis are provided in Tables 2-2 and 2-3 below. Table2-2 includes the hot leg results; Table 2-3 includes the cold leg results. The combined probability term included in Tables 2-2 and 2-3 below includes a probability of:

a,c,e

The divider plate factor used in each case is taken from EPRI Report 10104982; Divider Plate Cracking in Steam Generators; Phase 1 Report, Reference 12. The probability associated with each divider plate factor is based on engineering judgment and the relative few divider plate cracking indications reported even after long periods of operation and repeat inspections in the French SGs.

The H*/B* results are plotted in Figures 2-1 through 2-4 below. Figures 2-1 and 2-2 provide the hot leg results. Figures 2-3 and 2-4 provide the cold leg results.

**Table 2-2 Hot Leg Result Summary for B* and H*
Using Stacked Worst Case Property Input Values**

a,c,e

Case #	TEC Source	Combined Probability	Divider Plate Factor	Max. H* (in.)	Max. B* (in.)

Table 2-3 Cold Leg Result Summary for B* and H*
Using Stacked Worst Case Property Input Values

[

Case #	TEC Source	Combined Probability	Divider Plate Factor	Max. H* (in.)	Max. B* (in.)

]a,c,e

HOT LEG RESULTS

[a,c,e

Figure 2-1 Case #89, B* and H* Analysis Results for Model F Hot Leg Stacked Input Case.

]a,c,e

a,c,e

Figure 2-2 Case #92, B* and H* Analysis Results for Model F Hot Leg Stacked Input Case.
[

]a,c,e

COLD LEG RESULTS

a,c,e

Figure 2-3 Case #89, B* and H* Analysis Results for Model F Cold Leg Stacked Input Case.
[

]a,c,e

Figure 2-4 Case #92, B* and H* Analysis Results for Model F Cold Leg Stacked Input Case.

]^{a,c,e}

The results of the sensitivity study show that the H* distance remains the limiting criterion for establishing the inspection depths in the Wolf Creek steam generators at every radial location. The cold leg H* distances also continue to be more limiting than the hot leg distances.

- For the hot leg, the required H* distance is 13.32 inches from the top of the tubesheet. (Case #89)
- For the cold leg, the required H* distance is 14.87 inches from the top of the tubesheet. (Case #89)

These values include the uncertainties associated with the [ ]^{a,c,e} identified in Table 1.0 above when stacked in a manner analogous to the arithmetic process outlined in Reference 4, [EPRI 1012987; Steam Generator Integrity Assessment Guidelines: Revision 2, 2006.]. As an alternative method for checking the validity of the "stacked model" results, a simplified statistical process analogous to that described in the EPRI Integrity Assessment Guidelines was applied and a similar result was obtained for the combined uncertainties. This alternative check included the limiting and more conservative definitions of variability in each parameter defined above, as opposed to the 1.645σ recommended in the EPRI Steam Generator Integrity Guidelines.

The combined uncertainties, all biased in a direction to increase the H* distance, with conservative assignment of standard deviation from their means, results in a whole bundle probability of 2.6E-6 of not meeting the structural and leakage performance criteria specified in NEI 97-06, Revision 2.

The maximum H* distances are based on using a divider plate factor of 0.64 versus a divider plate factor of 1.0. It has been shown that, without the divider plate to stub runner weld present, the tube plate

vertical deflection is still limited to 36% less than if the divider plate was not present at all, Reference 12 (EPRI 1014982; Analysis of Primary Water Stress Corrosion Cracking and Mechanical Fatigue in the Alloy 600 Stub Runner to Divider Plate Weld Material.). In other words, most of the structural benefit of the divider plate is derived from the welds to the channelhead, and not from the weld to the tubesheet (stub runner). No degradation has been reported in the welds between the divider plate and the bowl, in contrast to the reports of degradation in the weld between the divider plate and the stub runner.

The results discussed in this response are not expected to change in the highly unlikely case that an input parameter takes on an "extreme" value due to some combination of installation artifacts or deviation from mean material properties. This is for two reasons:

1. The variability of the parameters that are most important to the analysis is known and the extreme values have already been considered. For example, the thermal expansion coefficient of the tube and the tubesheet is very important to the results of an H* analysis. However, the ANTER labs data shows that the variability of those parameters is limited to +/- 1.5% with 95% confidence interval. The conclusion, then, from the most recent data means that there will always be a difference between the TEC of the tube and the tubesheet and therefore there will always be differential thermal growth between the tube and the tubesheet. The sensitivity study results presented above include the effects of varying both the ANTER labs properties and the ASME code properties to the extreme limits of the available test data and still show adequate margin with respect to the desired inspection distances into the tubesheet. Note that significant margin exists despite the fact that the other input parameters are also being varied, many to the extreme range of the known data for that property (e.g., Young's Modulus of the tube and the tubesheet). Therefore, extreme values of most of the parameters critical to the H* and B* analysis (i.e., Young's Modulus of the tube, thermal expansion coefficient of the tube and the thermal expansion of the tubesheet) have already been evaluated in the analysis.

   The only critical parameter for which an extreme value has not been evaluated is the yield strength of the tube. The results of varying the tube yield strength to either extremely negative limits or extremely positive limits still provide adequate margin with respect to the desired inspection limits. For example, if the yield strength in the tube approaches a value of zero, the contact between the tube material and the tubesheet material will be nearly perfect. This would dramatically increase the residual contact pressure between the tube and the tubesheet and make it much more difficult for the tube to pull out under the limiting loads. On the other hand, assuming that the yield strength of the tube is triple the highest value (approaching a value of 5σ) the residual contact pressure from installation would tend toward zero. The results of a B*/H* analysis for the Model F SG, with no residual contact pressure from installation, but with mean ASME code material properties and design input values for all other parameters, is a B* of 11.15 inches and an H* of 14.87 inches for the limiting cold leg. Therefore, an extreme variation in tube yield strength is bounded by the analysis results from the "stacked" model cases discussed above.

2. The bellwether concept inherently addresses any postulated effect of an extreme value result. If a tube in the steam generator is postulated to exhibit the worst case value for every parameter that is used in the B*/H* analysis, and those parameter values were beyond those considered in any of the sensitivity studies described here, and the tube is assumed to be still in service, the expected

conditions would be such that the tube would leak during normal operating conditions. If the leak during normal operating conditions is significant, it will be located and plugged. A significant leak would require a gross crack that occurs in a short time (i.e., one operating cycle) or have a prior history of leakage. There is no known mechanism that would cause a complete circumferential throughwall crack in one operating cycle to cause a significant leak, which, in any case, would cause a plant shutdown if it were to occur. Even for the case of a severe circumferential crack, not of 360 degree extent, or a large axial crack, structural integrity of the tube would be maintained by the remaining tube ligaments. Therefore, the postulate of an extreme condition tube is extremely unlikely due to the normal plant leakage monitoring requirements.

It is concluded that the H* and B* inspection criteria conservatively provides significant margin in the tubesheet for all of the tubes in the bundle even if:

- The extremely unlikely case that a specifically stacked set of material properties variations and dimensional conditions, all biased in a direction to result in greater H* values, exist in the steam generator;

- The divider plate weld to the tubesheet is 100% degraded;

- Lower bound residual pullout strength and contact pressures are used.

3. *The H* analyses in References 1 and 2 are based, in part, on pullout resistance associated directly with hydraulic expansion process. This pullout resistance was determined by subtracting out the effects of differential thermal expansion between the tube and tubesheet test collar from the measured pullout load. The calculated differential thermal expansion effect was based, in part, on an assumed TEC value of 7.42E-06 in/in/°F for the 1018 steel tubesheet test collar. What is the impact of considering an alternative TEC value of 7E-06 in/in/°F (from Matweb.com for 1018 steel interpolated at 600 degrees Fahrenheit) on the computed pullout force determined from the pullout test and on the computed H* distances?*

Response to RAI No. 3:

The impact of varying values for thermal expansion coefficient for both the tube and the tubesheet is assessed in the response to RAI No. 2.

The effect of considering the alternate value of TEC for the tubesheet noted in the question for the analysis of the pullout test is bounded by the effect of using the same TEC in the analysis for H* and B*. It is not proper to selectively use different values of the same parameter in different phases of a single analysis of the same conditions. The effect of using a reduced TEC for both the pullout analysis and the tubesheet displacement analysis is non-conservative. The lower residual pullout strength resulting from analysis of the test data has a much smaller effect (increase) on H* and B* than the use of the same value for TEC in the H*/B* analysis. A lower value of TEC applied to the tubesheet analysis significantly reduces the tubesheet displacement, resulting in increased contact pressure between the tube and the tubesheet. As a consequence, the smaller value of tubesheet TEC significantly decreases the H*/B* values.

The use of the ANTER data plus one standard deviation value for the thermal expansion coefficient for the tubesheet material of 7.2E-6 in/in/°F is judged to be extremely conservative when used in concert with a reduced thermal expansion coefficient of 7.5 E-6 in/in/°F for the steam generator tubing for the reasons discussed in the response to NRC RAI Number 2. The value of 7.2E-6 in/in/°F is the at the extreme limit of the ANTER test data. The use of this value is in the most conservative possible with respect to theH*/B* analysis.

The impact of reducing the value for TEC to 7E-06 in/in/°F for the tubesheet without a corresponding change in the thermal expansion coefficient of 7.82E-6 in/in/°F for the tube would result in a less conservative (shorter) H*/B* distance. Therefore, the impact of the MATWEB.com value for thermal expansion coefficient for the tubesheet region on the computed pullout force has not been calculated.

4. *Reference 2, Enclosure I, Response to RAI question 7 - The Model D5 steam generator (SG) pullout data in Table 2 indicate that pullout force increases with temperature for the 3-inch long specimens and decreases with temperature for the 6-inch long specimens. For the 4-inch specimens, pullout force increases with temperature to 400°F and decreases with temperature beyond that point. Discuss the reasons for this apparent discrepancy in trends among the data. Discuss whether the reduction in tube yield strength with temperature might be sufficient for some specimens to limit any increase in contact pressure associated with differential thermal expansion between the tube and tubesheet.*

Response to RAI No. 4:

(Note: The specimen number for test number 1 in Table 2.0 of Reference 2, LTR-CDME-07-72 P-Attachment, response to RAI question 7, is D5H-R3-1 not D5H-R5-1 which may have contributed to the misinterpretation of the data.)

1. The decrease in tube yield strength with increasing temperature is not likely to reduce or limit the contact pressure between the tube and tubesheet. First, the loads and conditions on the limiting section in the tube are not sufficient to cause plastic yielding in the tube. See the response to RAI No. 5. A decrease in the tube yield strength is likely to increase the contact pressure between the tube and tubesheet up to the point of plastic yielding of the tube material. For example, consider a load state on the tube that would generate a state of plastic yielding in the tube material. In that case, the plastically yielded tube material would flow with no resistance in an isochoric manner (i.e., volume preserving deformation). This kind of deformation would have two effects on the interface between the tube and the tubesheet.

2. The tube material would be able to plastically flow into the crevices and surface peaks and valleys of the tubesheet local to the plastic tube material. This would create a state of near perfect intimate contact between the tube and the tubesheet; thereby preventing any leakage through the crevice and allowing for the dispersal of large amounts of strain energy which would further reduce the possibility of tube pullout.

3. Although the surface of the tubesheet could push back on the plastically yielded tube material, the internal pressure in the tube (the primary pressure of the SG) would keep the tube material in contact with the tubesheet regardless of the tubesheet deformation because there would be no stiffness in the tube material to resist the plastic flow.

In conclusion, it is highly unlikely the tube material in the tubesheet will plastically yield due to the loads and constraints applied to the tube (See RAI No. 5). However, in the event that the tube did plastically yield, the effect would be to increase both the leakage resistance and the pullout resistance of the tube. Therefore, it is more conservative to consider both the tube and the tubesheet material as elastic structures that retain their respective stiffnesses in the event that contact pressures and conditions allow the two material surfaces to deflect away from each other. This more conservative case is the condition that is considered in the H*/B* analysis.

The pullout strength for the Model D5 tubing and the Model 44F H*/ B* submittals is a lower bounding value based on pullout test results from both room temperature and elevated temperature testing. The

data plotted in both Figures 4-1 and 4-2 have had the effects of thermal expansion due to elevated temperature testing subtracted out, thus only the mechanical contribution of the joint are reflected in the figures. As can be seen from Figure 4-1 and 4-2 provided below, the average minus one standard deviation value for pullout strength essentially bounds the data cloud for both the Model 44F and Model D5 test data. Regardless of the tube size, it can be seen that using the empirically determined mean minus one standard deviation resulting value for pullout strength is a conservative value for the bulk of the data for both the Model D5 and 44F steam generators.

The data plotted in both Figures 4-1a and 4-2a have had the effects of thermal expansion due to elevated temperature testing subtracted out. It can be seen by Figures 4-1 and 4-2 that, for the different expansion lengths, the room temperature data does not always result in the lowest pullout strength for the Model D5 and 44F test specimens as well. For the specific example cited by the NRC staff, i.e., the Model F result for Wolf Creek, it can be seen that the Model D5 7-inch expansion length room temperature test specimen results in a higher tube pullout strength than the elevated temperature test results. For the Model 44F steam generator, however, the approximate 7-inch expansion length room temperature test specimen results in a lower tube pullout strength than that for the elevated 400°F test specimen and a comparable pullout strength to the elevated 600°F test result. Therefore, it is concluded that what is interpreted in the question as a data trend reflecting temperature effects is, in reality, normal variability among the different test specimens.

a,c,e

a) elevated temperature data adjusted to remove thermal expansion component

a,c,e

b) Room Temperature Data

Figure 4-1 Model D5 Pullout Test Results for Force/inch at 0.25 inch Displacement

a,c,e

a) (elevated temperature data adjusted to remove thermal expansion component)

a,c,e

b) Room Temperature Data

Figure 4-2 Model 44F Pullout Test Results for Force/inch at 0.25 inch Displacement

As discussed in the response to NRC RAI Number 1 above, it is noted that the analysis of the residual contact pressure and the pullout force for the Wolf Creek Model F steam generators used a theory of elasticity model. In order to obtain a consistent approach for defining the tube pullout strength, it was decided to only use room temperature results to determine tube resistance to pullout so that the temperature effects do not have to be subtracted out of the data. The mean minus one standard deviation room temperature values for tube pullout strength for the Model F, Model D5, and 44F steam generators are repeated here for convenience:

Room Temperature Tube Pullout Force (F/L) Values

Model Steam Generator	Original Pullout Force Value (lbf/in)	Revised Pullout Force value (Lbf/in)

a,c,e

1. Based on Theory of Elasticity model.
2. Based on first principles approach
3. Based on first principles approach and room temperature test data only

As discussed in the response to NRC RAI Number 1, the use of room temperature data only does not significantly change the previous values for pullout force used for the Model D5 and 44F steam generators when both room temperature and elevated temperature data are considered.

The NRC staff's concern whether a reduction in tube yield strength with increasing temperature might be sufficient for some specimens to limit any increase in contact pressure associated with differential thermal expansion between the tube and tubesheet was considered. As stated in the response to NRC RAI No. 7 in LTR-CDME-07-72, Reference 2, the data in Table 2.0 is intended to show that for an expansion length as short as 2.95 inches, a significant increase in pullout force occurs at elevated temperatures (e.g., pullout force increases from [ ]^{a,c,e} when temperature increases from 70°F to 600°F, respectively). Therefore, since the test results inherently include the variation of yield strength with temperature, the results indicate that yield strength reduction with temperature does not limit the increase in contact pressure due to thermal expansion.

5. *Following up on question 4 above, is there a possibility that any tubes could be stressed beyond the compressive yield strength (at temperature) of the tube material due to differential thermal expansion, internal pressure, and tubesheet hole dilation for the range of yield strengths in the field? Describe the basis for either yes or no to this question. If yes, how has this been factored into the contact pressures, accumulated pullout resistance load as a function of elevation, and H* in Tables 7-6 through 7-10 and 7-6a through 7-10a of Reference 2, Enclosure 1?*

Response to RAI No. 5:

It is not possible for a SG tube with an intact cross section to compressively fail due to the applied pressures calculated in the H* and B* analysis. The basis for this statement is a stress analysis of the tube material using the Tresca yield criteria. The analysis approach and results follow:

The maximum applied contact pressure from Tables 7-6 through 7-10 and Tables 7-6a through 7-10a in Reference 2 [LTR-CDME-07-72 P-Attachment] is 5355.38 psi or approximately 5.4 ksi. The maximum contact pressure occurs in the cold leg, during FLB at the bottom of the tubesheet (21.03 inches below the top of the tubesheet). For 11/16 inch Alloy 600 tubing, the minimum yield strength is [ ]^{a,c,e} at room temperature, Reference 8 [WCAP-12522]. At a temperature of 650°F the tensile yield stress [ ]^{a,c,e} Reference 8 [WCAP-12522]. For a material element at the outside surface of the tube wall (the tube material in contact with the tubesheet wall), assuming the full axial load is applied to the tube despite its location in the tubesheet, the state of stress is equivalent to that of an element in a thin-walled pressure vessel with the third principal stress not equal to zero.

For the FLB condition, the principal stresses on the tube wall element are:

$$\sigma_1 = \sigma_{XX} = \frac{p_{PRI} r}{t} = \frac{2650 psi \cdot 0.3515 in}{0.040 in} = 23586.9 psi = 23.3 ksi$$

$$\sigma_2 = \sigma_{YY} = \frac{p_{PRI} r}{2t} = \frac{2650 psi \cdot 0.3515 in}{2 \cdot 0.040 in} = 11643.4 psi = 11.6 ksi$$

$$\sigma_3 = \sigma_{ZZ} = P_{CONTACT} = -5355.38 psi = -5.4 ksi$$

Applying the Tresca theory, or maximum shear stress yield criteria, gives:

$$\frac{Y}{2} = \tau_{MAX} = \left| \frac{\sigma_1 - \sigma_3}{2} \right|$$

$$Y = 36.8 ksi > \left| 23.3 ksi - (-5.4 ksi) \right| = 28.7 ksi$$

This shows that the tube has a safety factor of at least 1.3 with respect to yielding using the minimum yield strength for Alloy 600 at elevated temperature. At room temperature conditions, the safety factor increases to nearly 1.6. If the material properties and conditions in the steam generator are varied for a worst case analysis then the maximum contact pressures in the tubesheet will be reduced. Any reduction

in contact pressure between the tube and the tubesheet make it even less likely that a tube will yield in compressive failure.

In conclusion, it is not possible for an intact tube to yield in compression under the state of stress created by the transient event with the maximum applied contact pressure.

6. *Reference 2, Enclosure I, Response to RAI question 17 - The response states near the bottom of page 30 of 84 that Case 1 results shown in Table 3.0 are for the limiting cold leg analysis and reflect the following assumption: "Although the pullout test data indicated positive residual mechanical joint strength, the residual joint strength is ignored for SLB [steam line break] accident condition[s] to conservatively account for postulated variability of the coefficient of thermal expansion." The NRC staff notes, however, that the limiting H* value shown in Table 3.0 for Case 1 is that necessary to resist three times the normal operating pressure end cap load, not that needed to resist 1.4 times SLB. It is the staff's understanding based on review of Tables 7-6 through 7-10 and 7-6a through 7-10a that the residual mechanical joint strength (522 lb/inch) was reflected in the H* computations for normal operating and accident conditions, including SLB. Discuss and clarify these apparent discrepancies.*

Response to RAI No. 6:

The tables in Reference 2, Enclosure I, Response to RAI question 17 print residual pullout value for the analysis using a cell reference from the calculation spreadsheet. This cell reference was not deleted to make it clear that the residual mechanical joint strength was excluded from some portions of the analysis. The residual mechanical joint strength was not included in the H* computations for accident conditions but was included for normal conditions. The result of the analysis shows that the NOP case is limiting despite the elimination of the residual joint strength for the SLB case.

7. *Reference 2, Enclosure I, Table 7-6 - This table states that the required pullout force is 1680 lb. Table 7-6 indicates that for a tubesheet radius of 12 inches the needed depth of engagement is less than 10.52 (about 10.2 using linear interpolation). However, the table states that an engagement depth slightly greater than 10.52 (i.e., 10.54) is needed. Discuss and explain this apparent (minor) discrepancy.*

Response to RAI No. 7:

The H* distance is determined using an automated MS-EXCEL spreadsheet routine written in VBA code. Beginning at the bottom of the tubesheet, the code integrates the resistance forces over the length of the tubesheet and compares the results to the external load applied, i.e., 3 times the end cap load. The stability of the calculation routine depends on the increment size: A too-small increment results in code instability; a too-large increment size can result in hunting for a solution. If the integrated resisting force is greater than the applied force, the prior reference location, i.e., the bottom of the tubesheet, initially, the code performs the integration again based on the shorter distance. As the net force approaches zero, the increment is automatically reduced. This iteration and incrementation is continued until the resisting force is less than the applied force. The final net-zero distance is established by interpolating between the closest negative and positive net forces.

It is possible that a minor difference, in this case 0.020 inch, can result from the variation of the calculation increment.

After a solution has been obtained with the iteration code, a constant factor of 0.3 inch (taken from the top of the tubesheet down) is added to the result to account for the potential variation in the location of the bottom of the expansion transition (BET). Compared to this constant factor applied for potential variation of the BET from the top of the tubesheet, a 0.02 inch variation of the calculated value of H* is negligible.

8. *Reference 1, Enclosure I, Table 6-4 - The listed F/L values are based on allowing 0.25 inch slippage. Reference 1 does not address the potential for limited, but progressive incremental slippage under heatup/cooldown and other operational load cycles. Nor does Reference 1 address the effects of slippage on normal operating leakage and on accident-induced leakage or the ratio of normal operating and accident induced leakage. The response to RAI question 5 in Reference 2, Enclosure I, does not provide any further insight into this issue. That response specifically addressed test results for tubes with a hard roll expansion, and the staff believes that the slippage versus axial load characteristics for such an expansion may be entirely different than for a hydraulic expansion. Discuss and address the potential for progressive incremental slippage under heatup/cooldown and other operational load cycles. In addition, address the potential for slippage under operational and accident conditions to affect the ratio of accident-induced leakage to operational leakage.*

Response to RAI No. 8:

Cyclic loading testing was conducted on five tubes, including A600TT tubes, which were hydraulically expanded into a test block (Reference 7 – NCE-88-271, "Assessment of Tube-to-Tubesheet Joint Manufacturing Processes for Sizewell B Steam Generators Using Alloy 690 Tubing," November 1988). The tubes were loaded to a given load between [ ]^{a,c,e} The axial position of the primary side end of the tube was measured before loading and after unloading. The direct measurements of the displacement of the primary end of the tubes were in reasonable agreement with displacements recorded from the secondary side by the displacement gage. Figure 8-1 below shows the load-displacement curves. Reference 7 concludes that the tubes underwent rigid body displacement (breakaway) at a [ ]^{a,c,e} relative to the maximum pullout load. Based on the much steeper unloading and reloading curves relative to the initial loading curves (See R12C4 and R12C5), it can be concluded that the tubes did slip at small loads.

There is no effect on the ratio of the normal and accident leakage for a 360° circumferential flaw in the event of relative slippage between the tube and tubesheet interface. If any slippage occurred it would be an indication of a degradation of the frictional interface between the tube and the tubesheet. Degrading this interface and lowering the frictional resistance of the tube portion within the tubesheet would change the necessary pullout load, but not the contact pressure between the tube and the tubesheet. Therefore, the leak resistance coefficient, k, would not be changed and the relationship between the contact pressure and the leak rate coefficient would not be changed. Also, the Bellwether Principle still applies to the situation. Regardless of the friction between the tube and the tubesheet, the increase in leakage is directly proportional to the difference in the primary and secondary side pressures. In the absence of resistance to leakage from the tube-to-tubesheet interface, Darcy's model for axial flow in a porous medium, predicts that any increase in leak rate would be equal to the increase in the differential pressure, which is bounded

by a factor of two (2). Therefore, if the leak rate under normal operating conditions was considered acceptable, the leak rate under accident conditions would also be acceptable and any increase in leakage during an accident would be conservatively bounded by a factor of two (2).

If it is assumed that a tube continues to incrementally slip, the cumulative distance of slippage would result in eventual contact with adjacent (lateral or vertical) tubes. This condition would be detected during normal inspection of the tubes soon after contact had occurred. The nominal spacing between tubes varies from about 0.3 inch at the inner rows to about 0.48 inch at the outer rows. Displacement of a tube by this amount would have no effect on B* since the difference between H* and B* exceeds this value.

Figure 8-2 shows the difference between H* and B* for both the hot leg and the cold leg. The minimum difference, approximately 1.8 inches, occurs on the HL at the periphery of the bundle. Since H* bounds B* in all cases, B* will apply at all locations even if the tube is postulated to slip by 1.8 inches.

Peripheral tubes, which may not have adjacent tubes, are discussed in the response to RAI No. 9.

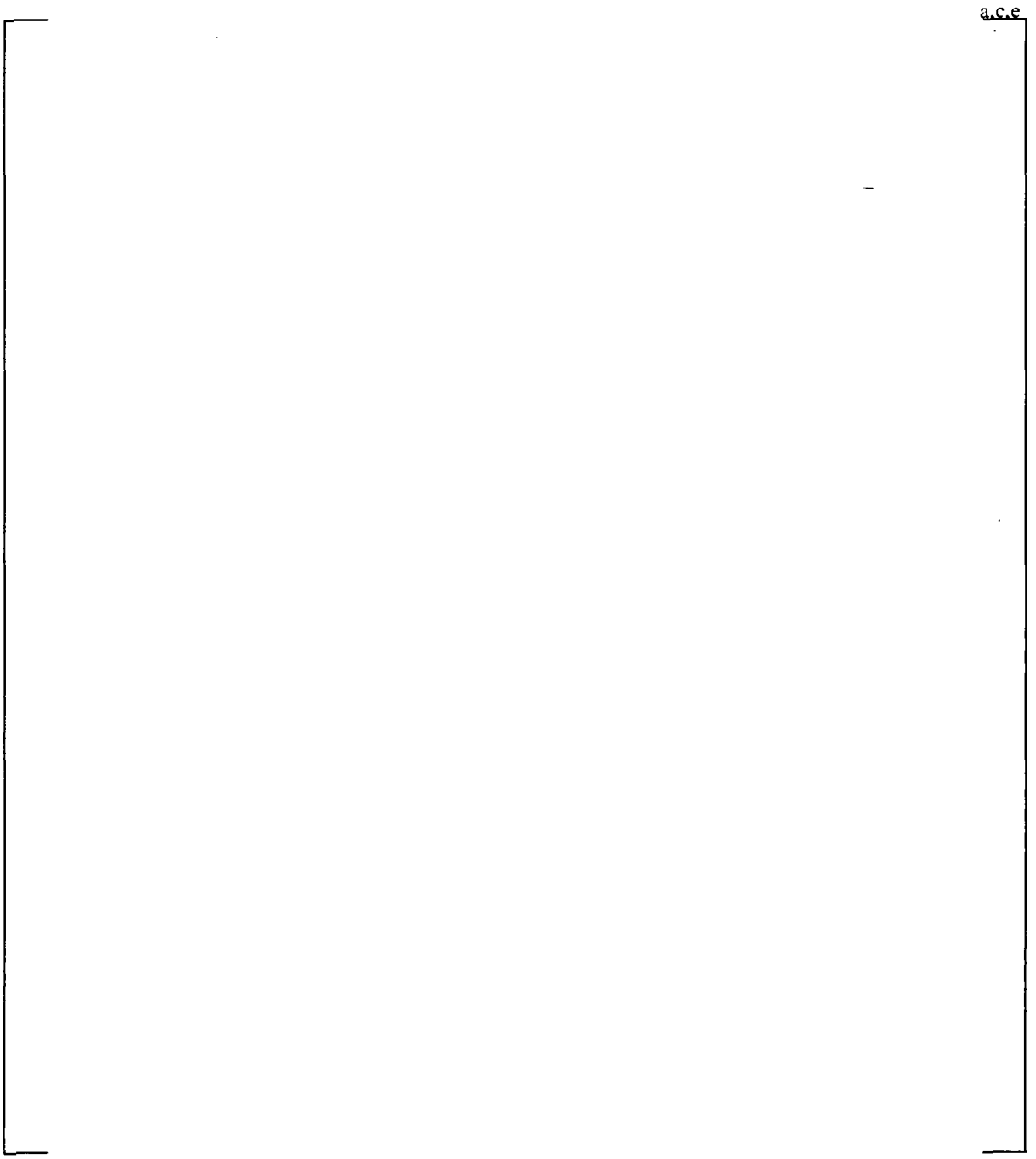

Figure 8-1 Load-Unload-Reload Pullout Curves

a,c,e

Figure 8-2 Difference Between H* and B*

9. *Discuss your plans for revising the proposed technical specification (TS) amendment to monitor the tube expansion transition locations relative to the top of the tubesheet to ensure that the tubes are not undergoing progressive, incremental slippage between inspections.*

Response to RAI No. 9:

No revisions to the Technical Specifications are proposed.

The response to RAI No. 8 concluded that, based on individual pull tests using a test block of tubes expanded in a tubesheet, [

]^{a,c,e} However, the test conditions were very conservative in that no tubesheet bow was simulated. In an operating SG, the application of tube loads depends on the SG primary side being pressurized, resulting in tube sheet bow. All tubes are constrained from motion by tube hole contraction below the tubesheet mid-plane for the bulk of the tubes or above the mid-plane for the tubes near the periphery of the tubesheet. For any motion to occur, it is tacitly assumed that a 360 degree throughwall circumferential crack exists below H*. If even a small ligament exists, the axial end cap force will be resisted by the tube-end weld at the bottom of the tubesheet. Further, the tests were performed at room temperature. Consequently, the two most significant factors affecting H* were not simulated.

If a 360° throughwall circumferential crack is assumed just below H* and that a tube continues to incrementally slip, the cumulative distance of slippage is limited by eventual contact with adjacent (lateral and/or vertical) tubes after a short distance. The maximum nominal distance between u-bends is 0.482 inch in rows 52 and greater. In smaller radius rows, the axial spacing is incrementally less due to smaller indexing of the tube straight legs. Because of axial constraints provided by the tube bundle, and lateral restraint provided by the presence of the AVBs, the maximum axial displacement of a tube is limited to less than one pitch, 0.980 inch, even if the u-bend of the postulated moving tube moves toward the adjacent column. As noted in RAI No. 8, the minimum margin between H* and B* is 1.8 inches; therefore a postulated extreme displacement such as this would not affect the efficacy of H*/B*.

An extreme displacement condition as described above would result in tube to tube contact well before a significant displacement had been achieved. Tube-to-tube contact would be detected during normal inspection of the tubes soon after contact had occurred. If tube-to-tube contact is detected, normal inspection procedures would require investigating the source of the contact and corrective action would be required.

No significant slippage of tubes has been reported to date in the industry. The requirements of Reference 16 (EPRI SG Inspection Guidelines) assure that all tubes have been inspected to date at Wolf Creek, both by bobbin and by RPC in the region ±3 inches relative to the top of the tubesheet on the HL. The Wolf Creek practice is to inspect the peripheral two rows of tubes on both the HL and CL at the top of the tubesheet ±3 inches, at a minimum, with RPC as a conservative measure to guard against damage due to foreign objects. No indications of gross slippage (i.e., the expansion transition moved above the top of the tubesheet) have been observed. This is an indication that either no circumferential separation has occurred in the expansion region or that significant slippage does not occur.

H* bounds B* by a minimum of 1.8 inches at all locations; therefore, leakage is not a concern because of the Bellwether principle. If a tube is found not to leak, regardless of the position of the the bottom of the

expansion transition (BET) relative to the top of the tubesheet (assuming motion has occurred), accident induced leakage will also be zero. If a tube is leaking within the performance limits at normal operating conditions, it will also not exceed the accident induced leakage limits. Leakage exceeding the normal operating limits requires shutdown of the plant and elimination of the source of the leakage. Consequently, the difference between H* and B* represents a conservative limit for tube motion, since, at the next inspection, if a flaw is found to exist above H*, the tube will require plugging. Therefore, continued monitoring of the BET at inspections is not necessary because, until significant motion (up to 1.8 inches) of the tube has occurred, there is no potential for accident induced leakage to exceed acceptable values.

A postulated condition of a circumferential separation occurring at H* within one inspection cycle is not a credible event. Since even a small ligament is sufficient to assure axial restraint of the tube, a 360° circumferential sever is required for tube motion to occur. The growth of a crack to a 360° circumferential throughwall condition requires a significant period of time after crack initiation, spanning at least several inspection cycles. If a circumferential crack were to develop at the H* distance, and if it is postulated that the tube experiences incremental motion, normal inspection of the tube to H* would identify the crack well before separation could occur, and the tube would be plugged. The factor of safety against tube pullout under normal operating conditions is approximately 3, and the 3DPNO condition envelopes all accident condition pullout loads.

In summary:

- Incremental motion, like that observed in manufacturing testing, is not expected because of the operating constraints in an operating SG. The tests that exhibited slight incremental motion did not simulate the operating conditions (temperature and pressure) that would lead to additional constraint provided by tubesheet bow and the thermal effects.

- It is not necessary to monitor tubes for small displacements. Since the Bellwether Principle applies, normal leakage monitoring will determine the need to shut down the plant when primary to secondary leakage is detected. Therefore, excessive accident induced leakage within the tubesheet expansion region can never occur. If a tube is found to be leaking, normal inspections to H* will determine if a flaw exists above H*. In that event, the tube must be plugged. All tubes except the peripheral tubes can be monitored during normal inspections for potential tube to tube contact. If tube to tube contact is observed, the source of the contact will be determined and appropriate action taken to repair the condition.

- The minimum difference between H* and B* is approximately 1.8 inches. Therefore, motion of up to 1.8 inches will not affect leakage, and provides a definitive, observable degree of displacement. This extent of motion is not possible in the interior of the bundle; therefore, any concern about displacement should focus principally on the peripheral tubes. For the peripheral tubes, normal bobbin inspection will detect significant displacement since the expansion transition will be reported above the top of the tubesheet.

- For all tubes, a circumferential sever is required for any motion to occur. The development of a 360° circumferential crack from crack initiation requires significant time. Normal inspection to H* will identify a circumferential crack within the H* distance if incremental motion is postulated.

10. *Reference 1, Enclosure I, Section 7.1.4.2 - This section provides a brief discussion of SLB, feed line break (FLB), and loss-of-coolant accident (LOCA) in terms of which is the most limiting accident in terms of tube pullout potential. Expand this discussion to indicate whether SLB and FLB are the most limiting accidents among the universe of design basis accidents (DBA) (or other faulted conditions in the design basis) in terms of both tube pullout, and the margin between the calculated accident-induced tube leakage for each DBA and the assumed accident-induced tube leakage in the safety analysis for that DBA.*

Response to RAI No. 10:

The following accidents model primary-to-secondary leakage in the Wolf Creek USAR:

- Section 15.1.5, Steam Generator Tube Rupture
- Section 15.3.3, Reactor Coolant Pump Shaft Seizure (Locked Rotor)
- Section 15.4.8, Spectrum of RCCA Ejection Accidents (Control rod ejection)
- Section 15.1.5, Steam System Piping Failure (Steam line break)
- Loss of Non-Emergency AC Power to the Station Auxiliaries (BLACKOUT)

An evaluation of these transients has been conducted to determine the duration of time that the primary-to-secondary pressure differential exceeds the normal operating condition primary-to-secondary pressure differential (Reference 13, LTR-SGDA-07-197, "Wolf Creek Model F Steam Generator Faulted Transient Delta-P Evaluation," 8/31/07). It has been determined that the duration of time that the primary-to-secondary pressure differential exceeds the normal operating pressure differential for a locked rotor [ ]^{a,c,e} and that the SLB event remains the limiting accident. The leakage limit that is defined for the locked rotor event and the control rod ejection event is 1.0 gpm. The leak rate for the locked rotor event and the control rod ejection event can be integrated over one minute to compare to the limit. Since the time above the normal operating pressure differential is less than [ ]^{a,c,e} the time integration should permit an increase in acceptable peak leakage at the peak pressure differential by at least a factor of 2. As the allowable primary to secondary leak rate is limited to 150 gpd (0.1 gpm) in the Wolf Creek SGs during normal operating conditions, accident induced leakage is expected to remain less than [ ]^{a,c,e} This leakage rate is bounded by the current accident analysis assumption. See Tables 10-1 and 10-2 and Figures 10-1 and 10-2 below.

For tube pullout considerations, the limiting load applied to the tube is 3 times the normal operating pressure differential. This value bounds 1.4 times both the SLB and FLB loads.

WCGS USAR Section 15.2.6, "Loss of Non-Emergency AC Power to the Station Auxiliaries" (BLACKOUT) also models SG primary to secondary leakage. However, based on a review of Reference 14, the maximum primary-to-secondary pressure differential [ ]^{a,c,e} during this upset transient never exceeds the normal operating pressure differential of 1443 psi. Therefore, there is no adverse impact on the existing radiological consequences calculated in the WCGS USAR with the implementation of the H*/B* criteria.

Table 10-1 Primary-to-Secondary Side Pressure Differential Time-Histories for RCP Locked Rotor and Control Rod Ejection Transients (Wolf Creek Model F Steam Generators)

Time sec	Normal Operation ΔP psi	RCP Locked Rotor (Dead Loop) ΔP psi	RCP Locked Rotor (Active Loop) ΔP psi	Time sec	Control Rod Ejection ΔP psi

a,c,e

Table 10-2 Primary-to-Secondary Side Pressure Differential Time-History for Main Steam Line and Feedwater Line Breaks (Wolf Creek Model F Steam Generators)

Time sec	Normal Operation ΔP psi	Feedwater Line Beak ΔP psi	Time sec	Steam Line Break ΔP psi

a,c,e

a,c,e

Figure 10-1 Plots of the Primary-to-Secondary Side Pressure Differential Time-Histories for RCP Locked Rotor and Control Rod Ejection Transients (Wolf Creek Model F Steam Generators)

a,c,e

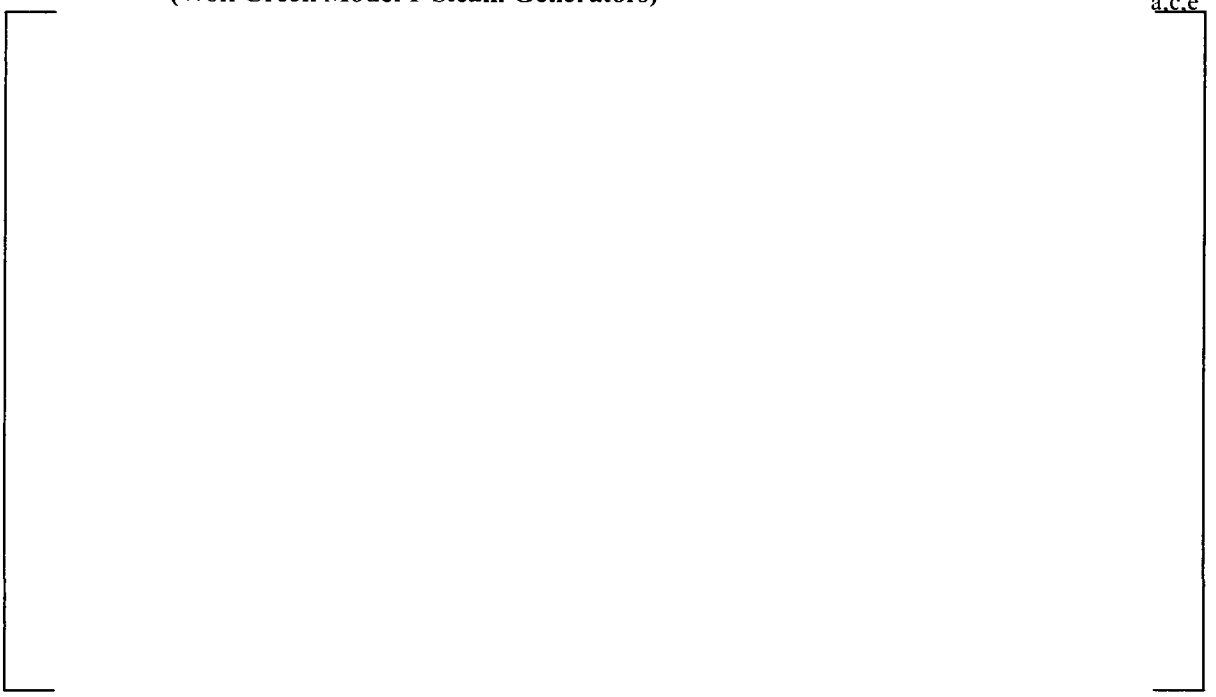

Figure 10-2 Plot of the Primary-to-Secondary Side Pressure Differential Time-History for Main Steam Line Break

11. Figure 11 of Reference 2, Enclosure 1 contains loss coefficient data for Model F SG tubing that was not included in Figure 6-6 of Reference 1, Enclosure 1. This data was for contact pressures ranging from about 1200 psi to about 2000 psi. Why was this data not included in Figure 6-6? Discuss if this is this because of low expansion pressures and if the data that is not included in Figure 6-6 is room temperature data. [If yes, then the NRC staff observes that the room temperature loss coefficients for the Model F specimens are relatively invariant with contact pressure above a contact pressure threshold of around 700 psi. The 600 degree F data is also invariant with contact pressure. Thus, loss coefficient may not be a direct function of contact pressure once a threshold degree of contact pressure is established. The difference in loss coefficient data between the 600°F data and the room temperature may be due to parameter(s) other than contact pressure. This other parameter(s) may not be directly considered in the B analysis.]*

Response to RAI No. 11:

The reasons for not including the data are discussed in the response to NRC RAI No. 11 from Enclosure I to WCNOC letter WO 07-0012.

The additional data include:

1. Test results from the Model F specimens that were not prepared in accordance with criteria of the test specifications (i.e., the test specification expansion pressure was not achieved).

2. Test results from Model D5 specimens that resulted in no leakage. The Model D5 testing was specifically oriented toward leakage; therefore, since a zero-leak test does not provide usable data for leakage, these tests were not previously reported.

The data that were added includes both room temperature data and elevated temperature data.

The Staff's observations about the leak rate data and the relationship between the loss coefficient and contact pressure for the Model D and Model F tests are noted. However, Westinghouse believes, based on the data, that there is a definable relationship between the loss coefficient of a TS crevice and the contact pressure between the tube and tubesheet. The data available provides the information necessary to define a conservative log-linear relationship between contact pressure and loss coefficient. See Figure 11-1 for a plot of the total Model F and Model D data set with a curve of the 95% confidence fit obtained by a log-linear regression of the combined Model D and Model F data sets.

Figure 11-1 Plot of Loss Coefficient, k, as a Function of Contact Pressure, P_c.

The results plotted in Figure 11-1 illustrate four important characteristics in the Model F and Model D data and the resulting 95% confidence interval fit of the combined data set.

These results indicate that the Model D loss coefficient data is [

]^{a,c,e}

[

]a,c,e

If only the Model D data were used, [

]a,c,e

Therefore, the available test data is considered valid and is applied in a very conservative manner via the Darcy model for axial flow through a porous medium. The Staff has noted in the past that the Darcy model is a more conservative approach than either the Bernoulli model or a converging orifice model. A different model is likely to give a less conservative result compared to the current bounding approach using the fit of the combined data set. In conclusion, using the 95% confidence fit of the combined Model F and Model D data set is an extremely conservative approach which results in a curve that bounds most of the loss coefficient data and maximizes the required B* distance.

12. Figure 13 of Reference 2, Enclosure 1 contains additional loss coefficient data taken from the crevice pressure study in the white paper. Provide a figure showing all individual data points from which Figure 13 was developed. Describe the specific applied pressure differentials from the crevice pressure study used to calculate the contact pressure for each data point.

Response to RAI No. 12:

The data supporting Figure 13 is provided below in Figure 12-1.

The pressure differentials used to calculate the contact pressures for each data point are listed in Table 12 -1. The crevice pressure differentials were calculated using bounding crevice pressure ratio values. The crevice pressure ratio (CPR) values were determined by taking the limiting median value as described in the White Paper [Appendix B] and are summarized in Table 12-2.

The crevice pressure ratios were applied based on the pressure differential in the leak test, for example, the data from the White Paper tests that had a ΔP of 1000 psi was applied to cases that also had a ΔP of 1000 psi to determine the appropriate contact pressure.

a,c,e

Figure 12-1
Loss Coefficient versus Contact Pressure (Combined Model F and Model D5)

Table 12-1

Data Supporting Figure 13 of the White Paper (Appendix B)

SG MODEL	PRIMARY SIDE TEST PRESSURE (PSI)	TEST TEMPERATURE (°F)	CONTACT PRESSURE (PSI)	CREVICE PRESSURE DIFFERENTIAL (PSI)

a,c,e

Table 12-2

Summary of Crevice Pressure Ratios from White Paper (Appendix B)

SG Type	Crevice Pressure Ratio	Primary Pressure

a,c,e

(Primary pressure units are psi)

13. *Although the means of the regression fits of the loss coefficient data for the Model F and Model D SGs are shown in Figure 13 of Reference 2, Enclosure I, to be within a factor of three of each other, the slope and intercept properties remain highly divergent, seeming to cast further doubt that loss coefficient varies with contact pressure (above some threshold value of contact pressure). Discuss this and describe any statistical tests that have been performed to establish the significance of correlation between loss coefficient and contact pressure. In addition, describe any statistical tests that have been performed to confirm that it is appropriate to combine the data sets to establish the slope and intercept properties of loss coefficient versus contact pressure.*

Response to RAI No. 13:

Figure 2 from Rev 0 of the White Paper (Rev. 1 is Appendix B of this document) are presented below as Figure 13-2 for ease of reference. The constant loss coefficient values noted in the White Paper are highlighted on the plot as well. Also please refer to the responses to RAI No. 11 and RAI No. 12.

No statistical tests were performed to evaluate combining the two data sets. A conservative approach was used that essentially bounds all of the available data, thus a statistical evaluation was not required.

While the data for the Model F tests results in a reasonable correlation; the Model D results in a slightly negative correlation. When the two data sets are combined, the linear regression results for the combined dataset is more conservative than interpolating between the regression fits of each of the Model D or Model F data. The high variability of the combined data set produces a 95% confidence interval fit that bounds the lower limit of almost the entire data population. See the Response to RAI No. 11.

If no correlation is assumed to exist, the intercept for the log linear equation is the average value of the population and the slope of the log linear correlation is zero. A lower bounding value for loss coefficient is also shown.

The maximum B* inspection distance for the case of the lower bounding limit of the loss coefficient, assuming mean ASME code material properties and mean design inputs, is 11.15 inches. In comparison, the maximum B* inspection distance for the case of the mean loss coefficient value, assuming mean ASME code material properties and mean design inputs, is approximately 6 inches. Since the lower 95% confidence fit for the combined data is well below the mean value and close to the lower bounding value, and essentially bounds the entire available data, it is conservative to use the lower 95% confidence fit for the B* calculation.

In conclusion, the 95% confidence fit of the entire data set results in a loss coefficient versus contact pressure relationship that bounds almost the entire set of data and produces highly conservative B* inspection distances. Even if the lower bounding limit of the loss coefficient values is used the B* inspection distance is less limiting than the H* inspection criteria.

a,c,e

Figure 13-2 Comparison of 95% Confidence Limit Scaled Model F and Model D Loss Coefficient Data Fits for the Case of No Flashing in the Crevice, Pc Calculated using TE and Varied Crevice Pressure with No Data Excluded

14. *Reference 2, Enclosure I, page 25 of 84 - For the case of assumed zero slope of loss coefficient versus contact pressure, two constant loss coefficient values were compared. Does the first assumed value come from Figure 14? If not, provide additional information on where this assumption comes from. If yes, explain the relationship between the assumed value and Figure 14. Does the second assumed value come from Figure 12? If not, provide additional information on where this assumption comes from. If yes, explain the relationship between the assumed value and Figure 12.*

Response to RAI No. 14:

See Figure 13-2 in the Response to RAI No. 13 for a plot that illustrates the two constant loss coefficient values. The first assumed value for zero slope loss coefficient comes from the lowest value from the Model D curve fit from Figure 14. The second assumed value for zero slope loss coefficient does not come from Figure 12. The second assumed value for zero slope represents the mean of all of the data points included in Figure 11 of Enclosure I to WCNOC letter WO 07-0012.

15. *Reference 2, Enclosure I, Figure 15 - clarify the title of Figure 15 in terms of whether it reflects consideration of residual mechanical strength in the joint during an SLB. Is Figure 15 for the hot or cold leg? Explain the following: (1) why the B* values at small tubesheet radii are less than those listed in Reference 1, Enclosure I, Table 11-1 and (2) why the contact pressures shown in Reference 1, Enclosure I, Figures 9-6 and 9-7 are different from those shown in Tables 7-6 and 7-8 of Reference 1, Enclosure I.*

Response to RAI No. 15:

- The results shown in Figure 15 of Enclosure I to WCNOC letter WO 07-0012 do include the consideration of mechanical strength in the joint during SLB.

- The results shown in Figure 16 of Enclosure I to WCNOC letter WO 07-0012 do not include the residual strength of the joint during SLB.

- The results shown in both Figure 15 and Figure 16 of Enclosure I to WCNOC letter WO 07-0012 are for the cold leg.

- The results shown in Figure 15 of Enclosure I to WCNOC letter WO 07-0012 are not used in the current determination of B* and H* inspection distances and were provided only as a means of comparison to the results shown in Figure 16 of Enclosure I to WCNOC letter WO 07-0012.

- The results shown in Figure 15 of Enclosure I to WCNOC letter WO 07-0012 and Figure 11-2 do not reflect the current level of technology nor the changes required to address recent RAI *(circa 2006-2007).*

- The B* and H* values at small tubesheet radii in Figure 15 of Enclosure I to WCNOC letter WO 07-0012are slightly less than those listed in Table 11-1 of Enclosure I to WCNOC letter ET 06-0004 for the cold leg. This is due to the correction of minor errors in the spreadsheet used to calculate the B* values.

- The contact pressures shown in Tables 7-6 and 7-8 of Enclosure I to WCNOC letter WO 07-0012 do not include the residual contact pressure due to hydraulic expansion.

16. *Reference 2, Enclosure I - Provide a description of the revised finite element model used to support the revised H* calculations in Tables 6-7 through 6-10 and Tables 6-7a through 6-10a. Compare this revised model to the original model which supported the Reference 1 analysis. Explain why the revised model is more realistic than the original model.*

Response to RAI No. 16:

Three finite element models were used to justify the contact pressure calculations for H* and B*.

- The first, original, finite element analysis is an axisymmetric model, as shown in Enclosure I to ET 06-0004, that calculates the radial deflection of the tubesheet under unit load conditions as a function of the tubesheet elevation and radius. For convenience, this model will be called Model O-1.

- The second finite element model is a three-dimensional solid model that calculates the vertical deflection of the tubesheet as a function of tubesheet radius for various load cases assuming different stiffnesses and/or cracking in the divider plate. The output from the second finite element model defines the divider plate factor and was used to check the results from the first. For convenience, this model will be called Model O-2.

- The third finite element model was an improved version of Model O-2, which included changes further discussed below.

The original finite element model (Model O-1), that was used to calculate the tubesheet deflection, was not revised as it does not model the divider plate in the lower SG complex.

The second finite element model (Model O-2), originally used to determine the divider plate factor used in the H*/B* analysis, was revised to become Model O-3. The modifications to the O-2 model include a solid tubelane, the addition of the weldments and connections between the divider plate and the channelhead and tubesheet, non-axisymmetric boundary conditions and variable stiffness in the divider plate material. The revised model, O-3, more accurately reflects the true geometry, loading and material conditions of the tubesheet. Therefore, the revised model, O-3, more completely represents the actual SG configuration than the original FEA analytical model (O-2) did.

The divider plate factor was conservatively chosen as 1.00 for the development of Tables 7-6 through 7-10 and 7-6a through 7-10a. A divider plate factor of 1.00 means that no structural credit is taken for the presence of the divider plate and the divider plate is assumed to be entirely absent; no support is derived for the DP either in the bowl or at the tubesheet. This condition is not possible because the residual weld beads would retain the divider plate even if it were postulated that the welds had completely cracked. Further, there has been no evidence in the industry of cracking in the weld between the divider plate and the channel head, nor is such degradation expected because these welds are thermally stress relieved. The results of a study funded by EPRI (Reference 12) and data from original design documents from Westinghouse show that the majority of the structural benefit of the divider plate is derived from the divider plate connection to the channelhead. The divider plate factor for the case where the structural credit for the divider plate to tubesheet connection is negated is DP = 0.64. This

means that even in the event that the upper 5.00 inches of the divider plate, stub runner and weld material somehow disappears the tubesheet displacements are still reduced by a minimum of 36%.

The results shown in Tables 7-6 through 7-10 and Tables 7-6a through 7-10a are highly conservative because the DP value that should be used based on the available data on cracking indications in the divider plate is DP = 0.64.

Replacement figures and tables, based on the final models using the stacked worst case and a divider plate factor of 0.64 are provided in Appendix C of this letter report.

17. *Reference 2, Enclosure 1, Attachment 1 (The Westinghouse Letter Summary of Changes to B* and H*), page 14 - address the status of the divider plate evaluation being performed under EPRI sponsorship, and the schedule for completion of the various topics being addressed in the evaluation. Describe any inspections that have been performed domestically that provide insight on whether the extent and severity of divider plate cracks is bounded by the foreign experience. Discuss the available options for inspecting the divider plates.*

Response to RAI No. 17:

The status of the EPRI program is not related to the current B*/H* analysis and any results from the EPRI program will have no impact on the Wolf Creek B*/H* analysis , which does not take credit for the presence of a divider plate to stub runner weld or the region of the divider plate that has been observed to degrade. The analysis presented in Enclosure I to WCNOC letter WO 07-0012 utilizes a divider plate factor of 1 which assumes that the divider plate is non-existent. Since this is not a credible condition as discussed in the response to RAI No. 16, a divider plate factor DP=0.64 is used that assumes that the divider plate to stub runner weld is completely degraded, but that the divider plate to channel heads welds are intact. This is a valid assumption because these welds are thermally stress relieved, and no degradation has been reported in these welds.

18. *Discuss how the ability of the divider plates at Wolf Creek to resist tubesheet deflection (without failure) under operating and accident loads is assured in the short term, pending completion of the EPRI evaluation. Include in this discussion the actions that are planned in the near term to ensure that the divider plates are capable of resisting tubesheet deflection.*

Response to RAI No. 18:

Please refer also to the response to RAI No. 16.

The B* and H* inspection depths reported in Enclosure IV to WCNOC letter WO 07-0012 do not take any credit for the presence of the divider plate, either at the tubesheet or in the channelhead. This is reflected in the analysis via the divider plate factor which is set to 1.00 such that no displacements are scaled in the calculation of the contact pressure. The divider plate to stub runner weld is not required to restrict any deflections of the tubesheet in the Wolf Creek steam generators to support the B*/H* alternate repair criteria. Please see the response to RAI 17 and RAI 25 in Enclosure I to WCNOC letter WO 07-0012.

As noted in the responses to several RAIs above, the current analysis is based on the use of a divider plate factor of 0.64. This factor reflects the structural effect of a divider plate which is welded to the channelhead but assumes that the weld to the stub runner is entirely missing. Justification for the use of this divider plate factor (DP=0.64) was provided previously.

Therefore, divider plate inspections are not necessary to support the H*/B* criteria for the Wolf Creek steam generators because:

- the H*/B* values do not depend on a direct connection between the divider plate and the tubesheet, and the weld between the divider plate and
- the channelhead to divider plate welds were stress relieved, have shown no evidence of degradation and are not anticipated to crack.

19. *Reference 2, Enclosure 1, Attachment 1 - Provide a description of the Crevice Pressure Test. This description should address, but not necessarily be limited to the following:*

    a. *Description of test specimens, including sketches.*

    b. *Description of "pre-treatments" of test specimens (hydraulic expansion pressure, heat relief, etc.).*

    c. *Description of test setup, including sketches.*

    d. *Description of test procedure.*

    e. *What were the secondary side temperatures in Tables 1 and 2 corresponding to the listed secondary side pressures and how were the secondary side pressure and temperatures controlled and monitored?*

    f. *How long did each test run and how stable were the pressure readings at each of the pressure taps during the course of each test?*

    g. *What was the temperature of (1) the coolant in the crevice and (2) the tube and tubesheet collar as a function of elevation?*

    h. *How were the temperature distributions for item g determined? Were direct temperature measurements of the tubesheet collar performed as a function of elevation?*

Response to RAI No. 19:

The results of an experimental test program to determine the pressure profile within a steam generator tube-to-tubesheet crevice under leakage conditions are described in *STD-MC-06-11, Rev. 1 "Pressure Profile Measurements During Tube-to-Tubesheet Leakage Tests of Hydraulically Expanded Steam Generator Tubing." August 2007.* This report is provided as Appendix A of this letter report.

For convenience, a "road map" to where subparts a) through h) of RAI No. 19 are located in Appendix A of this report is provided below:

a. Description of test specimens, including sketches.

   A description of the test specimens along with sketches and pictures are included on Pages 4-1 through 4-3 of Section 4, "Experimental Description" of Appendix A of this letter report.

b. Description of "pre-treatments" of test specimens (hydraulic expansion pressure, heat relief, etc.).

   A description of a portion of the "pre-treatments" of the test are included in Figures 19-1 through 19-6 below. Additional description is provided on Pages A-27 and A-28 in Section 5, "Outline of Test Procedure" of Appendix A of this letter report.

c. Description of test setup, including sketches.

   A description of the test facility is provided on Pages A-17 through A-27 in Section 4.2, "Test Facility" of Appendix A of this letter report.

d. Description of test procedure.

   A description of the test procedure is provided on Pages A-28 through A-32 in Section 5.4, "Summary of Different Types of Leak Test Procedures" of Appendix A of this letter report. The test matrix is shown in Table 5-3 on Page A-33 in Section 5.5, "Test Matrix" of Appendix A of this letter report.

e. What were the secondary side temperatures in Tables 1 and 2 corresponding to the listed secondary side pressures and how were the secondary side pressure and temperatures controlled and monitored?

   A summary of the leak rate test procedures is provided on Pages A-28 through A-32 in Section 5.4, "Summary of Different Types of Leak Rate Test Procedures" of Appendix A of this letter report. Only secondary side pressure was monitored. The corresponding temperature can be obtained from the steam tables.

f. How long did each test run and how stable were the pressure readings at each of the pressure taps during the course of each test?

   The crevice pressure profile test results are provided on Pages A-34 through A-64 in Section 6, "Results" of Appendix A of this report. A discussion of the leak rate test results is provided on Pages A-73 through A-85 in Section 7, "Discussion" of Appendix A of this letter report.

g. What was the temperature of (1) the coolant in the crevice and (2) the tube and tubesheet collar as a function of elevation?

The temperature of the coolant in the crevice was not measured. Only the inlet temperature was measured. See Section 5.4 of Appendix A of this letter report.

h. How were the temperature distributions for item g determined? Were direct temperature measurements of the tubesheet collar performed as a function of elevation?

No measurements were taken of the temperature of the tubesheet collar. See Section 5.4 of Appendix A of this letter report.

a,c,e

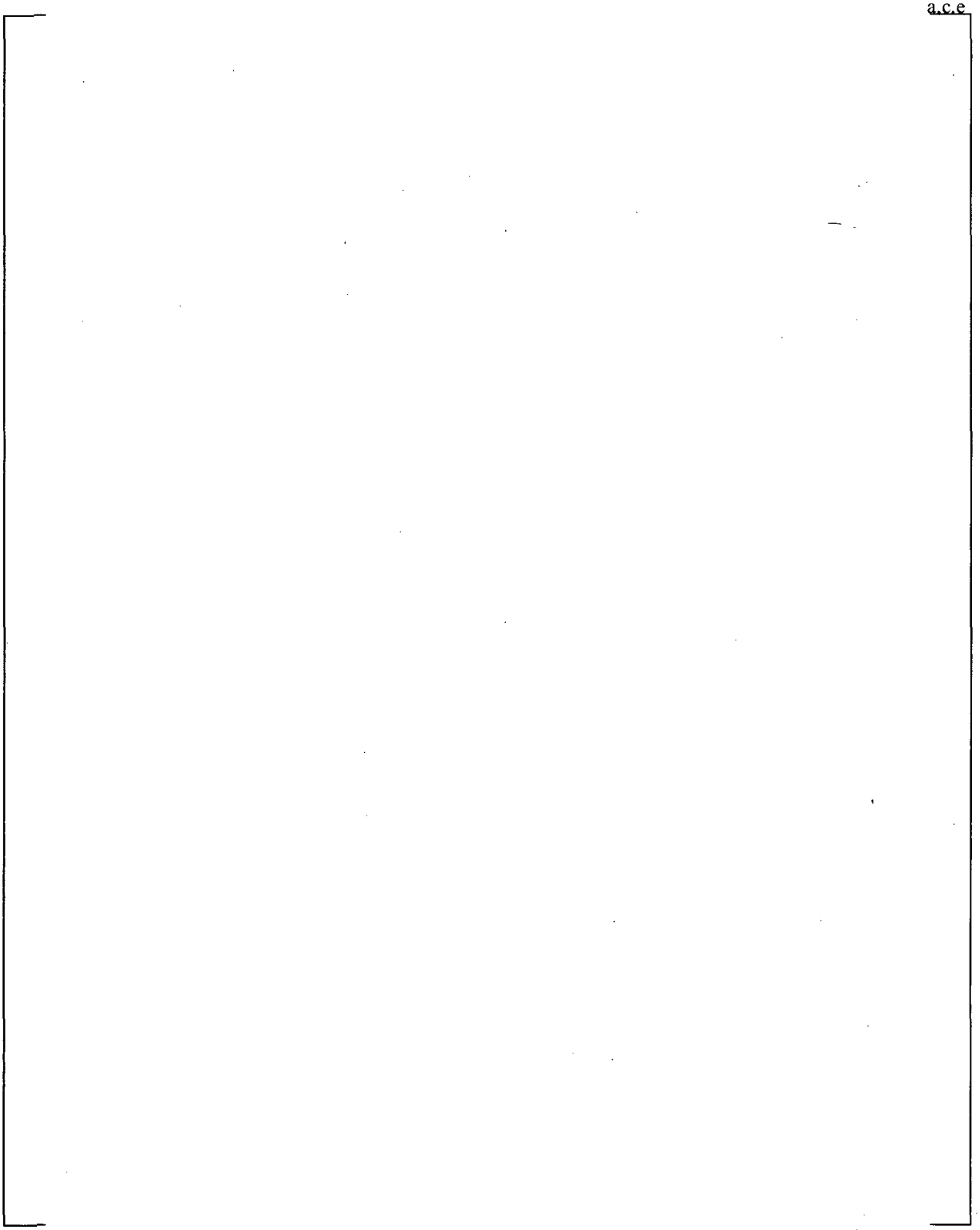

Figure 19-1

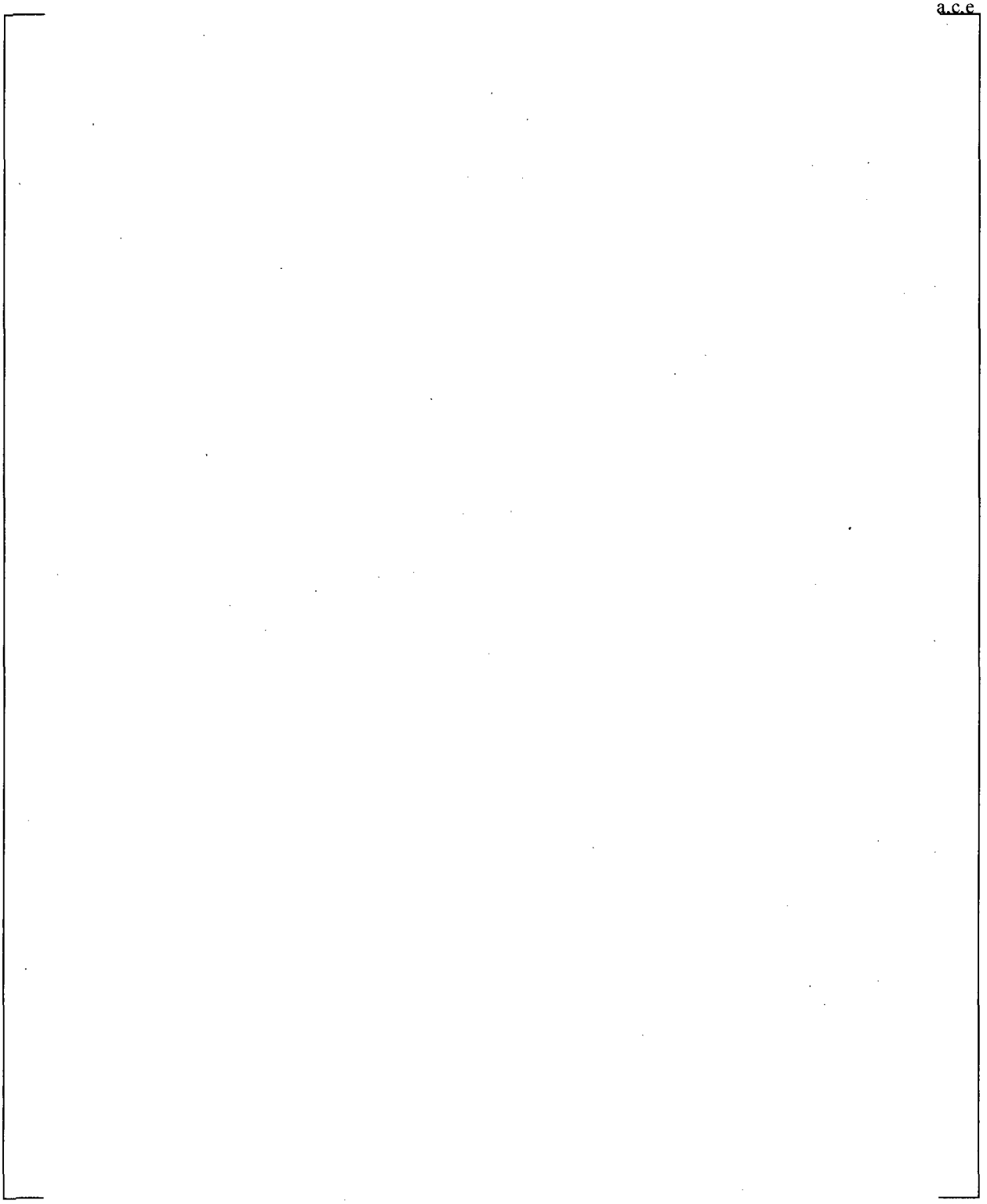

Figure 19-2

a,c,e

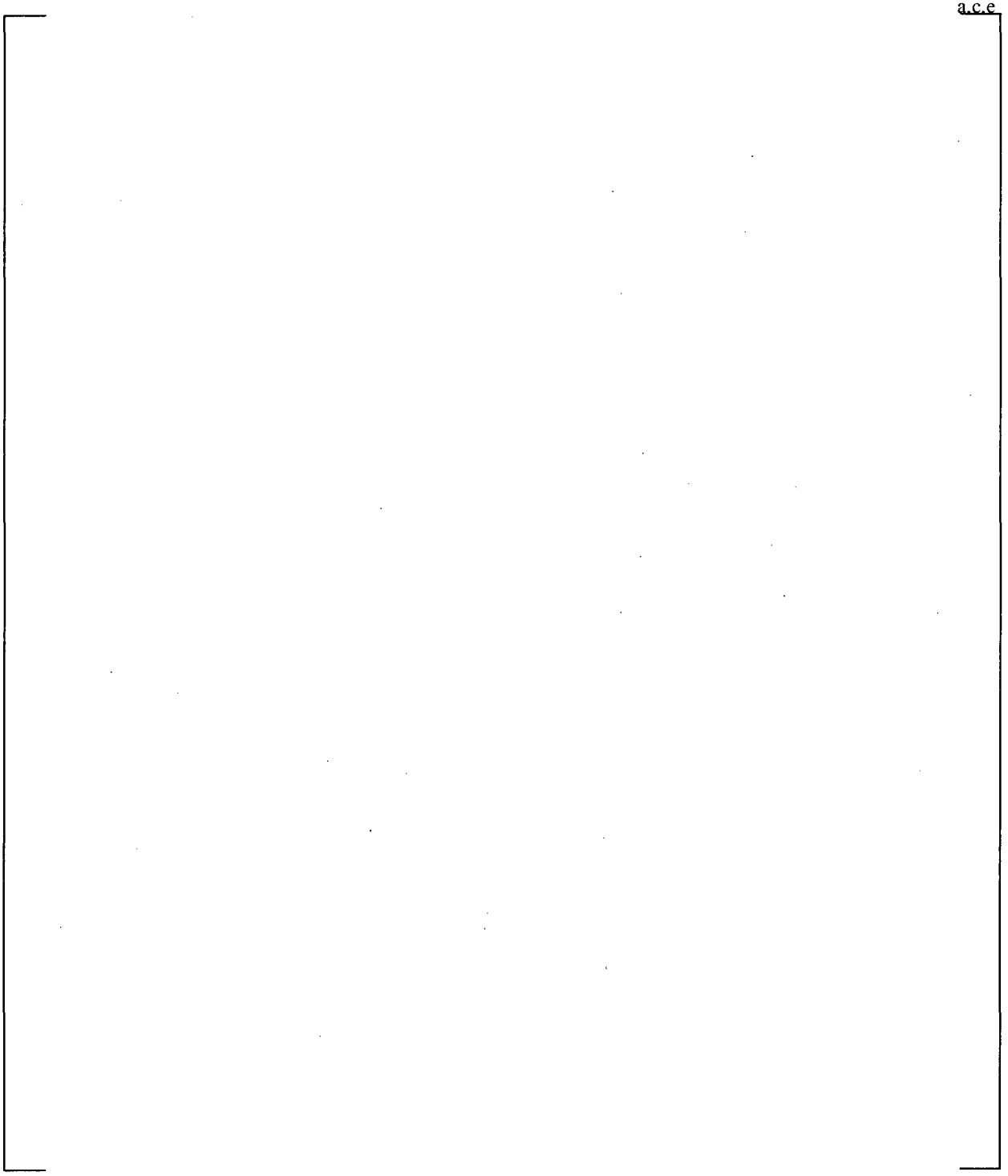

Figure 19-3

a,c,e

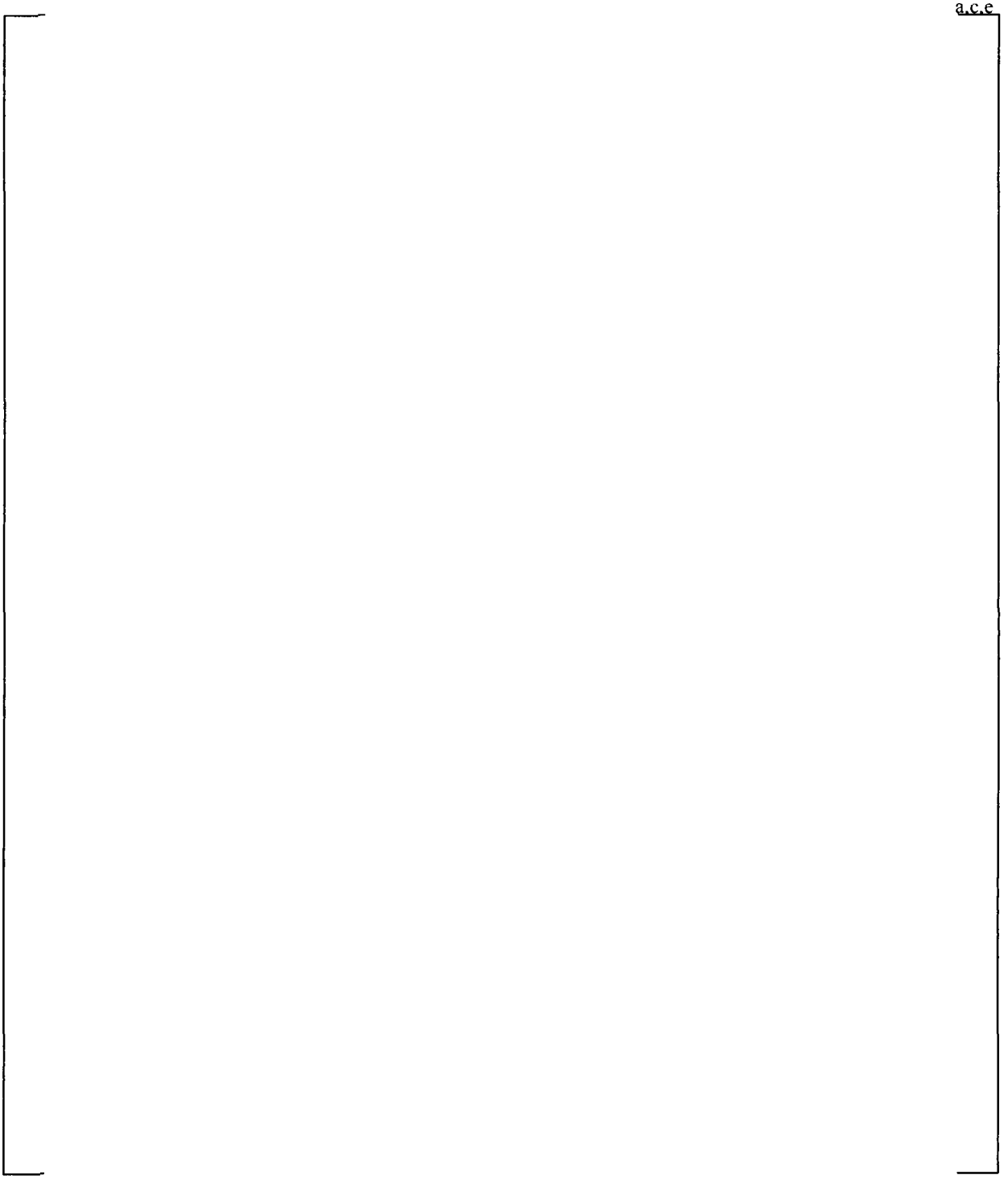

Figure 19-4

a,c,e

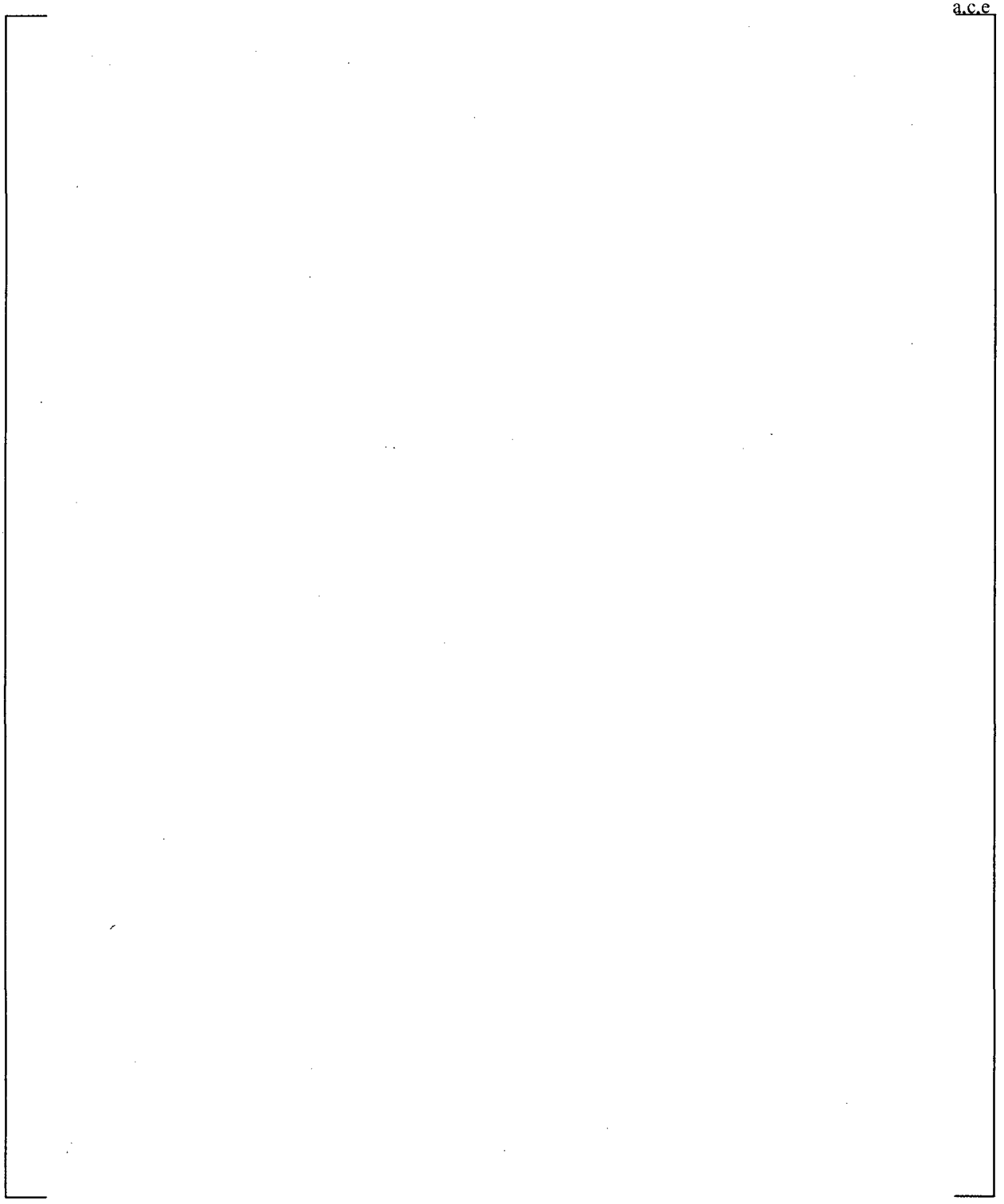

Figure 19-5

a,c,e

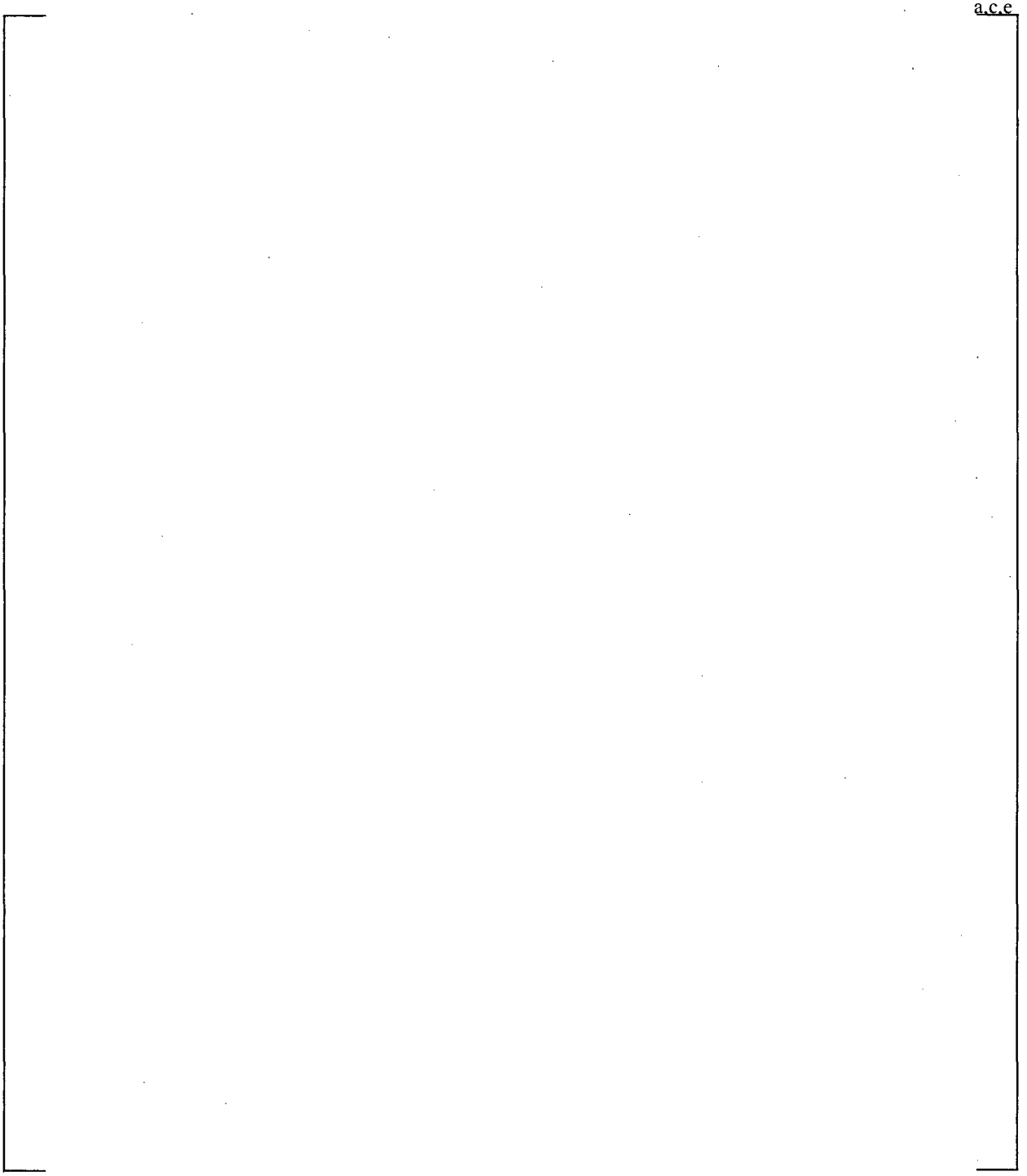

Figure 19-6

20. *Reference 2, Enclosure 1, Attachment 1 - The pressure tap locations in Figure 2 are different from those shown in Figure 3. Discuss and explain this difference or provide corrected figures.*

Response to RAI No. 20:

The abscissa values, the horizontal axis, in Figure 2 of the White Paper are correct. The abscissa values used in the original Figure 3 were incorrect. The corrected Figure 3 is provided below as Figure 20-3.

a,c,e

Figure 20-3

Corrected Figure 3 from the White Paper

21. *Reference 2, Enclosure 1, Attachment 1 - Figures 2 and 3 assume crevice pressure at the top of tubesheet is at the saturation pressure for the primary system. Discuss and explain the basis for this assumption. Why wouldn't the crevice pressure trend to the secondary side pressure near the top of the tubesheet?*

Response to RAI No. 21:

Figures 2 and 3 in the White Paper show only the average, or mean, saturation pressure for all of the test results plotted.

The saturation pressures come from measured test data and are not assumptions. The results are presented in Tables 1 and 2 in the White Paper.

The pressure does approach the secondary side pressure near the very top of the specimen (within less than 1 inch from the top) in both the SLB and NOP cases, as shown in Tables 1 and 2 in the White Paper.

The ability of the fluid pressure in the crevice to reduce to the level of the secondary side pressure is limited by the physical constraints of the crevice. The results of the tests suggest that the crevice is too tight for the water to expand in volume and thereby reduce in pressure. This is because the contact pressure between the tube and the simulated tubesheet collar is too great during the simulated operational conditions to allow a path through the crevice that is large enough to allow for the fluid to expand. The contact pressure near the top of the crevice, between the tube and the tubesheet, in the simulated tubesheet collars appears to decrease which allows for a more open crevice. As the crevice opens up, the fluid velocity and volume can increase which allows the fluid to approach the conditions on the simulated secondary side of the tubesheet

An updated version of the White Paper is provided as Appendix B to this letter report.

22. *Reference 2, Enclosure 1, Attachment 1 - Figure 3 refers to tests labeled SLB 9 and SLB 10 which are not listed in Table 2. Discuss and explain this, or provide a revised Table 2 and Figure 3 showing all test results.*

Response to RAI No. 22:

The attached White Paper (Appendix B of this letter report) has been revised to correct any typographical errors in the text and the figures.

The data in Table 2 of the White Paper is correct.

A revised Figure 3 is provided below as Figure 22-3.

a,c,e

Figure 22-3

Corrected Figure 3 from the White Paper

23. *Reference 2, Enclosure 1, Attachment 1 - Page 6 states in part that the following change should be made to the H*/B* analyses: "The driving head of the leaked fluid has been reduced." Discuss and clarify this sentence. The staff notes that resistance to leakage occurs from two sources: resistance from the flaw and resistance from the crevice. Because the crevice pressure was assumed to be equal to the secondary pressure, the original analysis assumed the entire pressure drop (the driving head) was across the flaw. The tests described in the white paper eliminate any pressure across the flaw (by using holes rather than cracks) and force the entire pressure drop to occur along the crevice. Thus, there is no net change in the total driving head between the primary and secondary sides. In fact, the driving head from the bottom to the top of the crevice would seem to have been increased.*

Response to RAI No. 23:

The Staff's understanding of the source of the leak resistance is correct. The Staff's interpretation of the crevice pressure test results is not correct. The test results indicate the crevice pressure distribution is distinct and different from the primary or secondary side pressures. The difference in pressure between the crevice and the secondary side of the tubesheet is especially evident at the lower tubesheet elevations. The driving potential on the fluid from the primary side (the interior of the tube) to the crevice has been reduced. The driving potential on the leaked fluid from the crevice to the secondary side is increased at the lower tubesheet elevations and decreased at the upper tubesheet elevations. However, the tightness of the crevice at the lower elevations prevents the fluid from directly conforming to the pressure gradient between the crevice and the secondary side of the simulated tubesheet collar. The implications of these results are discussed below.

The objective for incorporating the crevice pressure results into the B* and H* models was to obtain the largest penalty for both the leakage resistance (maximize the B* depth) and the resistance to pullout (maximize the H* depth) assuming a 360° sever in a tube and 100% degradation of the tube material below the severed portion of the tube. The limiting crevice pressure ratio determined using the approach described in the White Paper conservatively accounts for any changes in driving potential and limits the leakage resistance in the crevice too. Further, the limiting crevice pressure ratio approach maximizes the driving head on the leaked fluid from the tube to the crevice and minimizes the resistance of the crevice to leaked fluids at lower tubesheet elevations. See Figure 23-3 and Figure 23-5 for a plot of the difference in pressure between the primary side pressure in the tube and the measured pressure in the simulated tubesheet crevice during NOP and SLB. See Figure 23-4 and Figure 23-6 for a plot of the difference in pressure between the crevice pressure in the tube and the secondary side pressure during NOP and SLB. The two curves shown on each plot represent the different assumptions discussed in the White Paper. The zero slope curves in each plot are the result of the limiting median crevice pressure approach described in the White Paper. The varied slope curves in each graph are representative data plotted from the crevice pressure test results. The definition of the crevice pressure ratio is the pressure in the crevice divided by the primary pressure in the system. The definition of the depth ratio is the distance from the bottom of the tubesheet divided by the total tubesheet depth.

Figure 23-3 Plot of the pressure difference between the primary pressure in the crevice pressure test compared to the measured pressure in the crevice during NOP as a function of depth ratio.

Figure 23-4 Plot of the pressure difference between the measured crevice pressure compared to the measured secondary side pressure during NOP as a function of depth ratio.

a,c,e

Figure 23-5 Plot of the pressure difference between the primary pressure in the crevice pressure test compared to the measured pressure in the crevice during SLB as a function of depth ratio.

a,c,e

Figure 23-6 Plot of the pressure difference between the measured crevice pressure compared to the measured secondary side pressure during SLB as a function of depth ratio.

The impact of the limiting median crevice pressure approach is clear from these plots. Namely, that the crevice pressure test results indicate that both during NOP and SLB the driving head on the leaked fluid from the tube to the crevice is significantly reduced at the bottom half of the tubesheet (See Figure 23-3 and Figure 23-5). The reduction in driving potential from the tube to the crevice at the lower elevations of the tubesheet is significant because:

1. The observed cracking indications occur at the lower tubesheet elevations. This means that decreasing the driving head on the fluid into the crevice using a depth based crevice pressure approach is less conservative than using the limiting median crevice pressure ratio approach.

2. The tight crevice prevents the leaked fluid from reaching equilibrium with the secondary side pressure at the lower tubesheet elevations. This means that the driving potential of the leaked fluid from the tube to the crevice is more important at the lower elevations than the driving potential from the crevice to the secondary side.

Using the limiting median crevice pressure value throughout the tubesheet maximizes the driving head on the leaked fluid at the lower tubesheet elevations. Conversely, using the limiting crevice pressure ratio approach conservatively reduces the leak resistance of the tubesheet crevice at the lower elevations due to the higher crevice pressures. Therefore, if the pressure difference between the crevice and the secondary side pressure were included as a function of depth, as opposed to the limiting median crevice pressure approach, the leak resistance of the crevice would be significantly increased (See Figure 23-4 and Figure 23-6).

Concerning the top of the tubesheet, referring to Figure 23-3, the use of the constant, limiting median crevice pressure value (crevice pressure net) during normal operating conditions results in a conservatively lower pressure differential between the primary pressure and the pressure in the crevice (less contact pressure) for the top half of the recommended H* distance (14.87 inches), the limiting cold leg distance. This effect would be expected to cancel out the effect of the depth dependent pressure differential being less than the limiting crevice pressure value (which results in a non-conservative contact pressure) for the lower half of the H* distance. No change in the recommended H* distance is required. Referring to Figure 23-4 again, during normal operating conditions, the use of the median crevice pressure value results in a higher pressure differential between the crevice pressure net and the secondary side pressure for a majority of the B* distance which would result in a longer B* distance.

Addressing SLB conditions at the top of the tubesheet, referring to Figure 23-5, because the pressure differential is greater across the tube for most of the H* distance, use of the limiting median crevice pressure value results in a shorter H* distance than would be calculated if a depth dependent pressure differential is used for the SLB condition. However, the most limiting H* distance calculated for the WCGS steam generators is based on the NEI 97-06, Rev. 2 structural performance criterion of 3 times normal operating pressure differential. A 3 inch margin exists between the H* distance calculated for the normal operating versus SLB condition (14.87 inches versus 11.01[2] inches – see Appendix C of this letter

[2] This value is the calculated H* value for SLB conditions, excluding the 0.3 inch uncertainty to cover variability in the location of the BET.

report). The increase in H* distance that results if a depth dependent pressure differential across the tubes is used is calculated to be 1.2 inches. Therefore, no change to the limiting H* distance is required. Next, referring to Figure 23-6 which affects the B* distance during a SLB, the depth dependent crevice pressure value minus the secondary side pressure differential exceeds the median crevice pressure value for crevice pressure net minus the secondary side pressure for approximately half of the limiting calculated B* distance. This would lead to a greater driving head for primary to secondary leakage and a greater B* distance. However, for the other half of the B* distance, the median crevice pressure value minus secondary side pressure exceeds the depth dependent pressure value minus the secondary side pressure differential which would negate this non-conservatism in the model. The net result is judged to be no impact on the limiting calculated B* distance.

Based on the above, the limiting crevice pressure ratio approach results in a conservative H* and B* distance for all plant conditions.

24. *Reference 2, Enclosure 1, Attachment 1 - The top paragraph on page 10 states, in part, "the median value of the crevice pressure ratios provides a conservative value that is an average representation of the behavior at the top of the tubesheet. The median is typically a better statistical representation of the data than the mean because the median is not influenced by a smaller data set but by the total range in values in the sample set." The staff has the following questions regarding these sentences:*

a. *Discuss and clarify what data set "median value" applies to. For example, does the "median value" for the NOP data set in Table 1 mean the median value of the 15 pressure tap data points obtained during three tests, or does it mean a median value of a subset of these 15 data points? If a subset, what subset and why? Alternatively, does it mean the median value at each pressure tap location?*

b. *Discuss why this median value is a conservative representation of the behavior at the top of the tubesheet.*

c. *Discuss what is meant by "top of the tubesheet." For 17-inch inspection zone amendments, shouldn't this mean the upper 17-inches to ensure a conservative analysis? If not, why not? To ensure a conservative analysis for H* and B*, should not the objective be to establish crevice pressure as a function of elevation that can be directly applied into the H* and B* computations.*

d. *Discuss why the median is not influenced by a smaller data set and how the median is influenced by the total range of values in the sample set.*

Response to RAI No. 24:

Please refer to the figures and text in the response to RAI No. 23 in addition to the responses below.

The objective for incorporating the crevice pressure results into the B* and H* models was to obtain the largest penalty for both the leakage resistance (maximize the B* depth) and the resistance to pullout (maximize the H* depth) assuming a 360° sever in a tube and 100% degradation of the tube material below the severed portion of the tube. The choice of crevice pressure model affects both the structural calculations for H* and the leakage calculations for B*. The reasons why the limiting crevice pressure ratio approach is conservative are discussed below.

a. The "median value" with respect to the limiting crevice pressure ratio reported in the White Paper is the median value of the sorted data set of all test specimens including only the last two pressure readings after the outliers identified by the Dixon ratio test have been removed from the set. See the response to RAI No. 26 for a sample calculation of the Dixon ratio test and the resulting limiting crevice pressure ratio.

b. The median value approach described in the White Paper is a conservative representation of the behavior at the top of the tubesheet because it captures the significant difference between the NOP and SLB conditions at the top of the tubesheet and it provides the maximum penalty on both the H* and B* distances throughout the tubesheet.

c. The term top of the tubesheet refers to the uppermost elevation of the tubesheet, relative to the primary face. The entire length of the tube and tubesheet expansion joint crevice must be considered in this analysis because, in the event that primary fluid could leak through a flaw below the H*/B* inspection requirements, the proposed analysis must still be conservative. It is less conservative to model the crevice pressure as a function of depth into the tubesheet as opposed to the limiting crevice pressure approach described in the White Paper. (Please refer to the response to RAI No. 23.) This analysis does not target a specific inspection depth but rather, it defines a very conservative inspection depth that meets all structural and leakage performance requirements.

d. Both the mean and the median values are used to evaluate which application of the constant limiting crevice pressure ratio is the most conservative with respect to B* and H*. The most conservative result occurs when the median crevice pressure value is used.

There are many sources available for detailed discussions of the application of the mean and the median in statistics. The discussion in the paragraph below is paraphrased from a discussion board hosted by Purdue University (http://www.cyto.purdue.edu/hmarchiv/1998/ 0824.htm) and several text books. Similar comments can be found in reliability engineering text books (e.g., Statistics, Probability and Reliability for Civil and Environmental Engineers, McGraw-Hill, © 1997).

The median, or 50th centile, is the value that corresponds to the middle item in a ranked list (e.g, sorted by magnitude) of all recorded measurements in a data set. The median is a robust statistical measure in that it doesn't necessarily change in response to small numbers of outliers, or to skewing of the tails of a distribution, whereas the mean is tugged by both. This is why the median is typically described as a "resistant" measure. One situation where the median is probably the only valid measure is when data congregate at one or both extremes. However, as long as more than 50% of the data are clear of the extremes you get a valid median, but any type of mean (geometric or arithmetic) will be less accurate.

In a smaller data set, it is less likely to obtain a significant portion of outliers, but the presence of outliers can make a drastic change to statistical interpretations of a small data set. The Dixon Ratio test is used to assess the character (i.e., mostly average values, a small number of outliers, entirely composed of outlier values, etc.) of the data set and remove potential outliers that could influence the limiting crevice pressure ratio result. The use of the mean and the median to check the results of the crevice pressure ratio approach is conservative and ensures that the limiting value can be determined regardless of the character of the data set.

25. *Reference 2, Enclosure 1, Attachment 1 - Provide a copy of Reference 3. The cited web page appears to be no longer available. Also, provide copy of Reference 4.*

Response to RAI No. 25:

The URL given in the White Paper (Reference 3 in the White Paper) was moved by the academic institution responsible for the website. Enclosure IV to this submittal provides the requested information.

Reference 4 in the White Paper is provided in Enclosure V to this submittal, is considered as copyrighted material and should be treated as such.

26. *Reference 2, Enclosure 1, Attachment 1 - What were the specific data sets used to compute the Dixon Ratio values at the top of page 11?*

Response to RAI No. 26:

Note: The following response is based on the original White Paper. An updated White Paper is included as Appendix B to this letter report.

The specific data used to calculate the Dixon Ratio values, and the crevice pressure ratio values come from the data presented in Table 1 and Table 2 of the White Paper. The data in Table 1 and Table 2 were then adjusted using one of the crevice pressure model approaches described in the White Paper on page 8 and page 9 of the originally submitted White Paper. The different model approaches are:

a,c,e

See Figure 4 and Figure 5 in the White Paper for plots of the different model results during NOP and SLB conditions (provided below for convenience).

Table 1 Crevice Pressure Specimen Data from Steady State NOP Conditions

a,c,e

Table 2 Crevice Pressure Specimen Data from Steady State SLB Conditions

a,c,e

a,c,e

Figure 4 Plot of Crevice Pressure Model Comparisons using average test data results for the normal operating condition. (Ref. original White Paper)

Figure 5 Plot of Crevice Pressure Model Comparisons using average test data results for the SLB accident condition. (Ref. original White Paper)

Model 1 was determined to be the limiting approach to using the crevice pressure data. The results shown in Table 3 and Table 4 of the original White Paper, were obtained from the following data sets.

Table 26-1 Data Set for Calculating the Dixon Ratio Test NOP Results Using Model 1

a,c,e

Table 26-2 Data Set for Calculating the Dixon Ratio Test NOP Results Using Model 2

a,c,e

Table 26-3 Data Set for Calculating the Dixon Ratio Test NOP Results Using Model 3

a,c,e

Table 26-4 Data Set for Calculating the Dixon Ratio Test SLB Results Using Model 1

a,c,e

Table 26-5 Data Set for Calculating the Dixon Ratio Test SLB Results Using Model 2

a,c,e

Table 26-6 Data Set for Calculating the Dixon Ratio Test SLB Results Using Model 3

a,c,e

Note that the values of the depth ratio for each data set will change based on the assumptions of how the crevice pressure test data is used in the model (See Figure 4 and Figure 5, from the White Paper, above). No confidence limit or scaling on the data are used prior to the Dixon ratio test analysis because lowering the data would produce a less conservative result. Taking the values from the top of the tubesheet, the values associated with a depth ratio of 0.94 and 1.00 in Model 1 and 0.40 and 1.00 in Model 2 and Model 3, and putting them in rank order gives the results in the Table 26-7 and Table 26-8.

Table 26-7 Rank Ordered Data Set for NOP Condition a,c,e

Table 26-8 Rank Ordered Data Set for SLB Condition a,c,e

The equation used to calculate the Dixon Ratio test value for a data set changes based on the size of the data population and whether the higher or lower values are suspect. In this context it is desirable to remove the lowest crevice pressure ratio values because the lower the crevice pressure ratio the larger the difference in pressure between the primary and secondary side pressures. The equation for determining the Dixon ratio test value for the NOP case is:

$$\tau = \frac{x_2 - x_1}{x_n - x_1}$$

Where τ is the Dixon ratio test value, x_n refers to the largest value in the data set, x_2 refers to the second lowest value in the data set and x_1 refers to the lowest value in the data set. The equation for determining the Dixon ratio test value for the SLB case is:

$$\tau = \frac{x_3 - x_1}{x_{n-1} - x_1}$$

Where x_3 refers to the third lowest ranked value in the data set and x_{n-1} refers to the second largest value in the data set. Calculating the Dixon ratio test values yield the results shown in Table 26-9 and Table 26-10 below (also shown in the White Paper as Table 3 and Table 4).

Table 26-9 Comparison of Dixon Ratio Test Values for NOP

a,c,e

Table 26-10 Comparison of Dixon Ratio Test Values for SLB

a,c,e

The results in Table 26-9 and Table 26-10 were used to determine which crevice pressure model was the most limiting with respect to the NOP and SLB conditions. The NOP results indicated that data values in the neighborhood of x_1 ($x \sim 0.35$) were potential outliers. These values were removed from further consideration in all of the models for the NOP data sets as shown in Table 26-7 in the bold type font. The SLB results were more varied than the NOP results, so a conservative limit of twice τ (2τ) was used to determine which values in the data sets could be potential outliers. Applying these criteria to the data in Model 1 removed the lowest six data points from further consideration (as shown in the bold type font in Table 26-8. The data in Model 2 was determined to be entirely non-conservative because a limit of twice τ suggested that all of the data was a potential low value outlier. Further consideration of Model 2 was performed for the sake of consistency only. Applying the criteria to Model 3 showed that none of the data in the set was a potential outlier. The remaining data sets for Model 1, Model 2 and Model 3 were then used to calculate the average and median values using different assumptions. The summary of the calculations is provided in Table 5 of the White Paper, reprinted below for convenience.

Table 5 Limiting Crevice Pressure Ratios from 3 Models (Ref. White Paper)

a,c,e

[redacted]

The "Total Set" results refer to using the entire data set (e.g., all of the data in the column for each model) in Table 26-1 through Table 26-6. The "Included" results refer to using all of the available data (shown in bold and plain type font) in the columns in Table 26-7 and Table 26-8. The "Excluded" results refer to using only the non-bold data in Table 26-7 and Table 26-8. The conclusion of the limiting crevice pressure analysis shown in Table 6 of the White Paper proves that Model 1, Median Outlier Excluded, gives the most conservative and appropriate result for both the NOP and SLB conditions, i.e., the values of both H* and B* are maximized.

27. *Reference 2, Enclosure 1, Attachment 1 - In Table 5 under the heading of outliers, rows 1 and 2 refer to "total set," whereas lines 3 and 4 refer to "included." Does "included" mean the same thing as "total set." If not, how does it differ from "total set," and how does it differ from "excluded?"*

Response to RAI No. 27:

Please refer to the Response to RAI No. 26 as well.

The terms in Table 5 of the White Paper refer to:

- 1) The mean of the entire data set and the median of the entire data set (Total Set), 2) a skewed mean and median (Included), and 3) a skewed mean and median with potential data outliers removed (Excluded).

- The description "total set" refers to calculating the limiting crevice pressure ratio using the entire set of crevice pressure ratio data (from the bottom of the tubesheet to the top of the tubesheet). This title refers to items 1 and 2 above.

  - The description "included" refers to calculating the limiting crevice pressure ratio using the entire set of data from the last two data points nearest the top of the tubesheet. None of the outliers that could potentially skew the limiting crevice pressure result to a lower, and less conservative value, are eliminated from consideration. This title refers to item 2 above.

  - The description "excluded" refers to calculating the limiting crevice pressure ratio using the set of data from the top of the tubesheet, in the same fashion as the "included" data set, but with any potential outliers removed to obtain the most conservative result. The outliers are determined using Dixon's ratio test. This title refers to item 3 above.

  - The term "skewed" in this context refers to the bias in the data selection, that is, for the Excluded and Included analysis taking only the data from the upper portion of the samples. The term skewed should not be confused with the statistical implication of a skewed distribution.

28. *Reference 2, Enclosure 1, Attachment 1 - Provide a step-by-step description (including an example) of how the values in Table 5 were obtained.*

Response to RAI No. 28:

- The method for calculating the results in Table 5 is contained in Appendix A of Enclosure I to WCNOC letter WO 07-0012.

- A detailed example of how the values in Table 5 were calculated is provided in the response to RAI No. 26.

29. *Reference 2, Enclosure 1, Attachment 1 - Confirm that the "unaltered" case in Table 5 reflects the use of the improved tubesheet/divider plate model with a "divider plate factor" of 0.399.*

Response to RAI No. 29:

- The unaltered case is listed in Table 6 of the White Paper, which compares the various B* and H* depths
- The results in Table 6 reflect the crevice pressure results in Table 5 of the White Paper.
- The divider plate factor, and the divider plate, does not influence the results given in Table 5.
- As stated on Page 16 of the White Paper (Appendix A of Enclosure I to WCNOC letter WO 07-0012) the "Unaltered" case listed in Table 6 uses a divider plate factor of 0.399. Note that the current recommendation is to use a divider plate factor of 0.64, which conservatively removes the portion of the divider plate and welds that has been shown to exhibit cracking in some foreign steam generators.

APPENDIX A

STD-MC-06-11, Rev. 1

Pressure Profile Measurements During Tube-to-Tubesheet Leakage Tests of Hydraulically Expanded Steam Generator Tubing

August 30, 2007

STD-MC-06-11-NP, Rev. 1

Pressure Profile Measurements During Tube-to-Tubesheet Leakage Tests of Hydraulically Expanded Steam Generator Tubing

August 2007

Richard J. Jacko

Westinghouse Electric Co. LLC
Science and Technology Department
Pittsburgh, PA

*Electronically approved records are authenticated in the electronic document management system.

Westinghouse Electric Company LLC
P.O. Box 355
Pittsburgh, PA 15230-0355

Table of Contents

Table of Contents (cont.)

PAGE

LIST OF TABLES

PAGE

LIST OF FIGURES

LIST OF FIGURES (cont.)

LIST OF FIGURES (cont.)

LIST OF FIGURES (cont.)

LIST OF FIGURES (cont.)

PAGE

1 PURPOSE

This report describes the results of an experimental test program to determine the pressure profile within a steam generator tube-to-tubesheet crevice under leakage conditions. For this program, the tube-to-tubesheet joint of tubes were hydraulically expanded into simulated tubesheet collars that model the tubesheets of Westinghouse-designed steam generators. This test program was designed to collect empirical pressure profile and leakage data. The testing was performed in accordance with the test prospectus described in TP-SGDA-04-6 entitled, "Steam Generator Tubesheet Crevice Pressure Profile Testing" [10].

2 REFERENCES

1. WP-4.22, Revision 7, Field Service – Qualification and Functional Testing.

2. WP-4.18, Revision 3, Test Control.

3. WP-11.1, Revision 3, Control of Inspection, Measuring and Test Equipment.

4. WEC 23.11, Revision 0, Science and Technology Department/Nuclear Services, SQS Interface Agreement.

5. ASME Steam Tables, Properties of Steam and Water using the 1967 IPC formulation for Industrial Use, ASME, 1993.

6. Westinghouse Drawing 1B81396, latest revision, "D5 Tube Leakage Test Specimens, Final Assembly, 3", 6", 9" and 12" Hydraulically Expanded Samples".

7. Westinghouse Drawing 1B81387, latest revision, "D5 Tube Leakage Test Specimens 9 inch and 12 inch Hydraulic Expansions and Part Details".

8. Westinghouse Data Package, STD-DP-1997-8015.

9. Westinghouse STD Letter Report STD-MCE-03-49, A. Pearce and M. Nagle, Determination of Model D5 Tube-to-Tubesheet Leakage Resistance for H-Star Program for CBE/CDE/DDP/TCX.

10. TP-SGDA-04-6, "Steam Generator Tubesheet Crevice Pressure Profile Testing", 2/9/2005.

11. "PROPERTIES OF STEAM & WATER using the 1967 IFC FORMULATION FOR INDUSTRIAL USE and other IAPWS releases", 1992, AMERICAN SOCIETY OF MECHANICAL ENGINEERS

3 BACKGROUND

Relatively little work has been done to determine leak rates past a simulated tube-to-tubesheet joint made by hydraulic expansion. Due to the excellent stress corrosion cracking performance of hydraulically expanded steam generator tubing, there has been little driving force to fully characterize the result of through-wall defects. However, changes in mandated inspection practices have required utilities to perform time-intensive inspections to the lower portions of steam generator tubes. Defects in this lower region will not leak substantially, because leakage will be constrained by flow through the hydraulic expansion crevice. One reason for performing leak rate tests on this configuration is to be able to understand and model the processes involved so that realistic predictions of leak rates during normal operation and accident conditions can be calculated. If the calculated rates are appropriately small, the hope is that some of the time-intensive inspections can be reduced.

In 1997, leak rate testing of hydraulically expanded joints was reported in STD-DP-1997-8015 [8]. Another program was performed in 2003 and reported in STD-MCE-03-49 [9] by Pearce. Both tests appeared to raise some questions regarding corrosion in the gap between the expanded steam generator tubing and the simulated steel tubesheet material. The 1997 tests were performed in a small dedicated rig using deaerated water. The 2003 tests were done in an autoclave and used hydrogenated primary water. This autoclave testing applied appropriate primary and secondary side conditions to determine the leak rates across a simulated through-wall crack. Additional efforts were spent to obtain and maintain prototypic oxides on the test specimen surfaces in the testing performed in 2003 and beyond.

Still basic questions remained from these tests regarding the nature of the flow in the hydraulically expanded, tube-to-tubesheet crevice. It was not known whether most of the flow in the crevice was mostly water, mostly steam or a two-phase, water/steam mixture. The goal of this work was to instrument test samples with pressure taps along the steam generator crevice to determine the phase of the fluid at various points along the expansion. This information should assist in the ability to model the phenomena.

4 EXPERIMENTAL DESCRIPTION

4.1 TEST CONCEPT

The goal of this testing was to determine the pressure distribution in a hydraulically expanded, steam generator tube-to-tubesheet crevice during situations where there could be primary-to-secondary leakage through cracks present within the tubesheet crevice. During the testing, primary water flowed through artificial through-wall defects machined into the tube and entered the tight, hydraulically-expanded crevice and eventually flowed to the top of the crevice where it mixed with the simulated secondary-side environment. During this period of time, pressure was monitored at five different locations within the tube-to-tubesheet crevice. Pressure was also monitored at primary-side and secondary-side positions. The main goal of the experiments was to determine where in the crevice the leaking primary water flashed to steam. The volume expansion and flow characteristics of the two-phase water and steam mixtures are much different than those of single phase water. Therefore, an accurate model of steam generator tube leakage can only be determined if the position where the leakage changes from single phase water to two phase (water + steam) is known. This information is needed to model leak rates at these locations during both normal operation and accident conditions.

The test specimens were designed to meet plant conditions for Westinghouse-designed Model D-5 steam generators for Alloy 600 tubes that have simulated through-wall defects per Reference 7. The specimens are simulated steam generator tube-to-tubesheet joints where the tube is hydraulically expanded into a low alloy steel collar that simulates the constraint offered by the steam generator tubesheet. The collar is thick enough to simulate both the thermal and the mechanical properties of the tubesheet in a steam generator. One-eighth inch holes were drilled through-wall at the bottom of the tube to simulate through wall SCC cracks. This was done so that the crack geometry would not limit the pressure drop in the steam generator crevice. These through-wall defects allow pressurized primary water to flow into the annulus between the tube and the simulated tubesheet collar.

Figure 4-1 shows the drawing of the modifications made to the existing leak rate specimens to accommodate the pressure taps. Four pressure taps were located along a given circumferential orientation on the specimen. The fifth tap was located 180° away from the other four pressure taps. Small stainless steel pressure lines, 0.125 inch OD were brazed into the holes leading to the pressure taps at the tube-to-tubesheet joint as shown in Figure 4-2 for specimens numbered 7 and 8 used for these tests. Note that these two specimens had been tested in previous leak rate programs and background data exists.

a,c,e

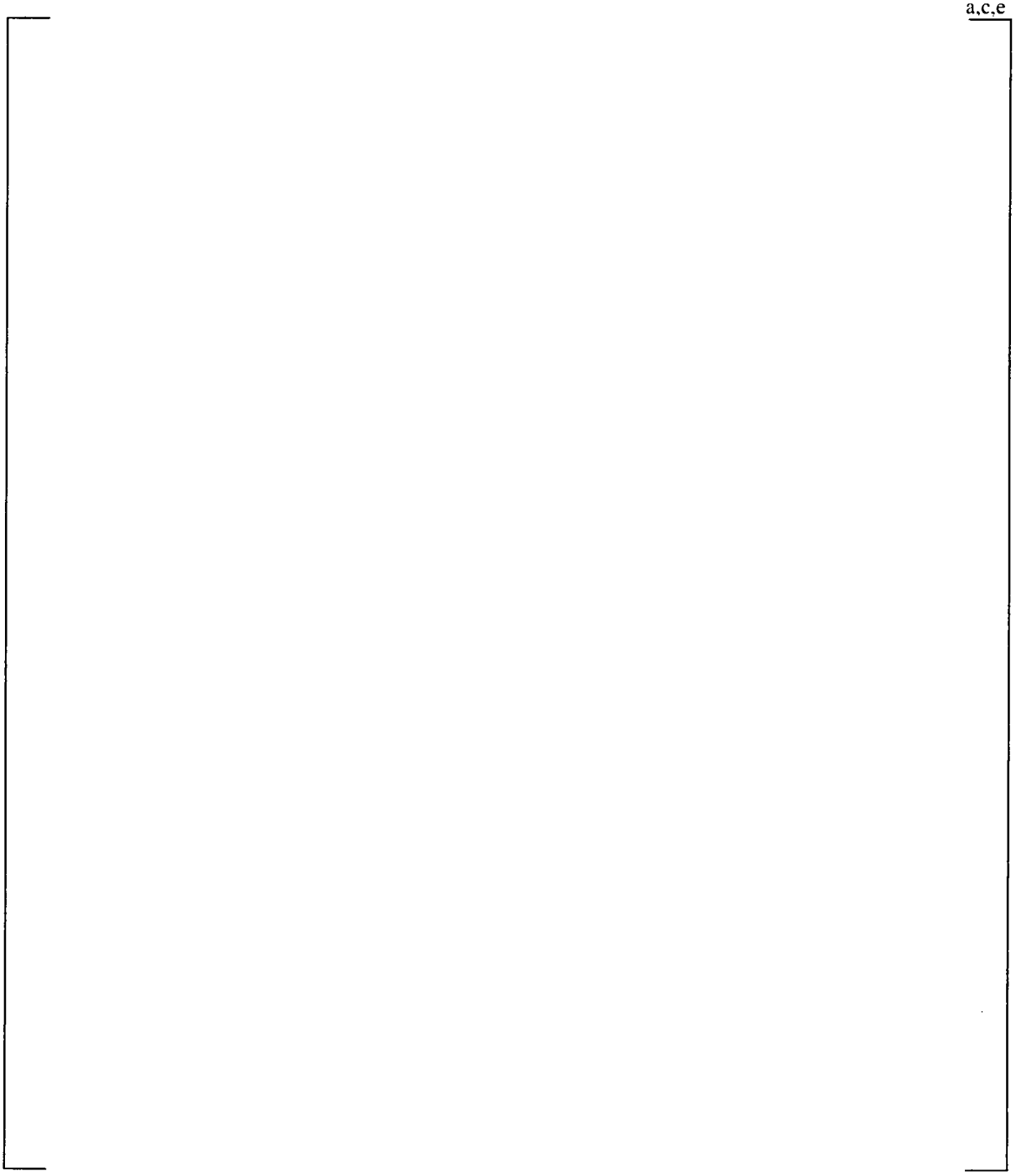

Figure 4-1 Drawing showing modifications to leak rate specimens 7 and 8 to install pressure taps in the tube-to-tubesheet crevice

a,c,e

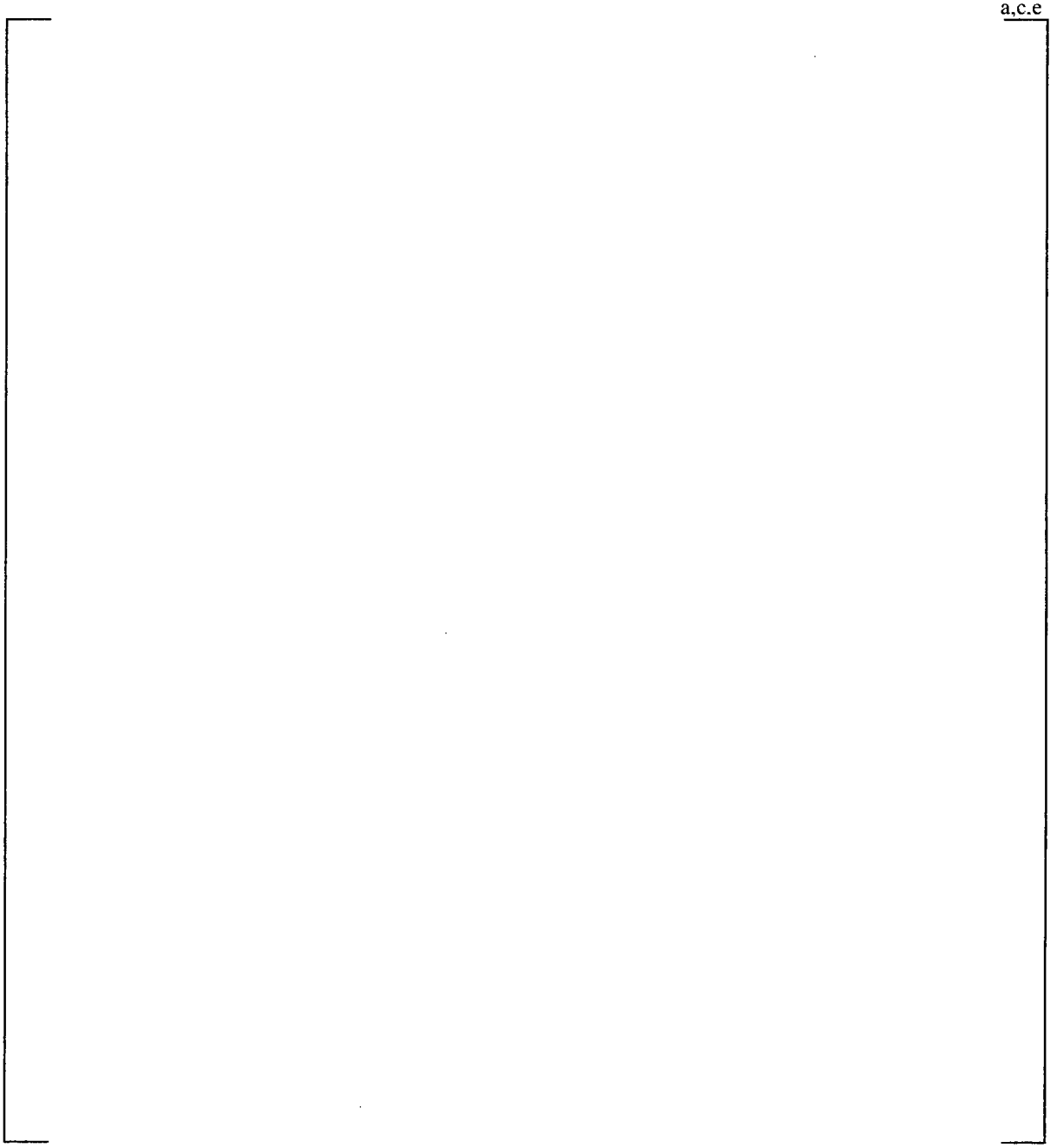

Figure 4-2 Photographs of specimens 7 and 8 with pressure tap lines brazed in place

4.2 TEST FACILITY

Figure 4-3 shows a schematic of the details of the testing facility. The facility operated in a slightly different manner depending on what type of leak rate test was being performed. Four different types of leak rate tests were performed during the course of this testing:

- Room Temperature Leak Rate Testing
- Elevated Temperature, Normal Operation Leak Rate Testing – primary water to superheated steam
- Elevated Temperature, Normal Operation Leak Rate Testing – primary water to pressurized water (single phase)
- Elevated Temperature, Accident Condition Leak Rate Testing – primary water to low pressure steam

For the room temperature tests, the test equipment consisted of [

]^{a,c,e}

The equipment used for high temperature tests is shown in Figure 4-4. For these tests, the specimen was contained in a [

]^{a,c,e}

For the normal operation tests, the leakage was calculated based on changes in [

]^{a,c,e}

[

]a,c,e

[

]a,c,e

Figure 4-5 shows the final specimen arrangement for the room temperature tests. [

]a,c,e

a,c,e

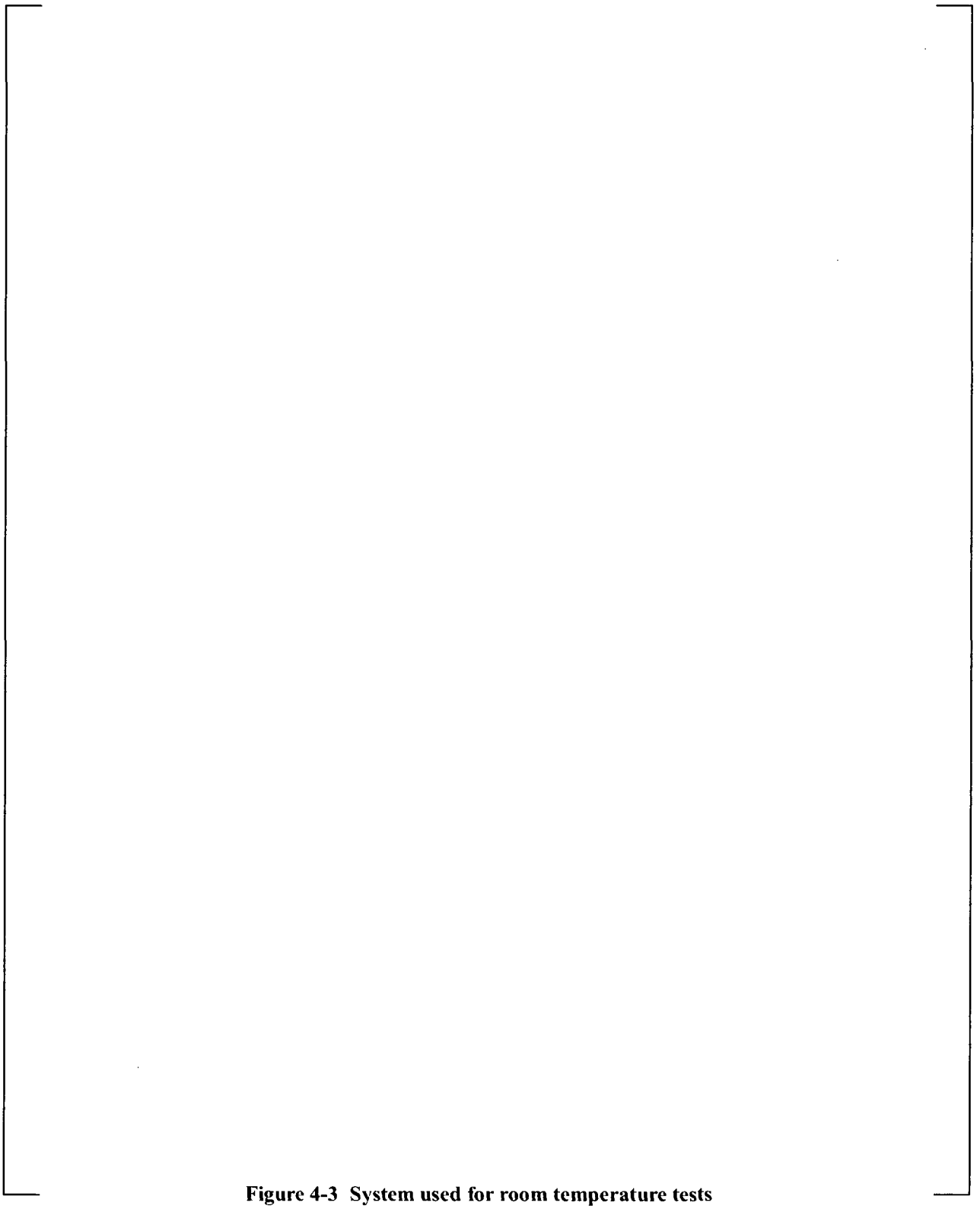

Figure 4-3 System used for room temperature tests

a,c,e

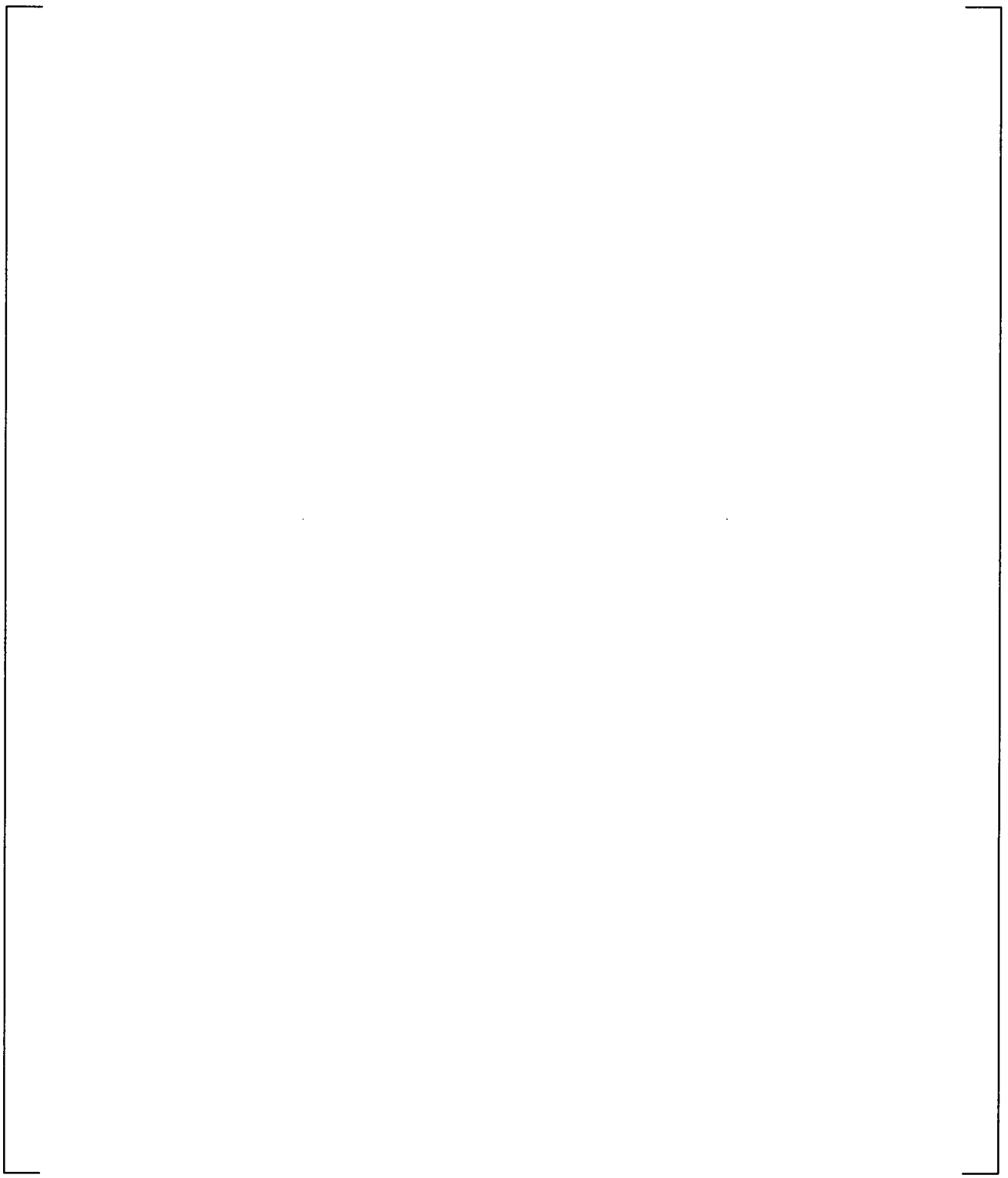

Figure 4-4 System used for high temperature tests

a,c,e

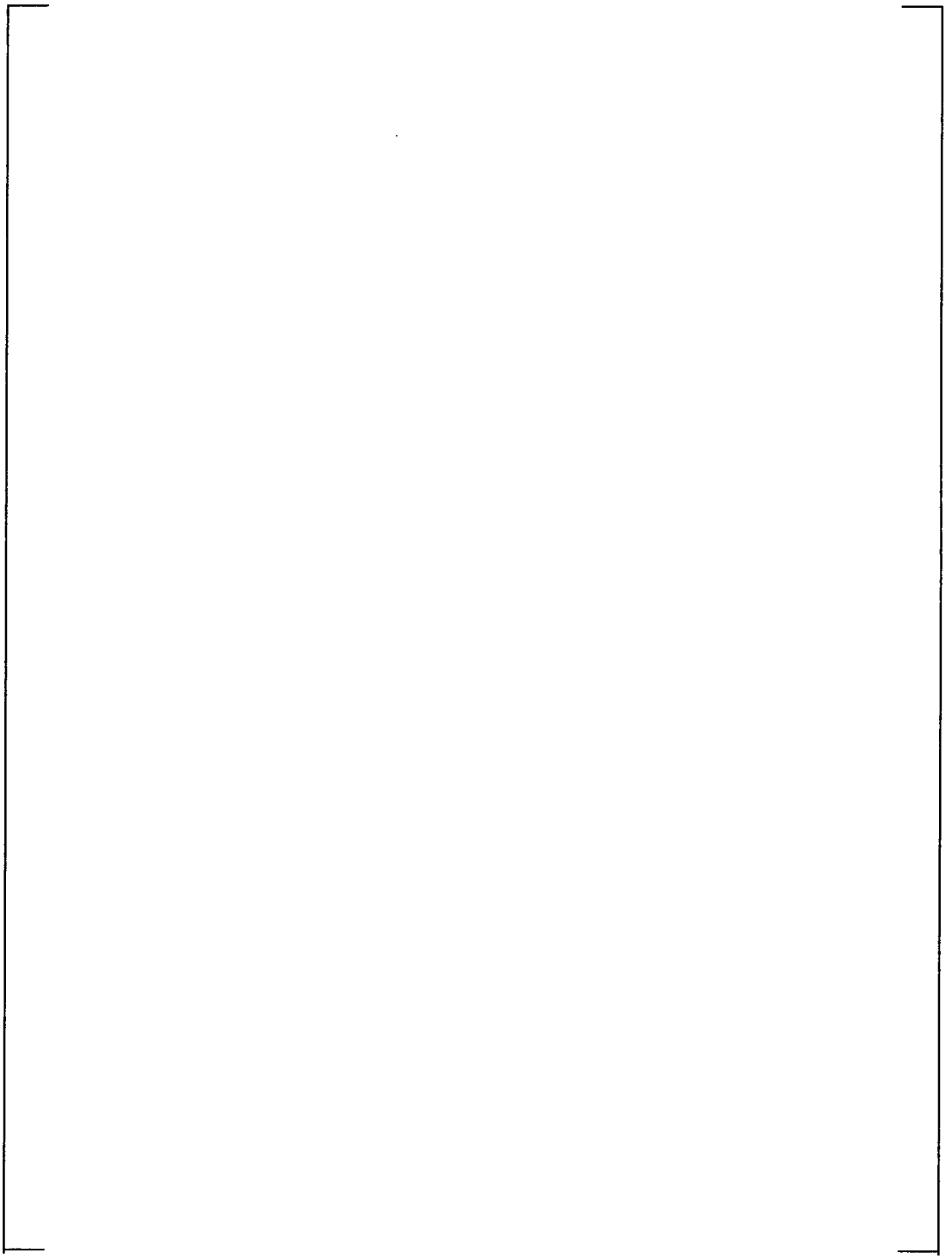

Figure 4-5 Final test specimen arrangement for room temperature leak rate tests

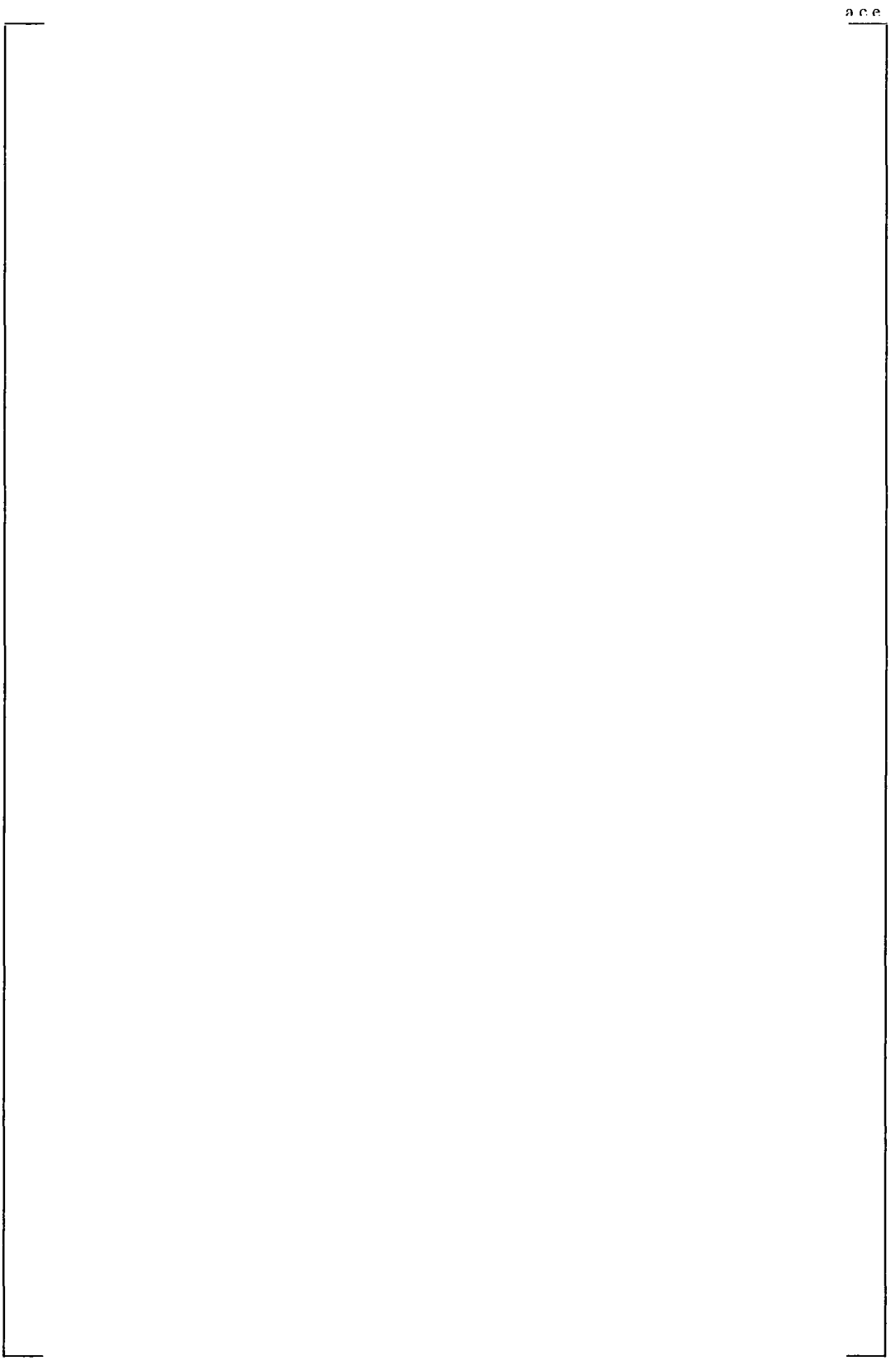

Figure 4-6 Initial, unsuccessful test specimen arrangement for room temperature leak rate tests

Figure 4-7 shows an autoclave used for the high temperature tests. [

]^{a,c,e}

Figure 4-8 shows two images of the arrangement for the high temperature tests. [

]^{a,c,e}

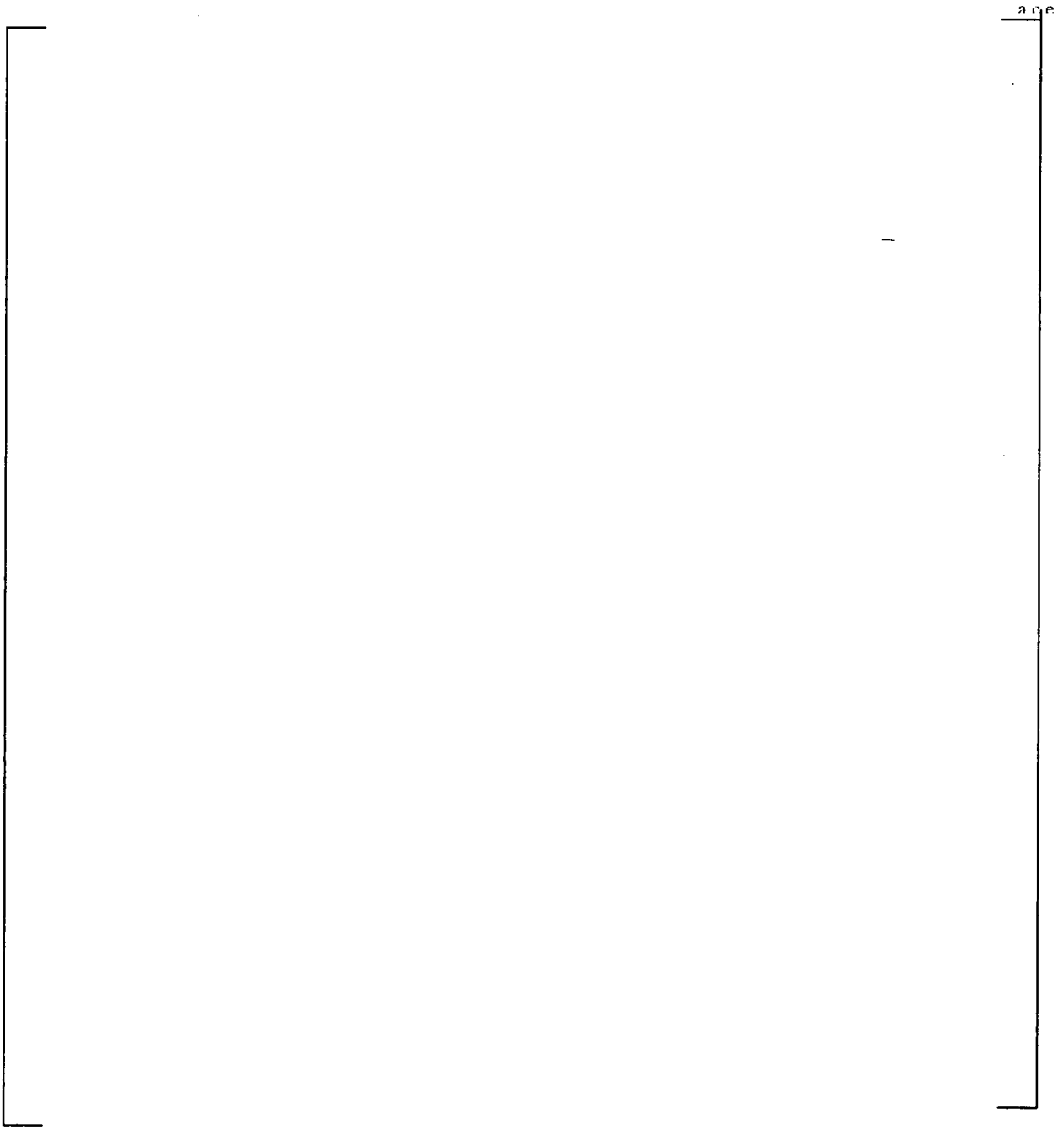

Figure 4-7 Image of the test autoclave used for the elevated temperature leak rate tests at STD.
[

]^{a,c,e}

a,c,e

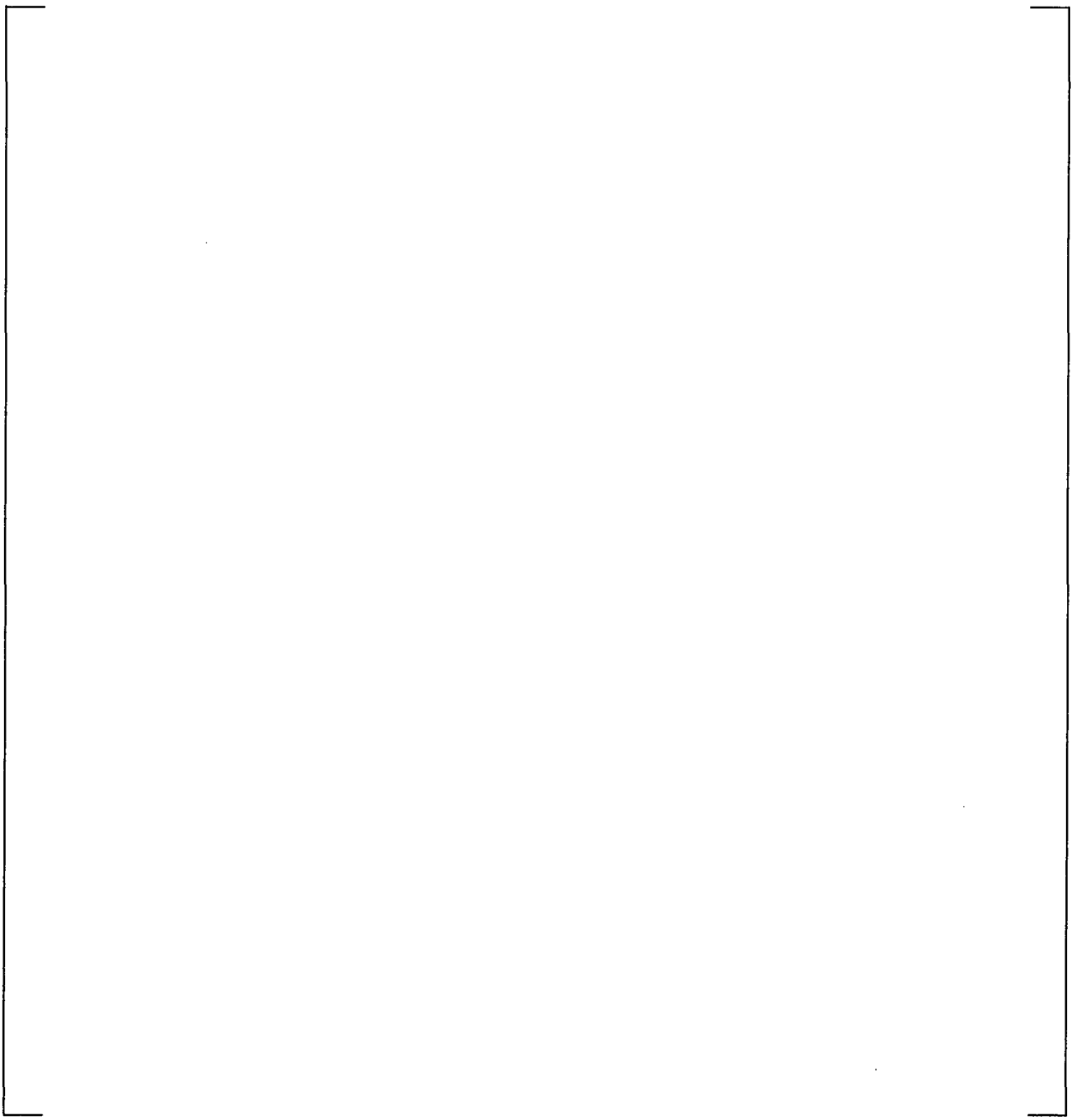

Figure 4-8 Test specimen is placed in a carbon steel cylinder that is attached to the autoclave head. [

]a,c,e

5 OUTLINE OF TEST PROCEDURE

The detailed test procedure used for these leak rate tests is listed in Westinghouse Science and Technology Department procedure MCT-147. Some additional details are listed below.

5.1 Specimen Conditioning

The test plan required that the oxides that form on the steel and Alloy 600 surfaces are typical of those that form under reducing PWR steam generator conditions. The test specimens were conditioned in a prototypic PWR environment prior to testing. The test specimens were fabricated using low alloy steels, nickel-based alloy tubing and stainless steel fittings. The corrosion resistances of these materials are quite different in high temperature water. [

]^{a,c,e}

5.2 Primary Water with Dissolved H_2

Simulated primary-side water was used during the leak rate testing. [

]^{a,c,e}

[

]a,c,e

5.3 Provisions to Minimize Corrosion

Because of the low alloy steel materials used in the specimen fabrication and the PWR steam generator, the specimens will be subject to corrosion when wet at room temperature. Any corrosion films that form on the outside of the specimen probably have no consequence on leak rates measured; however, corrosion products that form in the annulus between the inside of the low alloy steel cylinder and the external tube surface will directly influence the leak rates measured. For this reason, it is necessary to take efforts to minimize the presence of water and moisture

- prior to testing
- between test sequences and
- after testing.

To help minimize the presence of water or water vapor in the annulus between the low alloy steel cylinder and the nickel alloy tube, the tube specimens were [

]a,c,e

5.4 Summary of Different Types of Leak Rate Test Procedures

5.4.1 Room Temperature Leak Rate Testing

For room temperature leak rate testing, the flow configuration was previously described. The specimen is connected to the primary water source and the pressure accumulator. The specimen is [

]a,c,e

5.4.2 Elevated Temperature Normal Operation Leak Rate Testing – Primary Water to Superheated Steam

Previous testing indicated that using the [

]^{a,c,e}

The first step in this calculation process was to [

]^{a,c,e}

For normal operation tests, the leak rate was calculated based on [

]^{a,c,e}

Table 5-1 Density of Superheated Steam at Typical Test Conditions

P	P			Steam Density as f(Temperature, Pressure)								
psig	psia				Density in (grams/cm^3)					Temp. (deg F)		
		575	580	585	590	595	600	605	610	615	620	625
780	795	0.02457	0.02434	0.02412	0.02390	0.02369	0.02349	0.02329	0.02310	0.02292	0.02273	0.02256
790	805	0.02496	0.02472	0.02449	0.02427	0.02405	0.02385	0.02364	0.02345	0.02326	0.02307	0.02289
800	815	0.02534	0.02510	0.02486	0.02464	0.02442	0.02420	0.02400	0.02379	0.02360	0.02341	0.02322
810	825	0.02573	0.02548	0.02524	0.02500	0.02478	0.02456	0.02435	0.02414	0.02394	0.02375	0.02356
820	835	0.02612	0.02586	0.02562	0.02538	0.02514	0.02492	0.02470	0.02449	0.02429	0.02409	0.02390
830	845	0.02651	0.02625	0.02600	0.02575	0.02551	0.02528	0.02506	0.02485	0.02464	0.02443	0.02423
840	855	0.02691	0.02664	0.02638	0.02613	0.02588	0.02565	0.02542	0.02520	0.02499	0.02478	0.02457
850	865	0.02731	0.02703	0.02676	0.02651	0.02626	0.02602	0.02578	0.02556	0.02534	0.02512	0.02492
860	875	0.02771	0.02743	0.02715	0.02689	0.02663	0.02638	0.02615	0.02591	0.02569	0.02547	0.02526
870	885	0.02812	0.02782	0.02754	0.02727	0.02701	0.02676	0.02651	0.02627	0.02604	0.02582	0.02561
880	895	0.02852	0.02822	0.02794	0.02766	0.02739	0.02713	0.02688	0.02664	0.02640	0.02617	0.02595
890	905	0.02894	0.02863	0.02833	0.02805	0.02777	0.02751	0.02725	0.02700	0.02676	0.02653	0.02630
900	915	0.02935	0.02904	0.02873	0.02844	0.02816	0.02789	0.02762	0.02737	0.02712	0.02688	0.02665
910	925	0.02977	0.02945	0.02913	0.02883	0.02854	0.02827	0.02800	0.02774	0.02749	0.02724	0.02701
920	935	0.03019	0.02986	0.02954	0.02923	0.02894	0.02865	0.02837	0.02811	0.02785	0.02760	0.02736
930	945	0.03062	0.03028	0.02995	0.02963	0.02933	0.02904	0.02875	0.02848	0.02822	0.02796	0.02772
940	955	0.03105	0.03070	0.03036	0.03004	0.02972	0.02943	0.02914	0.02886	0.02859	0.02833	0.02808
950	965	0.03148	0.03112	0.03077	0.03044	0.03012	0.02982	0.02952	0.02924	0.02896	0.02869	0.02844
960	975	0.03192	0.03155	0.03119	0.03085	0.03053	0.03021	0.02991	0.02962	0.02933	0.02906	0.02880
970	985	0.03236	0.03198	0.03161	0.03126	0.03093	0.03061	0.03030	0.03000	0.02971	0.02943	0.02916
980	995	0.03280	0.03241	0.03204	0.03168	0.03134	0.03101	0.03069	0.03038	0.03009	0.02980	0.02953
990	1005	0.03325	0.03285	0.03247	0.03210	0.03175	0.03141	0.03109	0.03077	0.03047	0.03018	0.02990
1000	1015	0.03371	0.03329	0.03290	0.03252	0.03216	0.03182	0.03148	0.03116	0.03085	0.03056	0.03027
1010	1025	0.03417	0.03374	0.03334	0.03295	0.03258	0.03222	0.03188	0.03156	0.03124	0.03094	0.03064
1020	1035	0.03463	0.03419	0.03378	0.03338	0.03300	0.03264	0.03229	0.03195	0.03163	0.03132	0.03102
1030	1045	0.03510	0.03465	0.03422	0.03381	0.03342	0.03305	0.03269	0.03235	0.03202	0.03170	0.03139
1040	1055	0.03557	0.03511	0.03467	0.03425	0.03385	0.03347	0.03310	0.03275	0.03241	0.03209	0.03177
1050	1065	0.03604	0.03557	0.03512	0.03469	0.03428	0.03389	0.03351	0.03315	0.03281	0.03248	0.03216
1060	1075	0.03652	0.03604	0.03557	0.03513	0.03471	0.03431	0.03393	0.03356	0.03321	0.03287	0.03254
1070	1085	0.03701	0.03651	0.03603	0.03558	0.03515	0.03474	0.03435	0.03397	0.03361	0.03326	0.03293
1080	1095	0.03750	0.03699	0.03650	0.03603	0.03559	0.03517	0.03477	0.03438	0.03401	0.03366	0.03332
1090	1105	0.03800	0.03747	0.03697	0.03649	0.03604	0.03561	0.03519	0.03480	0.03442	0.03406	0.03371
1100	1115	0.03850	0.03796	0.03744	0.03695	0.03649	0.03604	0.03562	0.03522	0.03483	0.03446	0.03410
1110	1125	0.03901	0.03845	0.03792	0.03742	0.03694	0.03649	0.03605	0.03564	0.03524	0.03486	0.03450
1120	1135	0.03953	0.03895	0.03840	0.03789	0.03740	0.03693	0.03649	0.03606	0.03566	0.03527	0.03490
1130	1145	0.04005	0.03945	0.03889	0.03836	0.03786	0.03738	0.03693	0.03649	0.03608	0.03568	0.03530
1140	1155	0.04057	0.03996	0.03938	0.03884	0.03832	0.03783	0.03737	0.03692	0.03650	0.03609	0.03570
1150	1165	0.04111	0.04048	0.03988	0.03932	0.03879	0.03829	0.03781	0.03736	0.03693	0.03651	0.03611
1160	1175	0.04165	0.04100	0.04039	0.03981	0.03927	0.03875	0.03826	0.03780	0.03735	0.03693	0.03652
1170	1185	0.04220	0.04152	0.04090	0.04030	0.03975	0.03922	0.03872	0.03824	0.03779	0.03735	0.03694
1180	1195	0.04275	0.04206	0.04141	0.04080	0.04023	0.03969	0.03917	0.03869	0.03822	0.03778	0.03735
1190	1205	0.04331	0.04260	0.04193	0.04131	0.04072	0.04016	0.03964	0.03914	0.03866	0.03820	0.03777
1200	1215	0.04388	0.04315	0.04246	0.04182	0.04121	0.04064	0.04010	0.03959	0.03910	0.03864	0.03819
1210	1225	0.04446	0.04370	0.04299	0.04233	0.04171	0.04112	0.04057	0.04005	0.03955	0.03907	0.03862
1220	1235	0.04505	0.04426	0.04353	0.04285	0.04221	0.04161	0.04104	0.04051	0.04000	0.03951	0.03904
1230	1245	0.04564	0.04483	0.04408	0.04338	0.04272	0.04211	0.04152	0.04097	0.04045	0.03995	0.03948
1240	1255	0.04624	0.04541	0.04463	0.04391	0.04324	0.04260	0.04201	0.04144	0.04090	0.04039	0.03991

Table 5-2 Autoclave Inventory of Superheated Steam as a function of Temperature and Pressure [ ][a,c,e] a,b,c

5.4.3 Elevated Temperature Normal Operation Leak Rate Testing Primary Water to Pressurized Water (single phase)

Leak rates were determined with [

]^{a,c,e}

5.4.4 Elevated Temperature Accident Condition Leak Rate Testing – Primary Water to Low Pressure Steam

A similar procedure was used for analyzing leak rate tests conducted under steam line break conditions.

[

]^{a,c,e}

5.5 Test Matrix

The test matrix is shown in Table 5-3 below. NODP refers to normal operation differential pressure. SLB refers to Steam Line Break Accident Conditions. [

]^{a,c,e}

Table 5-3 The Test Matrix

a,c,e

[

]

6 RESULTS

Conditioning treatment for specimens 7 and 8 was conducted from 2/17/05 to 2/20/05 in STD autoclave Run A21R263. [

]^{a,c,e}

6.1 SPECIMEN #7

The test results for specimen 7 are presented in the order described in the test prospectus. The results are summarized in Appendix D-1. A starting and ending date and time are listed in Appendix D-1 along with information as specified in the test prospectus. An overall summary of the test conditions and leak rates are shown in Table 6-1 below.

Table 6-1 Summary of Test Conditions and Leak Rates for Specimen #7

a,b,c

Note: * denotes that leak rate determined during the last half of the final step.

Graphs showing the pressure, temperatures and leak rates are shown in Figures 6-1 through 6-14.

Specimen 7

Test Condition 1, Room Temperature, Normal Operation and Accident delta P Tests

[

]^{a,c,e}

Specimen 7

Test Condition 2, 600°F, Normal Operation Tests

This test was performed on 11-March-2005 and leak rate was determined by the change in autoclave pressure resulting from the leakage. The test records are shown in Figure 6-3. [

]^{a,c,e}

[

]a,c,e

Specimen 7

Test Condition 3, 600°F, Steam Line Break Test with a Primary Pressure of 2850 psia

This test was performed on 17-March-2005 and the leak rate measured directly by collecting the condensed steam. The target conditions were 600°F, a primary pressure of 2850 psia with atmospheric secondary pressure. [

]a,b,c

Specimen 7

Test Condition 4, 600°F, Steam Line Break Test with a Primary Pressure of 2575 psia

This test was performed on 17-March-2005 and the leak rate measured directly by collecting the condensed steam. The target conditions were 600°F, a primary pressure of 2575 psia with atmospheric secondary pressure. [

]a,b,c

Specimen 7

Test Condition 5, 420°F, Steam Line Break Test with a Primary Pressure of 2850 psia

This test was performed on 18-March-2005 and the leak rate was measured directly by collecting the condensed steam. The target conditions were 420°F and a primary pressure of 2850 psia with atmospheric secondary pressure. The data are presented in Figures 6-6 and 6-7. [

]a,b,c

[

]^{a,b,c}

This test was repeated to try to get conditions to be within the specified temperature range. The second attempt at this test is shown in Figure 6-7. The specimen temperature for this second attempt increased throughout the test. [

]^{a,b,c}

Specimen 7

Test Condition 6, 420°F, Steam Line Break Test with a Primary Pressure of 2575 psia

This test was also performed on 18-March-2005 and the leak rate was measured directly by collecting the condensed steam. The target conditions were 420°F, a primary pressure of 2575 psia with atmospheric secondary pressure. The data are presented in Figures 6-8. [

]^{a,b,c}

Specimen 7

Test Condition 7, 590°F, Steam Line Break Test with Primary Pressures of 2575 psia (7a), 2850 psia (7b) and 2900 (7c)

These tests were performed on 19-March-2005 and consisted of multiple steps each. The test records are shown in Figures 6-9, 6-10 and 6-11. [

]^{a,b,c}

[

]^{a,b,c}

Specimen 7

Test Condition 8, 420°F, Steam Line Break Test with Primary Pressures of 2575 psia (8a), 2850 psia (8b) and 1800 (8c)

[

]^{a,b,c}

[

]a,b,c

a,b,c

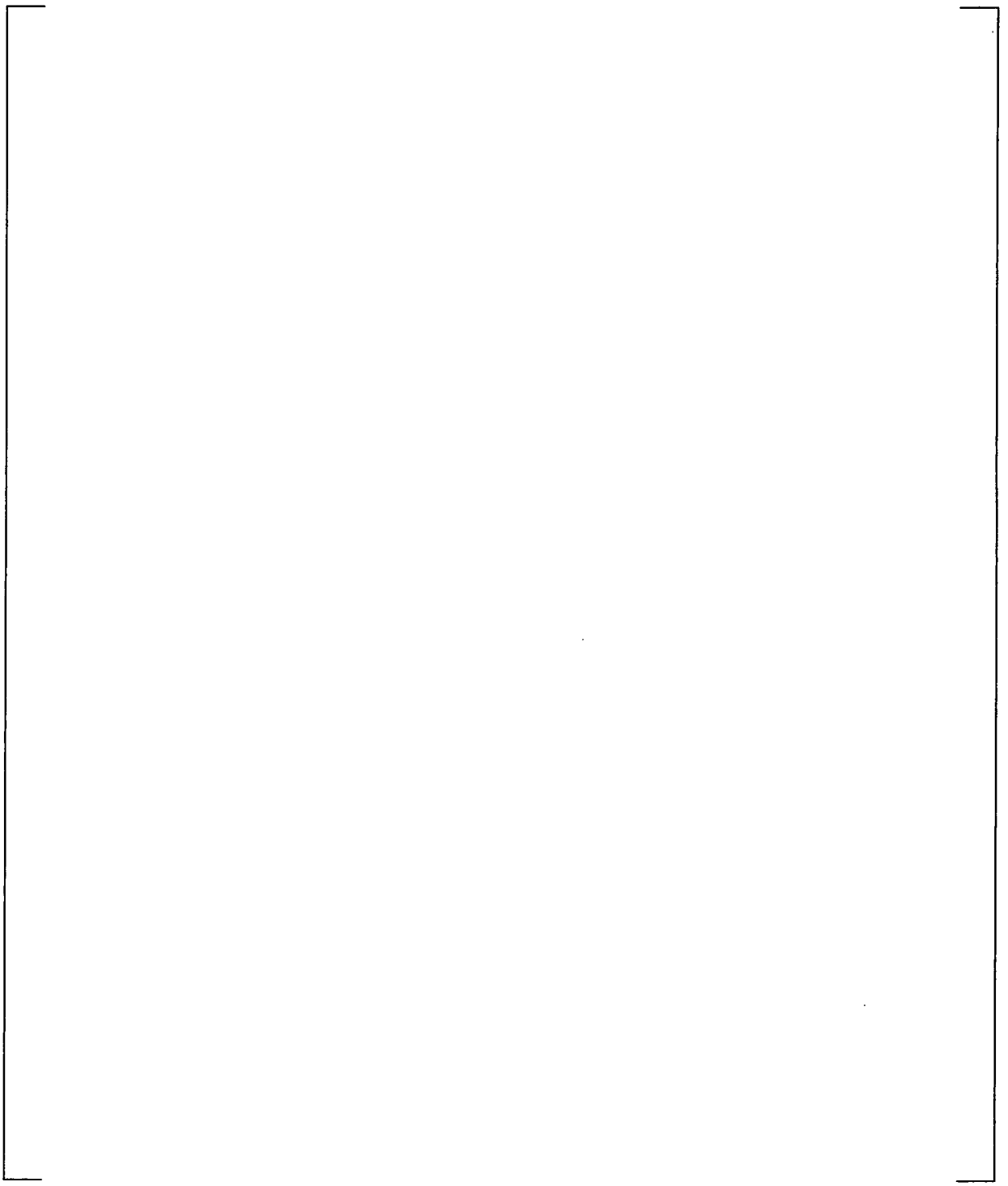

Figure 6-1 **Took approximately 30 min for all pressure tap lines to fill with fluid and pressurize. Leakage was observed after ~33 min. Leakage was steady from 33 to 59 minutes. Significant pressure drop within crevice.**

a,b,c

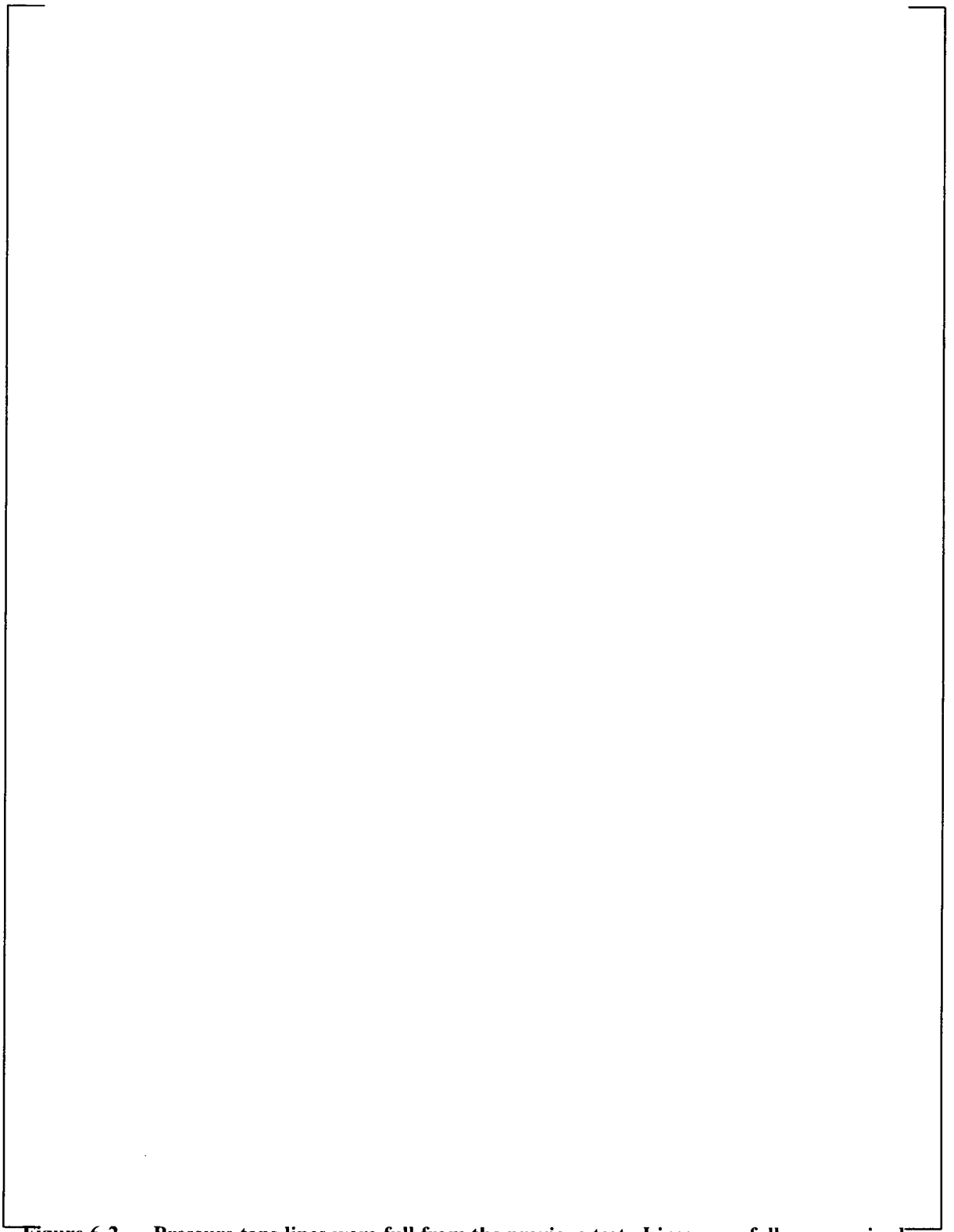

Figure 6-2 Pressure taps lines were full from the previous test. Lines were fully pressurized within 4 min. Leakage was steady from 5 to 25 minutes. Significant pressure drop within crevice.

a,b,c

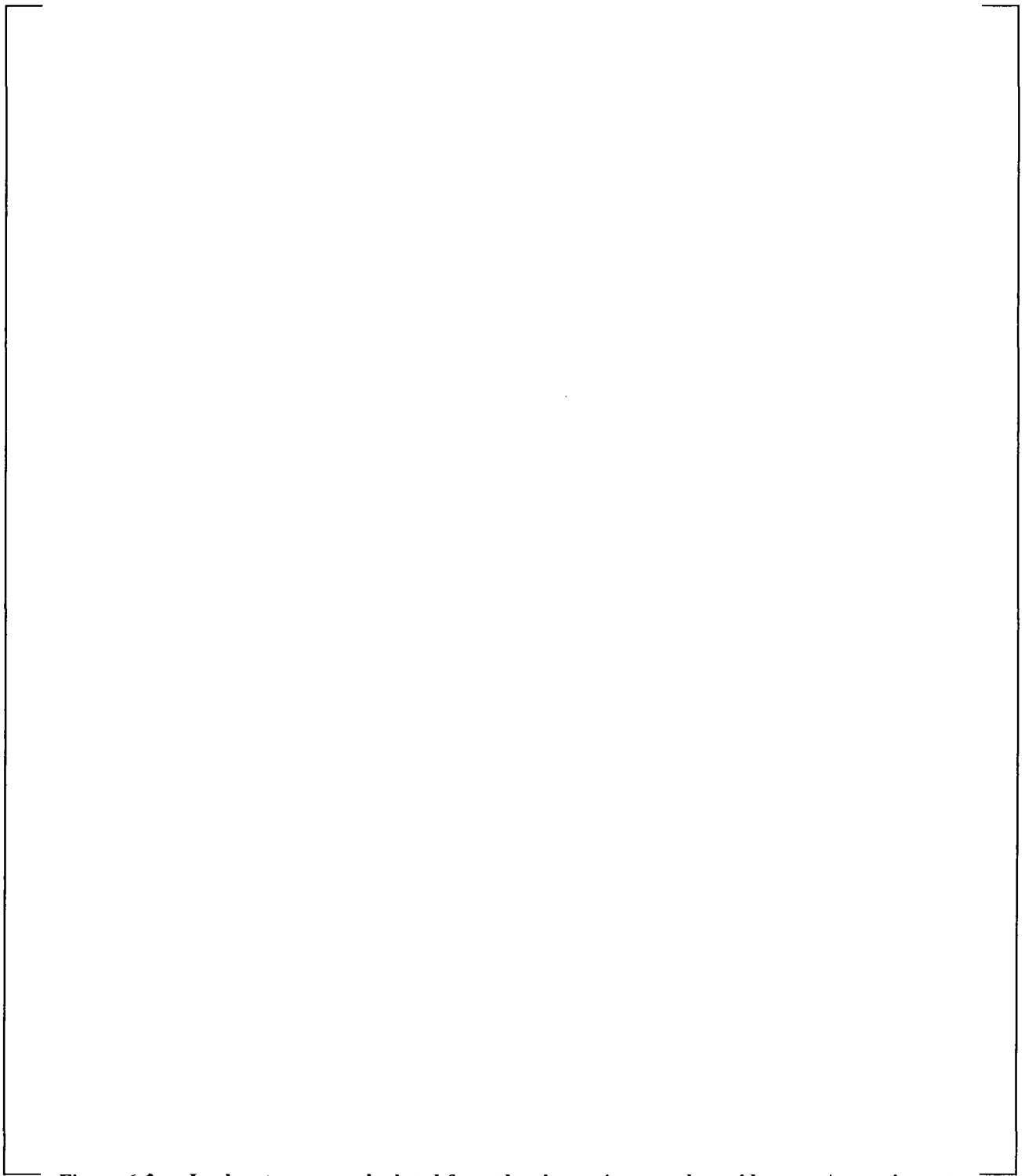

Figure 6-3 Leak rates were calculated from the change in secondary side water/steam inventory over the pressure range from 695 to 895 psia for this normal operation condition leak rate test. [

]^{a,b,c}

a,b,c

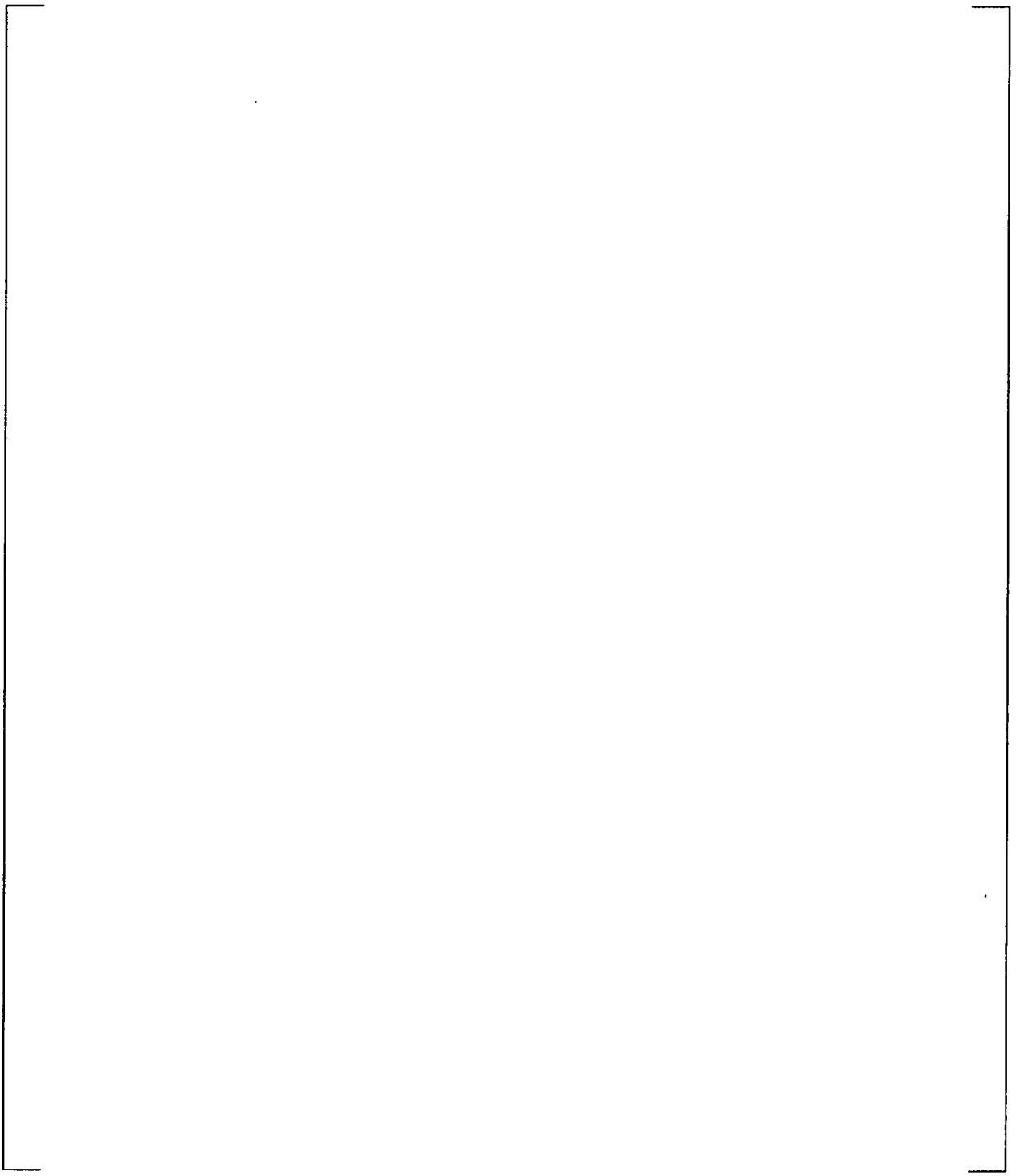

Figure 6-4 Specimen temperature exceeded the specified range after ~ 25 min. Leak rate was steady from 3 to 45 min. [

]a,b,c

a,b,c

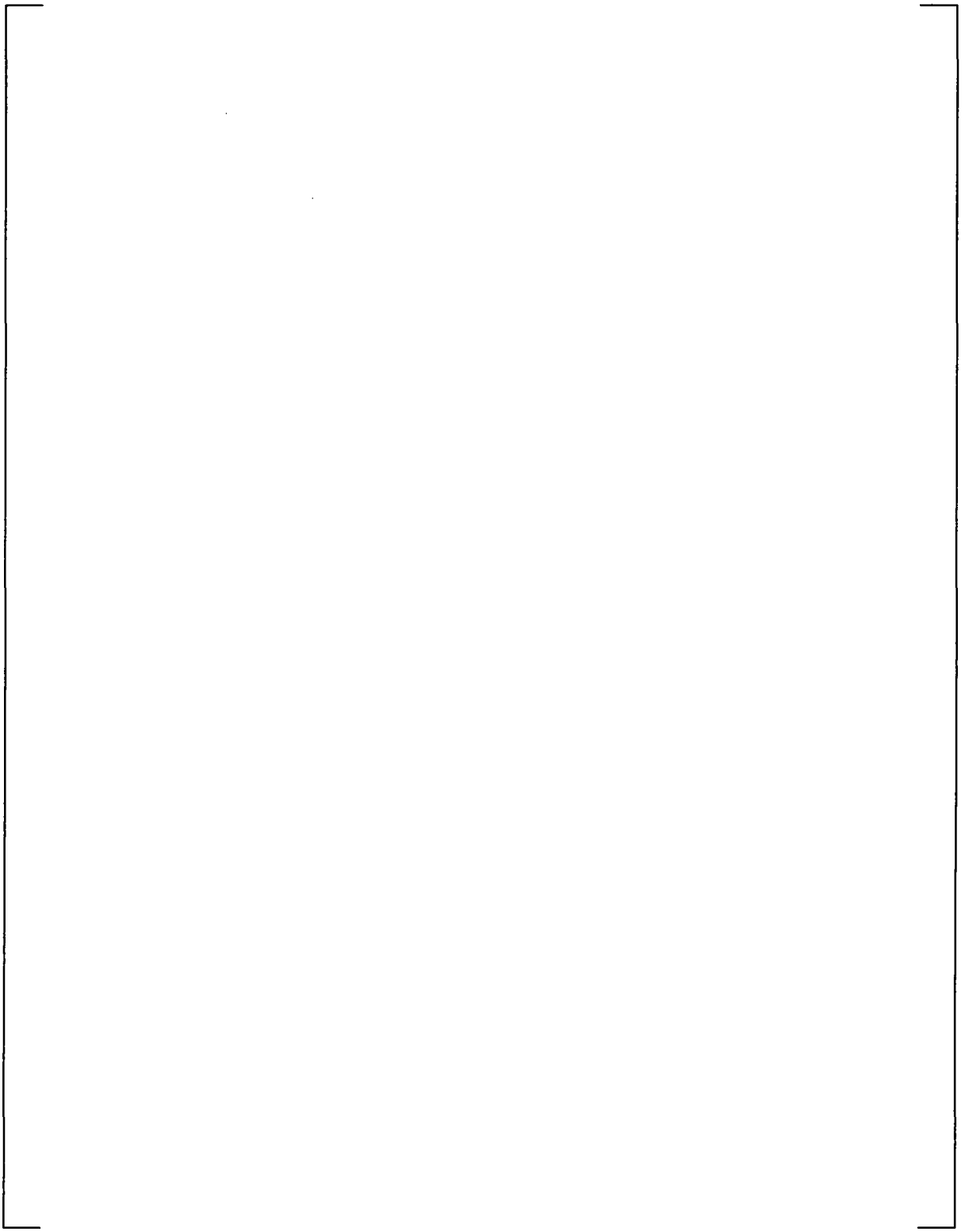

Figure 6-5 Leak rate was steady from 5 to 40 min. [

]a,b,c

a,b,c

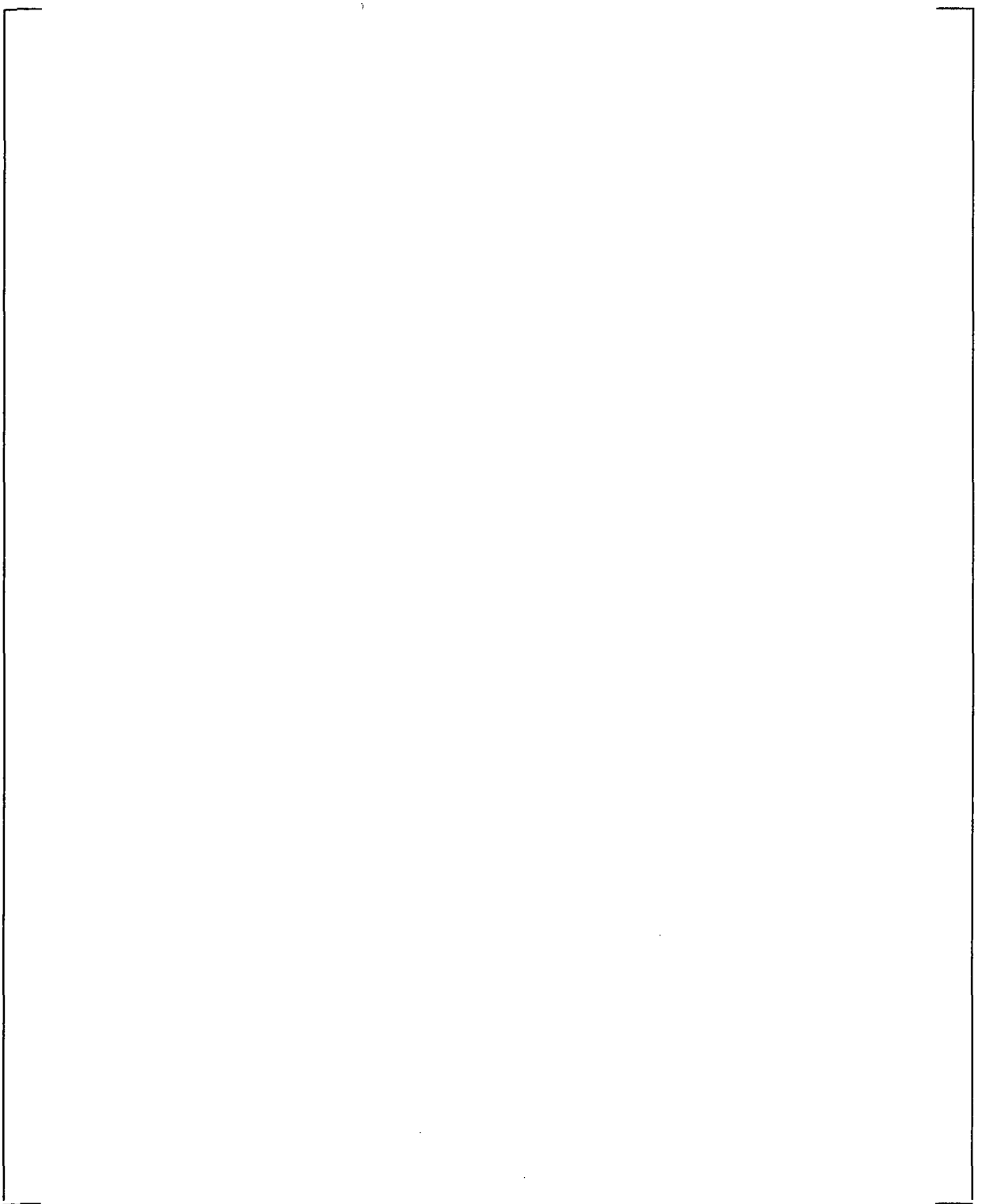

Figure 6-6 Specimen temperature averaged 466°F, P pri = 2800 psia. Leak rate was steady from 2 to 50 min. [

]^{a,b,c}

a,b,c

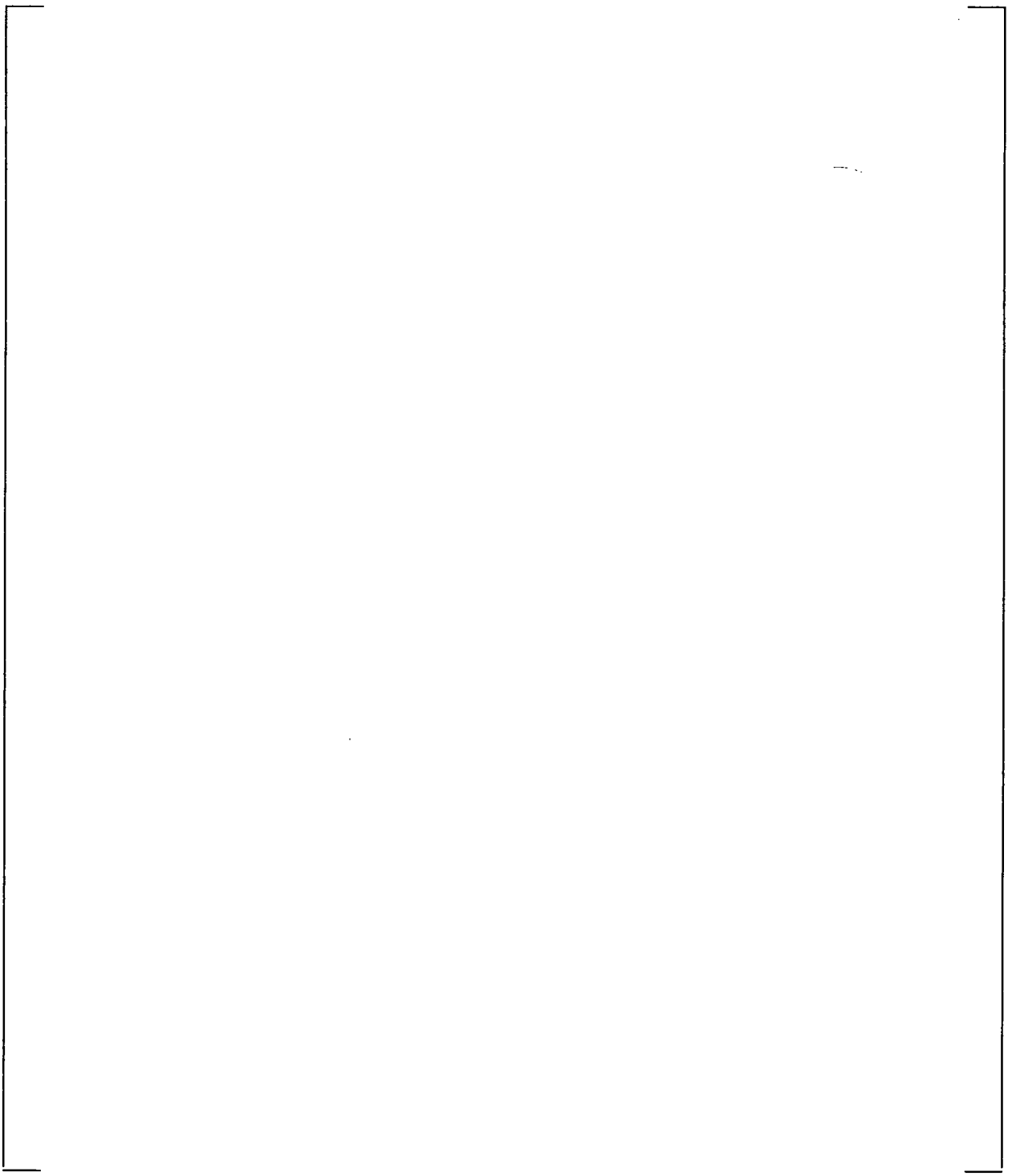

Figure 6-7 Specimen temperature changing throughout the experiment. Temperature was in the desired range from [

]^{a,b,c}

a,b,c

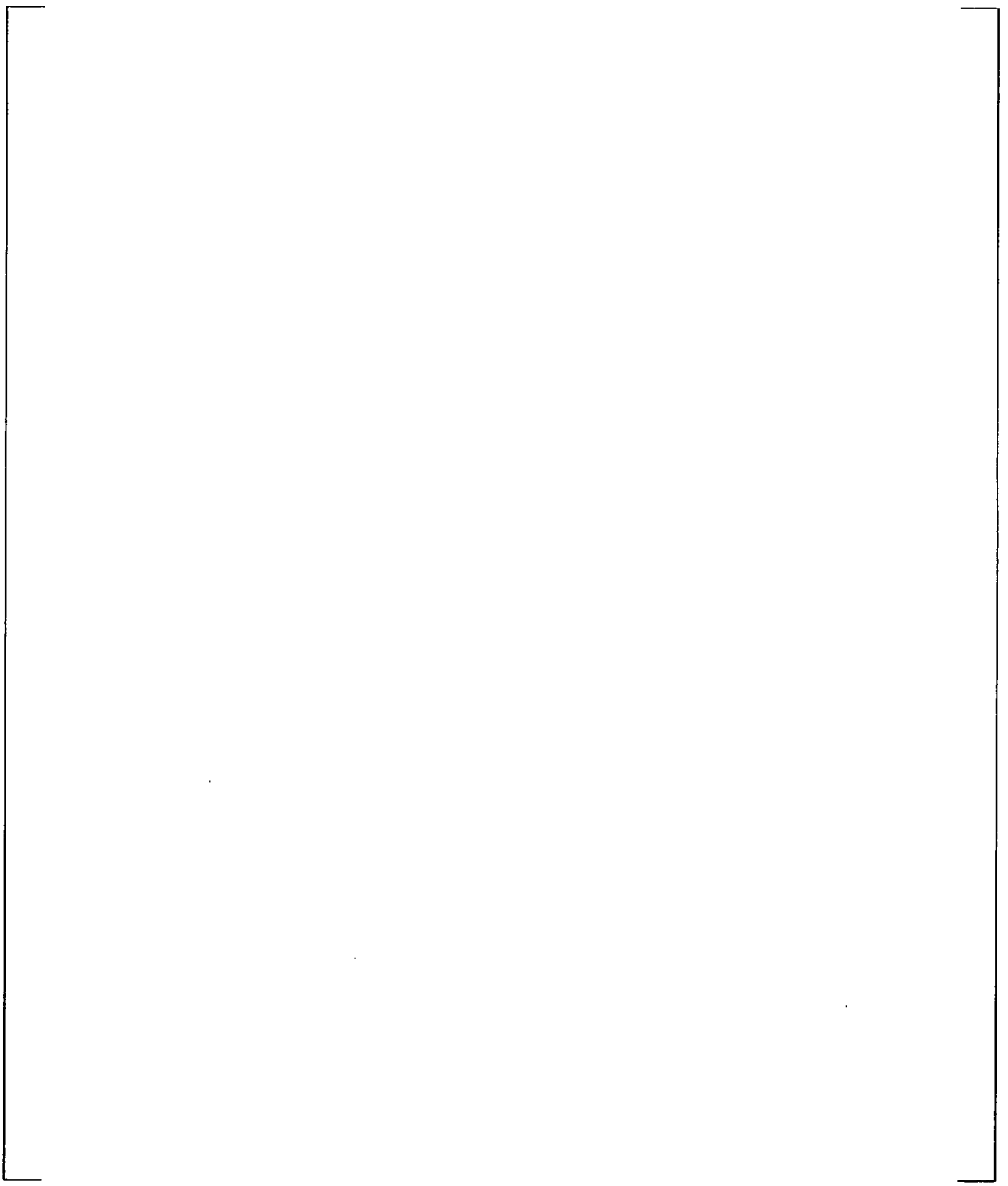

Figure 6-8 Specimen temperature lower than specified for most of the test. [

]^{a,b,c}

a,b,c

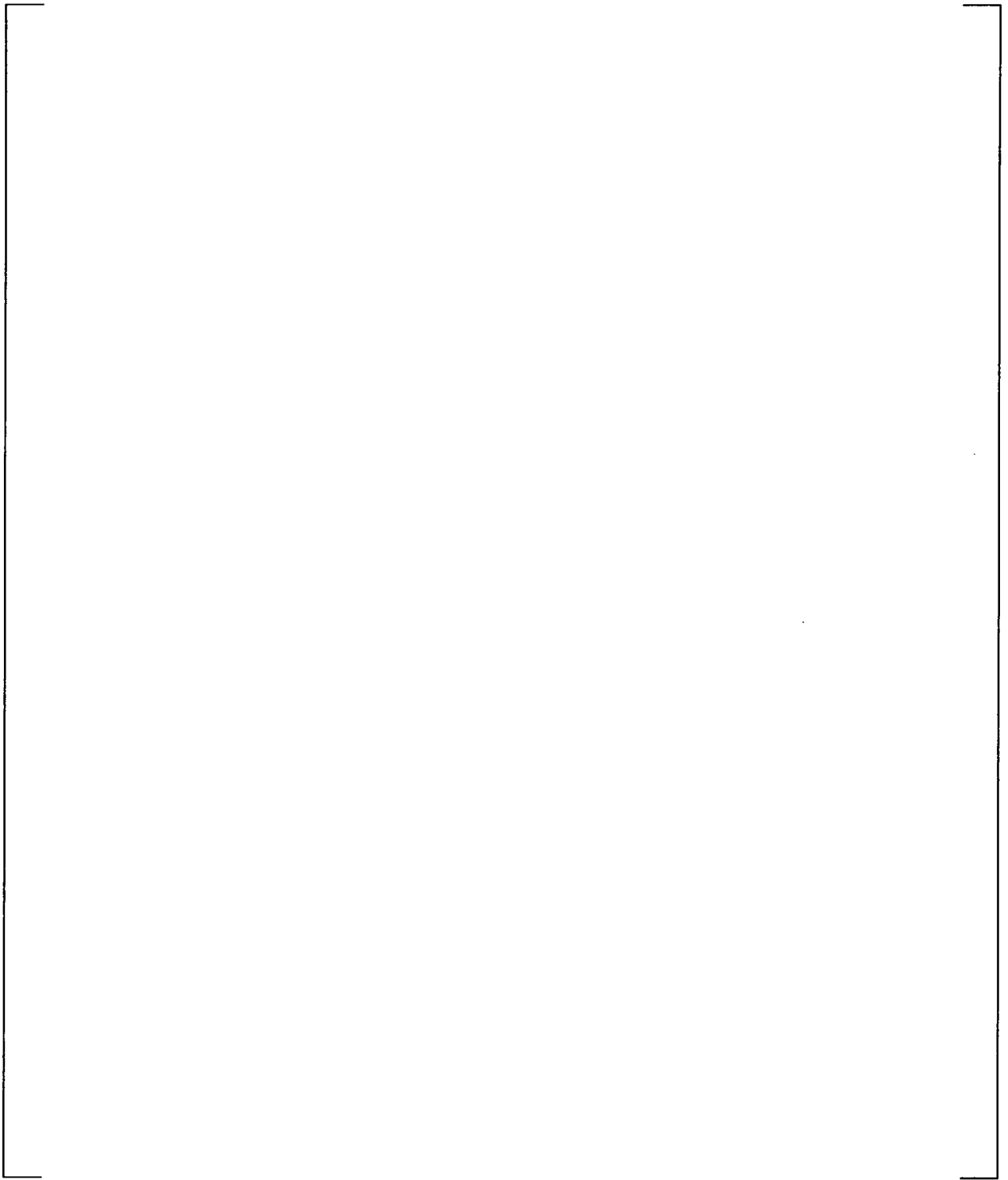

Figure 6-9 Specimen temperature decreased during the test. [

]^{a,b,c}

a,b,c

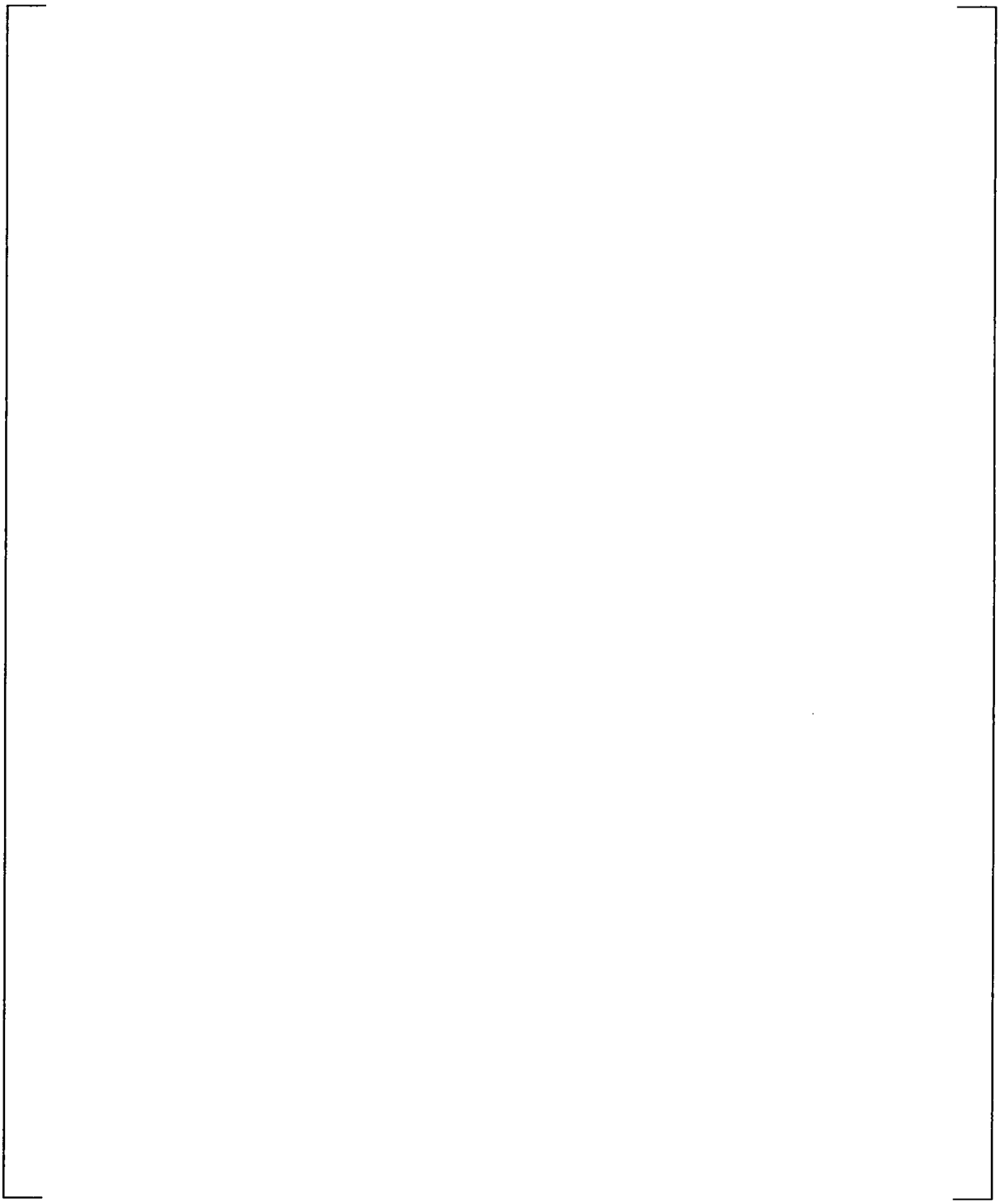

Figure 6-10 Primary pressure was increased each 10 minute period. [

]^{a,b,c}

a,b,c

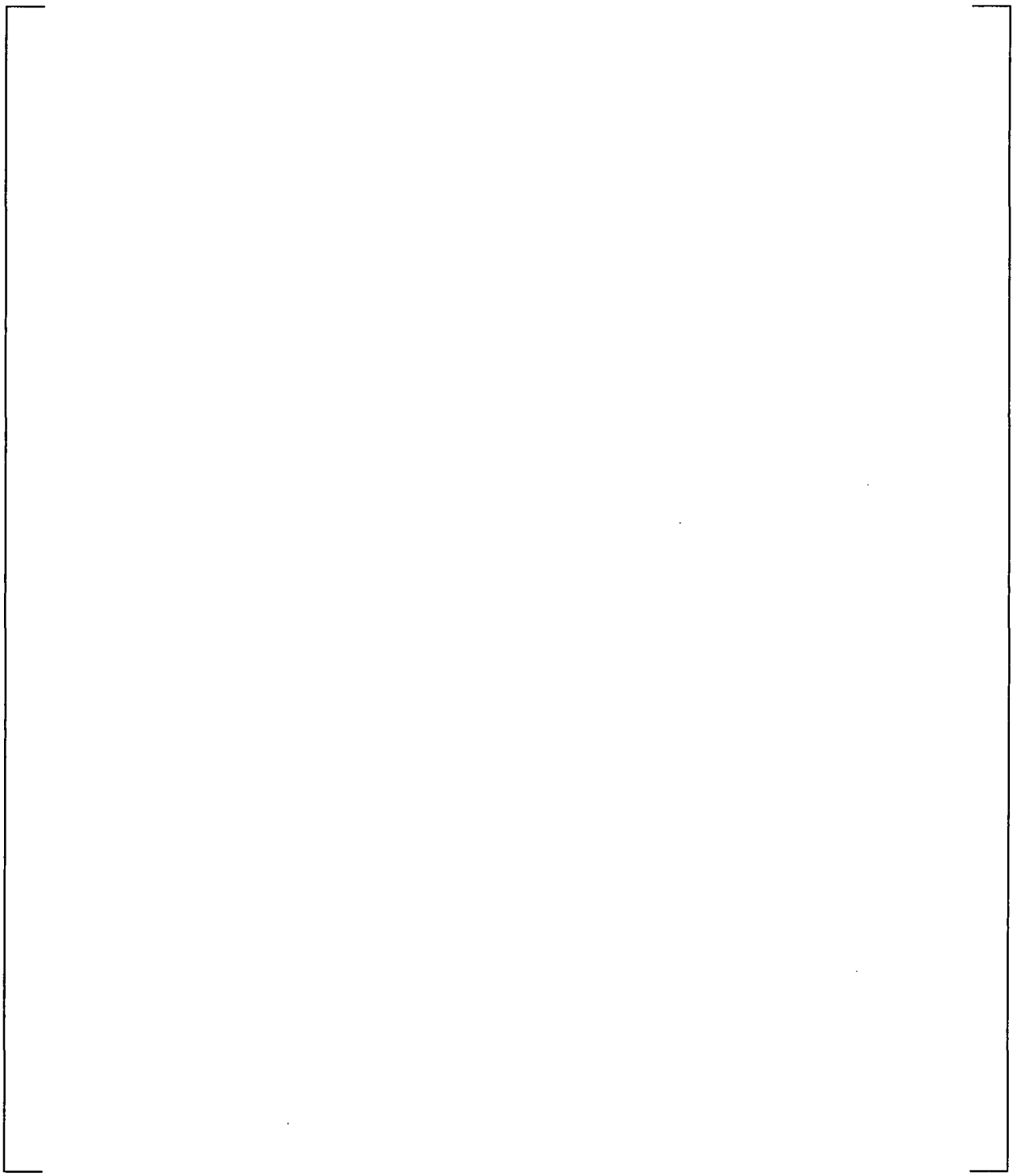

Figure 6-11 Primary pressure was increased each 10 minute period and the secondary side was filled with water. [

]a,b,c

a,b,c

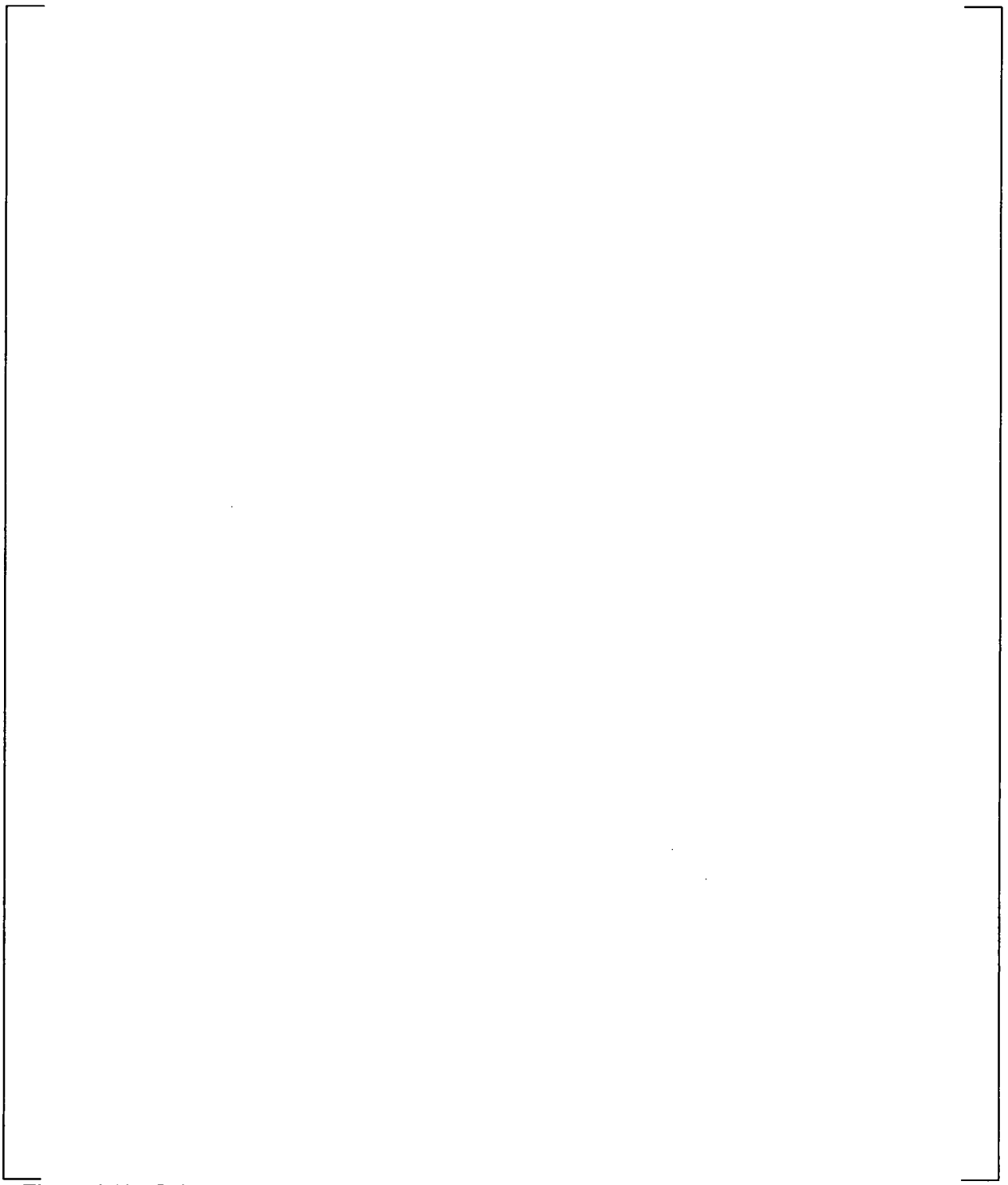

Figure 6-12 Primary pressure was increased each 10 minute period up to 2564 psia. [

]a,b,c

a,b,c

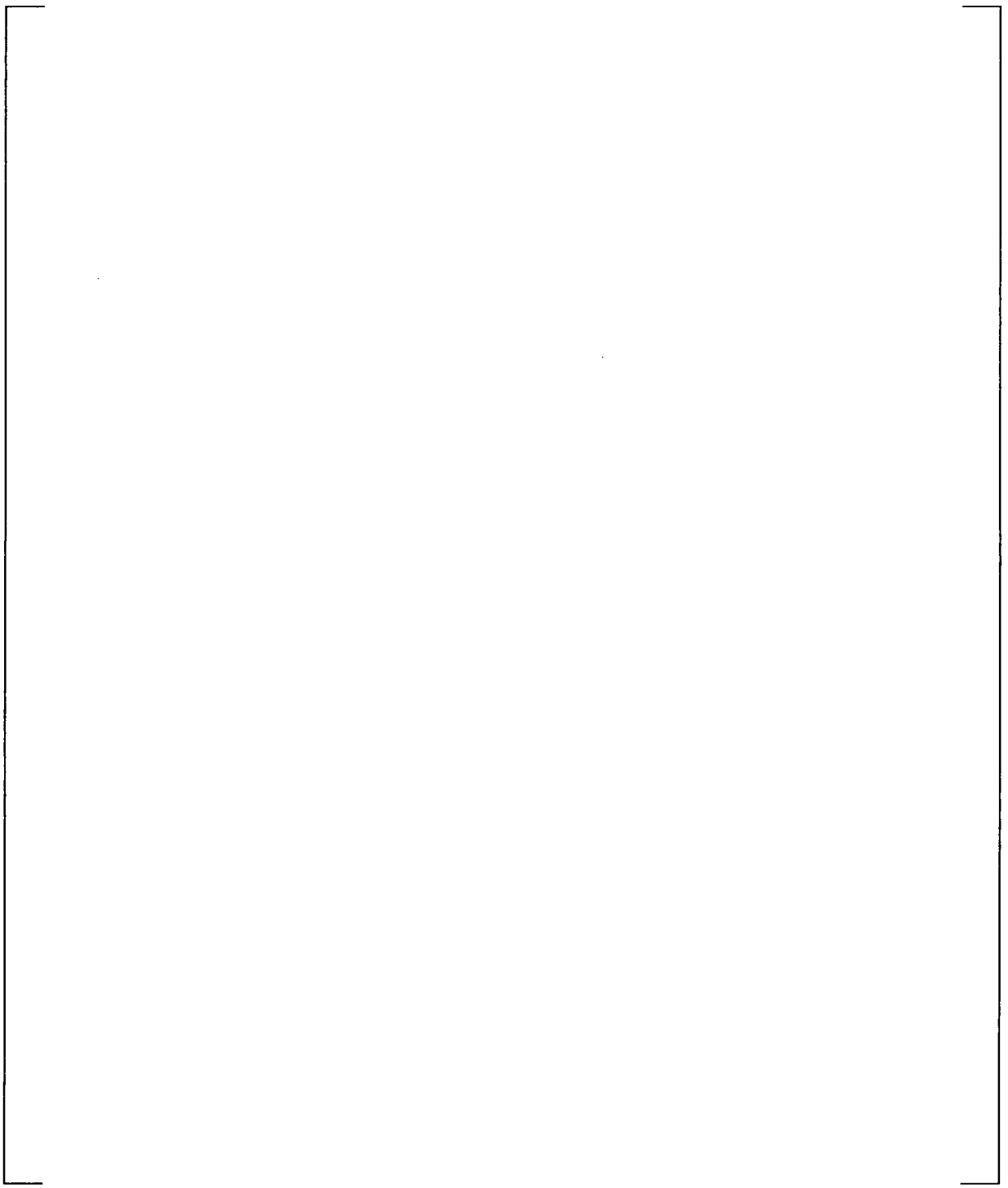

Figure 6-13 Primary pressure was increased each 10 minute period up to 2834 psia.]

]^{a,b,c}

a.b,c

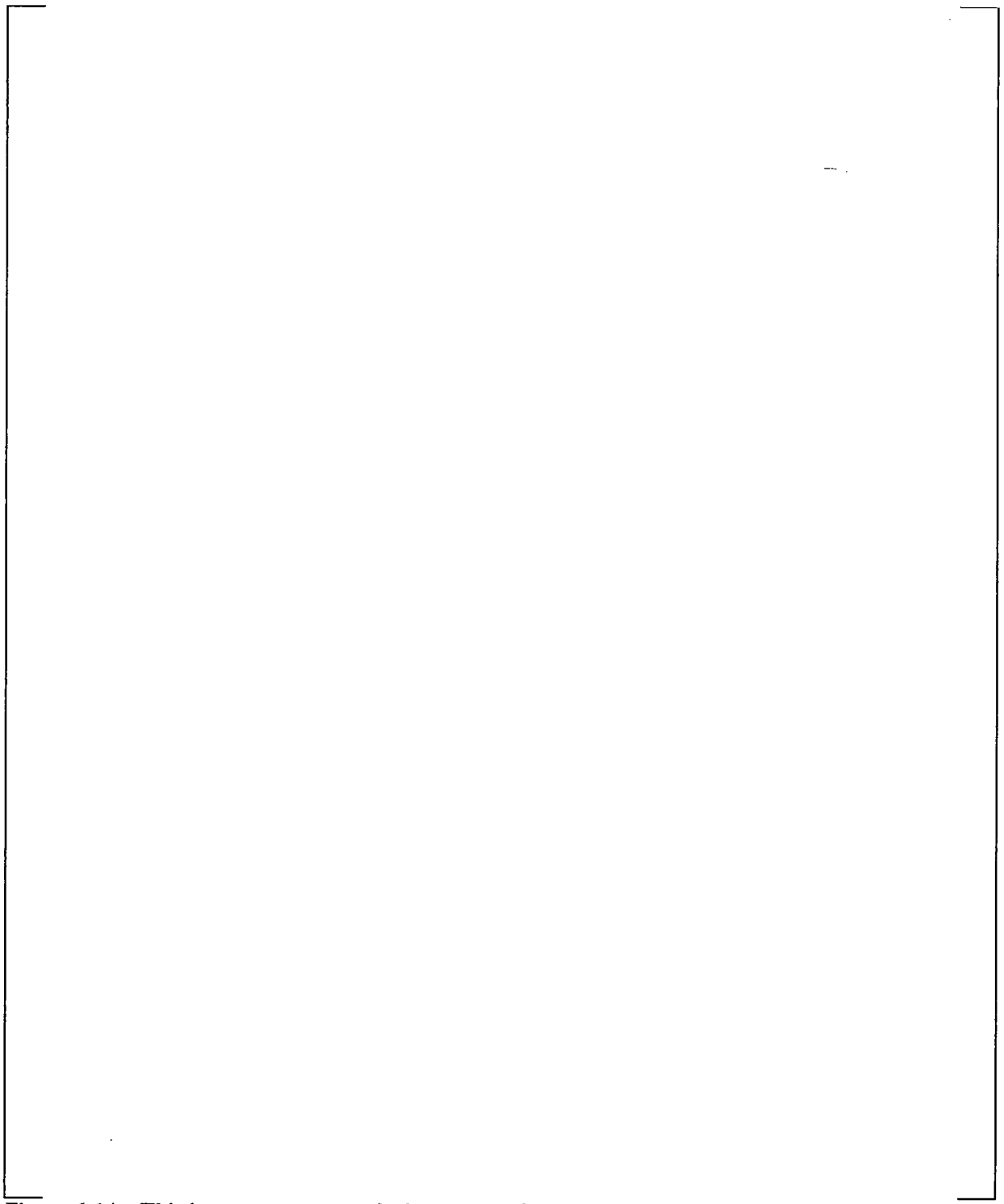

Figure 6-14 This is a water-to-water leak rate test. [

]a.b,c

6.2 SPECIMEN #8

The test results for specimen 8 are presented in the order described in the test prospectus. The results are summarized in Appendix D-2. A starting and ending date and time are listed in Appendix D-2 along with information as specified in the test prospectus. An overall summary of the test conditions and leak rates are shown in Table 6-2 below.

Table 6-2 Summary of Test Conditions and Leak Rates for Specimen #8

a,b,c

Note: * denotes that leak rate determined during the last half of the final step.

Graphs showing the pressure, temperatures and leak rates are shown in Figures 6-15 through 6-28.

Specimen 8

Test Condition 1, Room Temperature, Normal Operation and Accident delta P Tests

The room temperature tests were performed on 30-March-2005, and the results are shown in Figures 6-15 and 6-16. [

]^{a,b,c}

[

]a,b,c

Specimen 8

Test Condition 2, 600°F, Normal Operation Tests

This test was performed on 24-March-2005 and the leak rate was determined by the change in autoclave pressure resulting from the leakage. The test records are shown in Figure 6-17. [

]a,b,c

Specimen 8

Test Condition 3, 600°F, Steam Line Break Test with a Primary Pressure of 2850 psia

Two tests were performed for this condition on 24-March-2005 and the leak rate was measured directly by collecting the condensed steam. The test records are shown in Figure 6-18 and 6-19. [

]a,b,c

[

]a,b,c

Specimen 8

Test Condition 4, 600°F, Steam Line Break Test with a Primary Pressure of 2575 psia

This test was performed on 24-March-2005 and the leak rate was measured directly by collecting the condensed steam. The target conditions were 600°F and a primary pressure of 2575 psia with atmospheric secondary pressure. The data are presented in Figure 6-20. [

]a,b,c

Specimen 8

Test Condition 5, 420°F, Steam Line Break Test with a Primary Pressure of 2850 psia

This test was performed on 24-March-2005, and the leak rate was measured directly by collecting the condensed steam. The target conditions were 420°F, a primary pressure of 2850 psia with atmospheric secondary pressure. The data are presented in Figures 6-21. [

]a,b,c

Specimen 8

Test Condition 6, 420°F, Steam Line Break Test with a Primary Pressure of 2575 psia

This test was performed on 24-March-2005, and the leak rate was measured directly by collecting the condensed steam. The target conditions were 420°F and a primary pressure of 2575 psia with atmospheric secondary pressure. The data are presented in Figure 6-22. [

]a,b,c

[

]a,b,c

Specimen 8

Test Condition 7, 590°F, Steam Line Break Test with Primary Pressures of 2575 psia (7a), 2850 psia (7b) and 2900 (7c)

These tests were performed on 29-March-2005, and consisted of multiple steps each. The test records are shown in Figures 6-23, 6-24 and 6-25. The secondary pressure was atmospheric for 7a and 7b. [

]a,b,c

Specimen 8

Test Condition 8, 420°F, Steam Line Break Test with Primary Pressures of 2575 psia (8a), 2850 psia (8b) and 1800 (8c)

These tests were performed on 28-March-2005 and consisted of multiple steps each. The test records are shown in Figures 6-26, 6-27 and 6-28. [

]a,b,c

[

]a,b,c

The final condition (8c) for specimen 8 was a [

]a,b,c

a,b,c

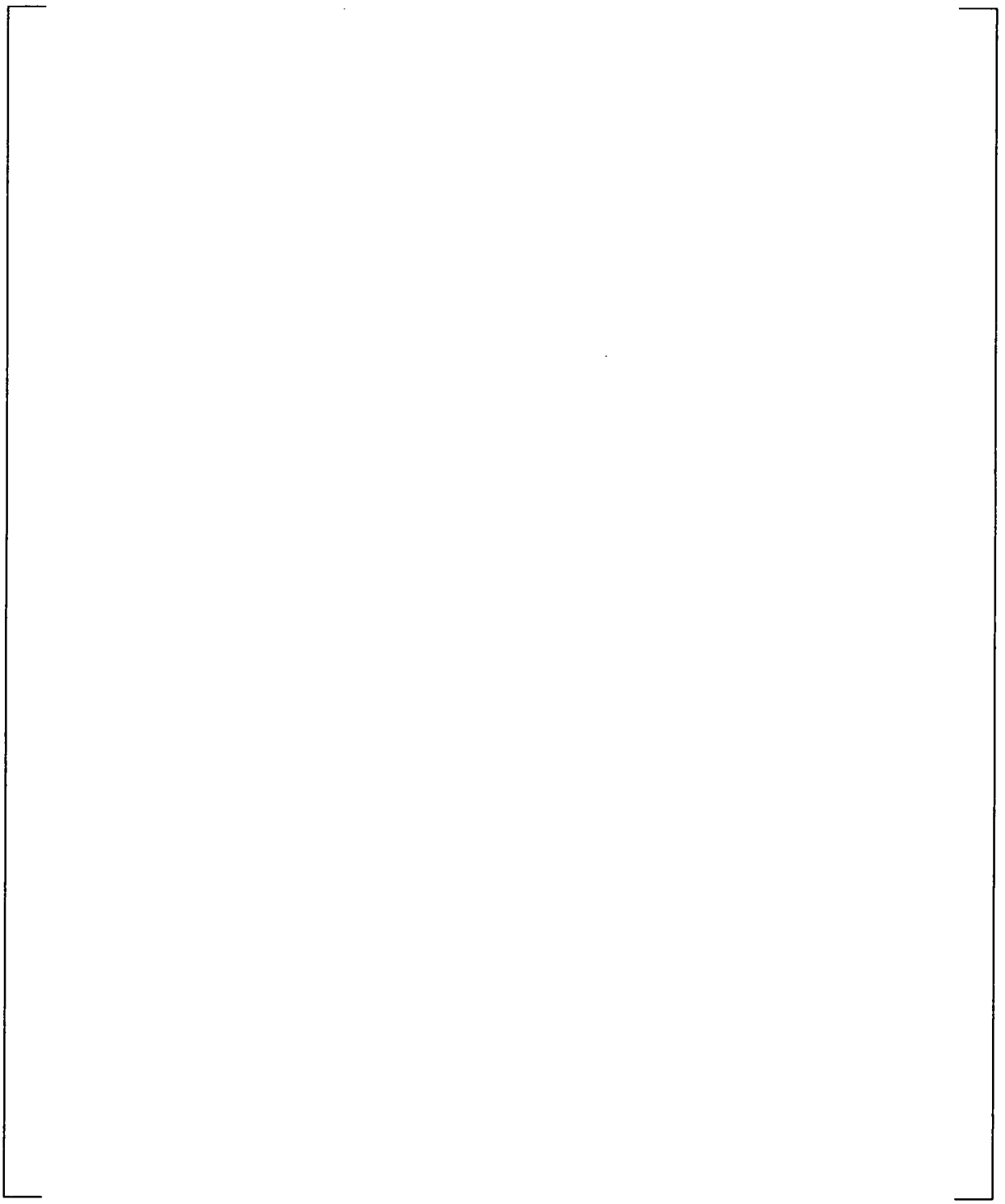

Figure 6-15 **Took approximately 9 min for all pressure tap lines to fill with fluid and pressurize. Leakage was observed after ~12 min. Leakage was steady from 12 to 59 min. Significant pressure drop observed within crevice.**

a,b,c

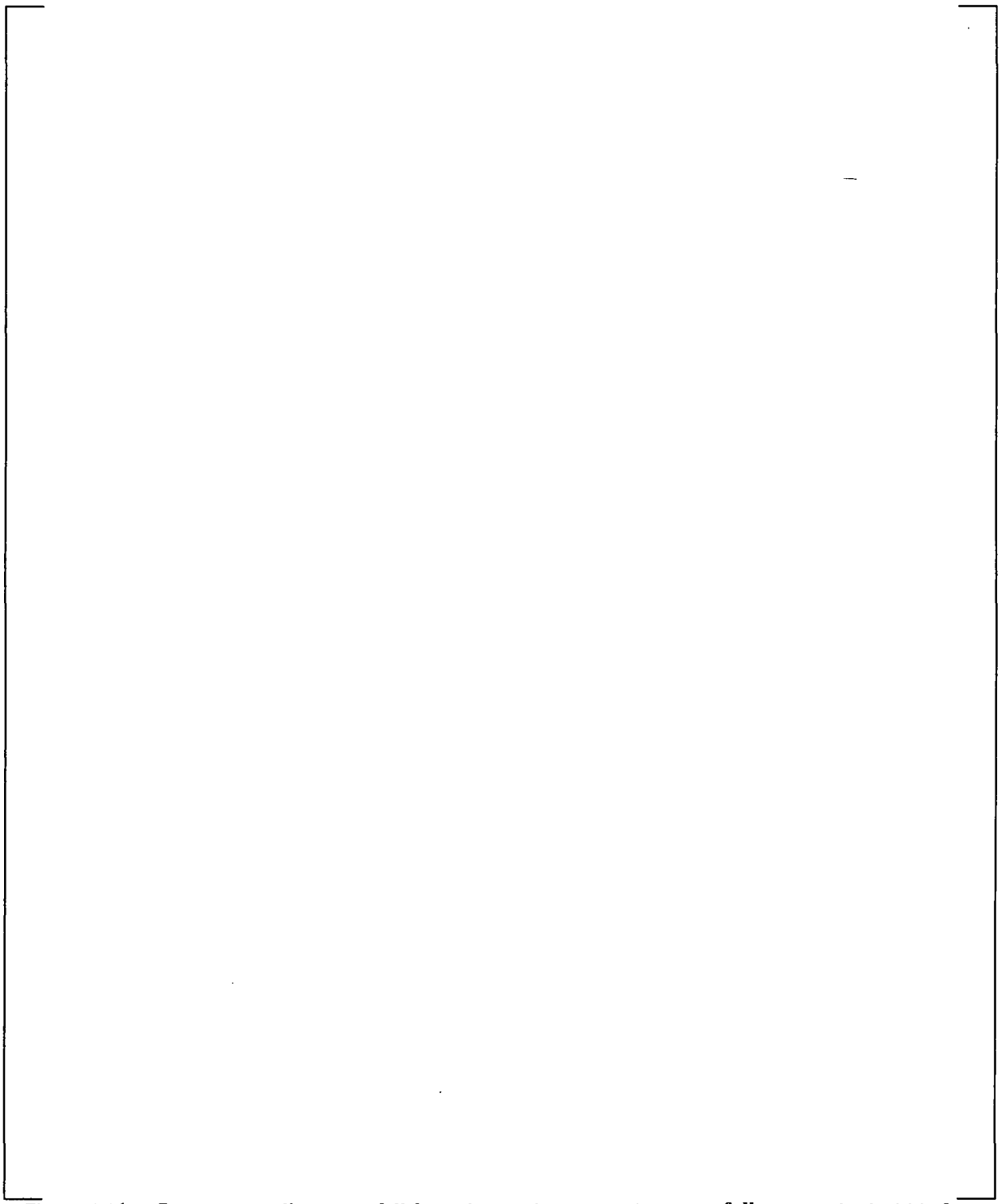

Figure 6-16 Pressure taps lines were full from the previous test. Lines were fully pressurized within 2 min. Leakage was steady from 4 to 28 min. Significant pressure drop within crevice.

a,b,c

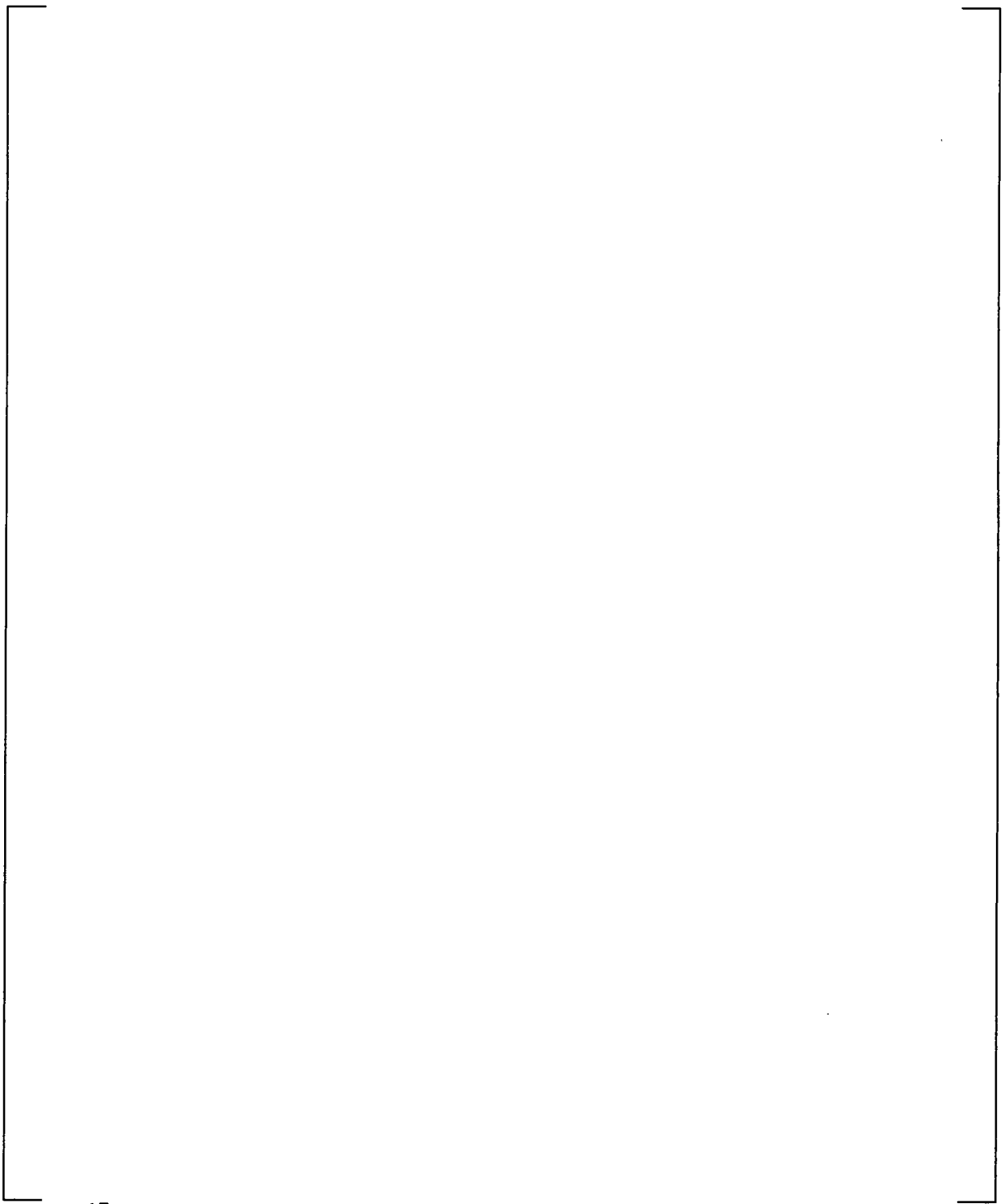

Figure 6-17 Leak rate was computed by the change in autoclave inventory [

]a,b,c

a,b,c

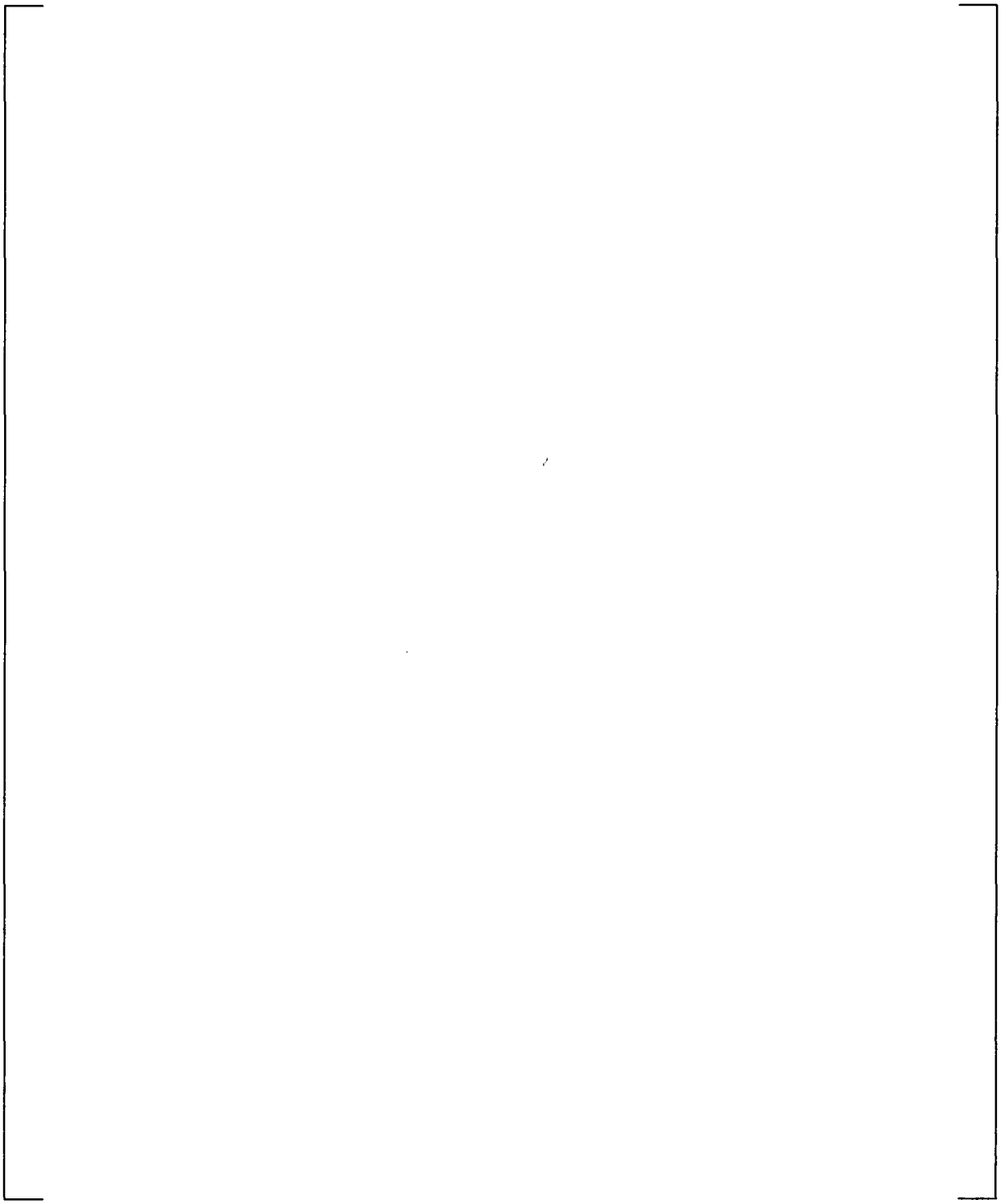

Figure 6-18 Specimen temperature below the specified range right after the test started. [

]^{a,b,c}

a,b,c

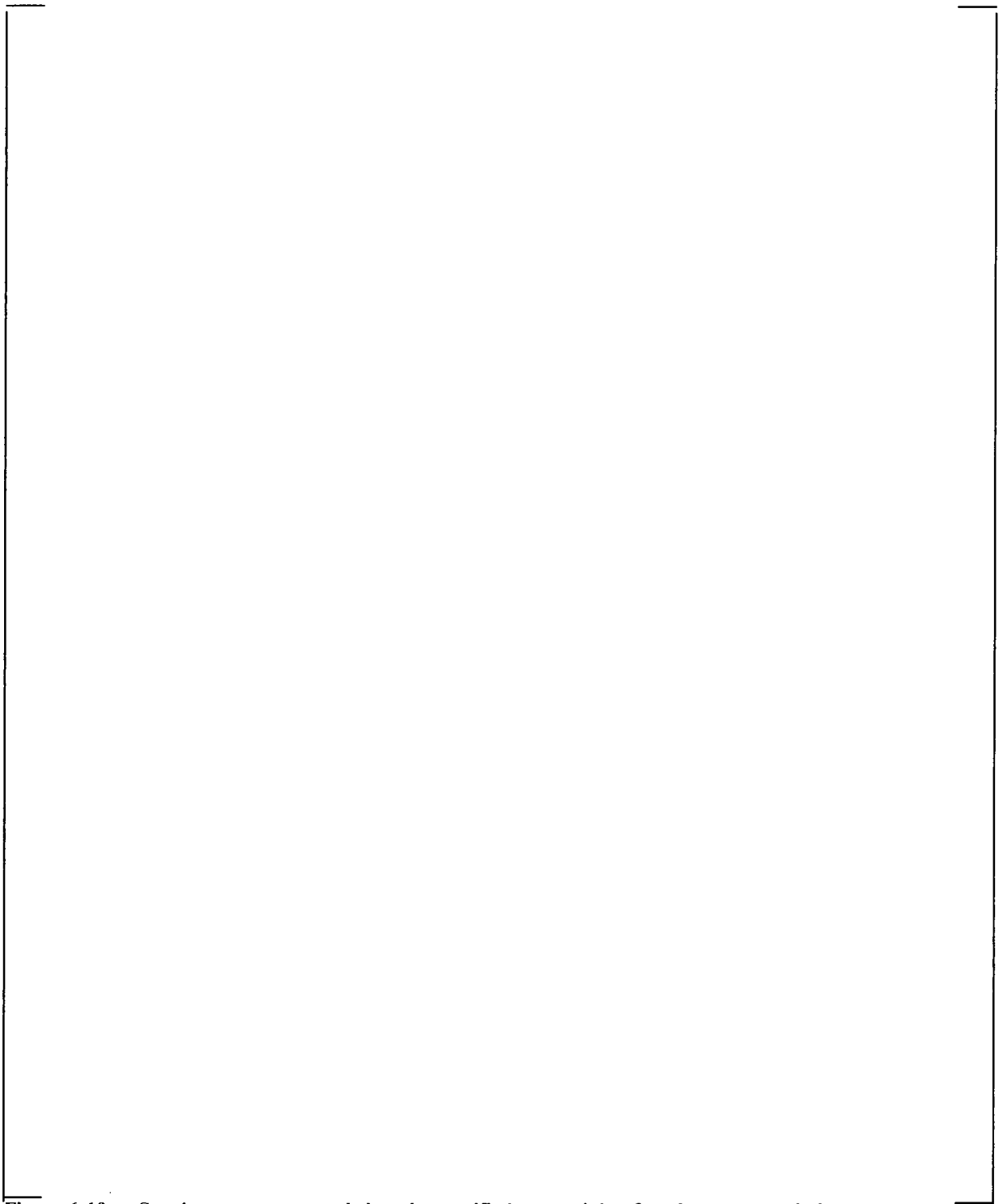

Figure 6-19 Specimen temperature below the specified range right after the test started. [

]a,b,c

a,b,c

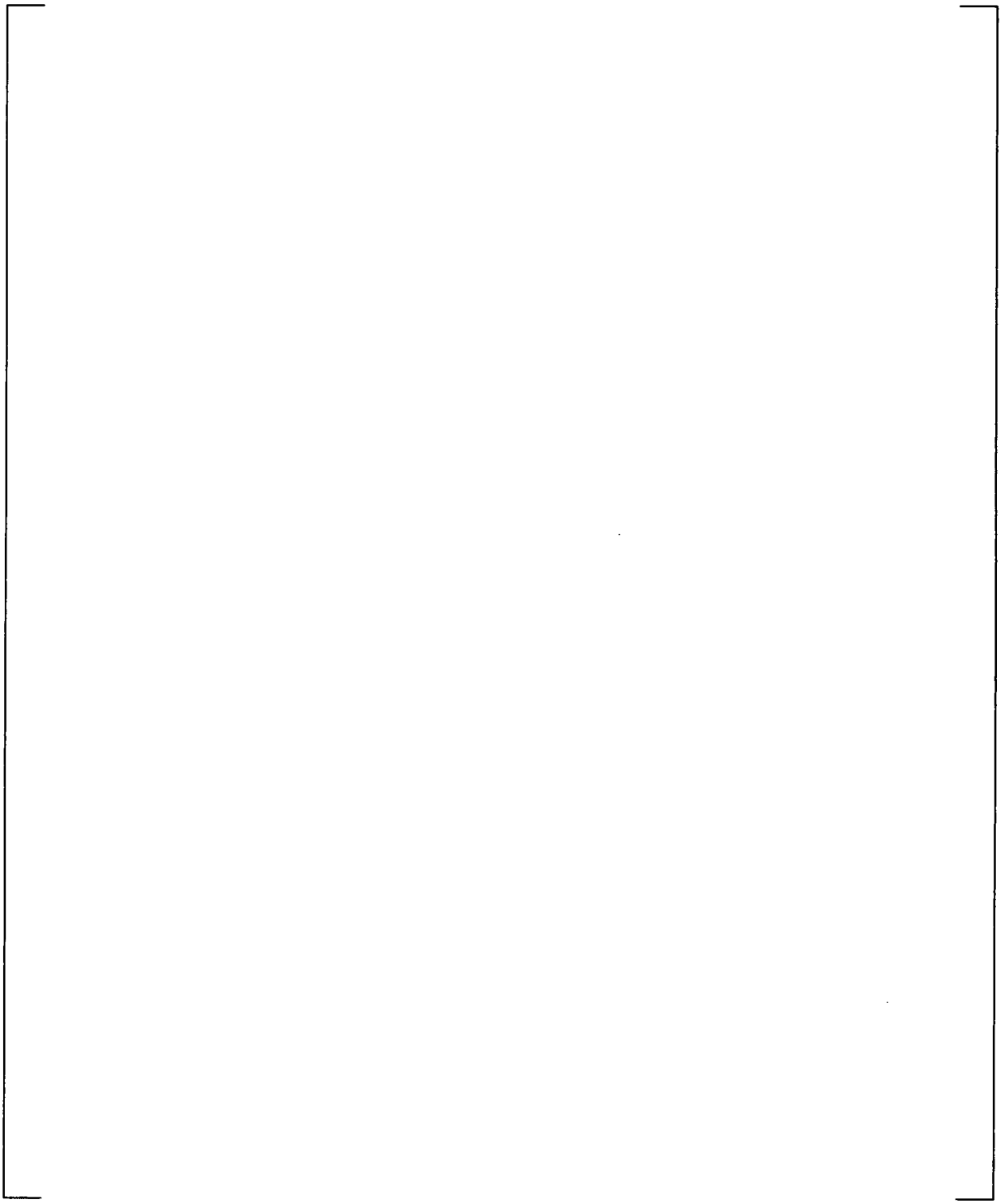

Figure 6-20 Temperature stability problems complicated this test. |

|a,b,c

a,b,c

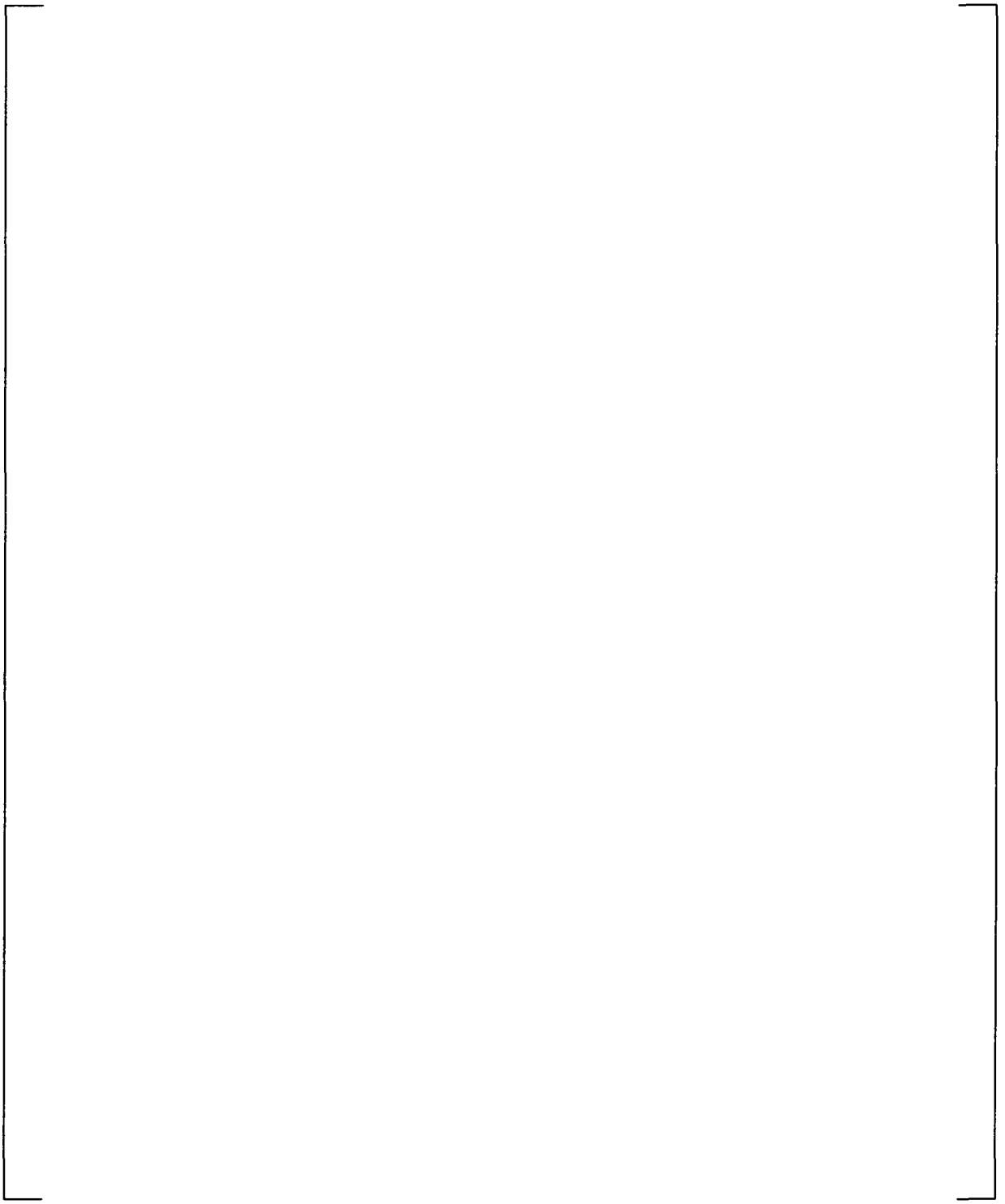

Figure 6-21 Specimen temperature was below the specified range 382°F. [

]^{a,b,c}

a,b,c

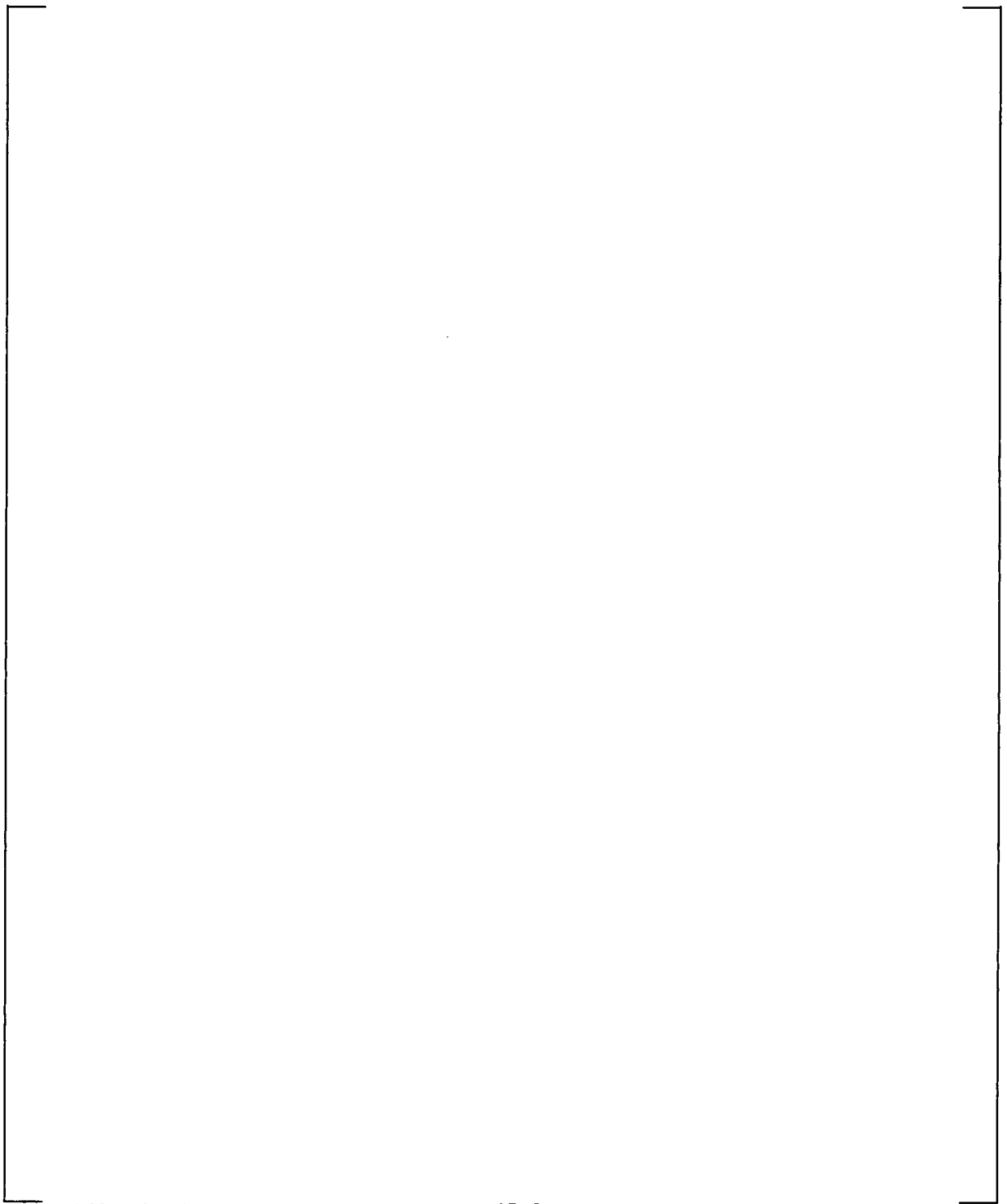

Figure 6-22 Specimen temperature higher than specified for most of the test. |

]^{a,b,c}

a,b,c

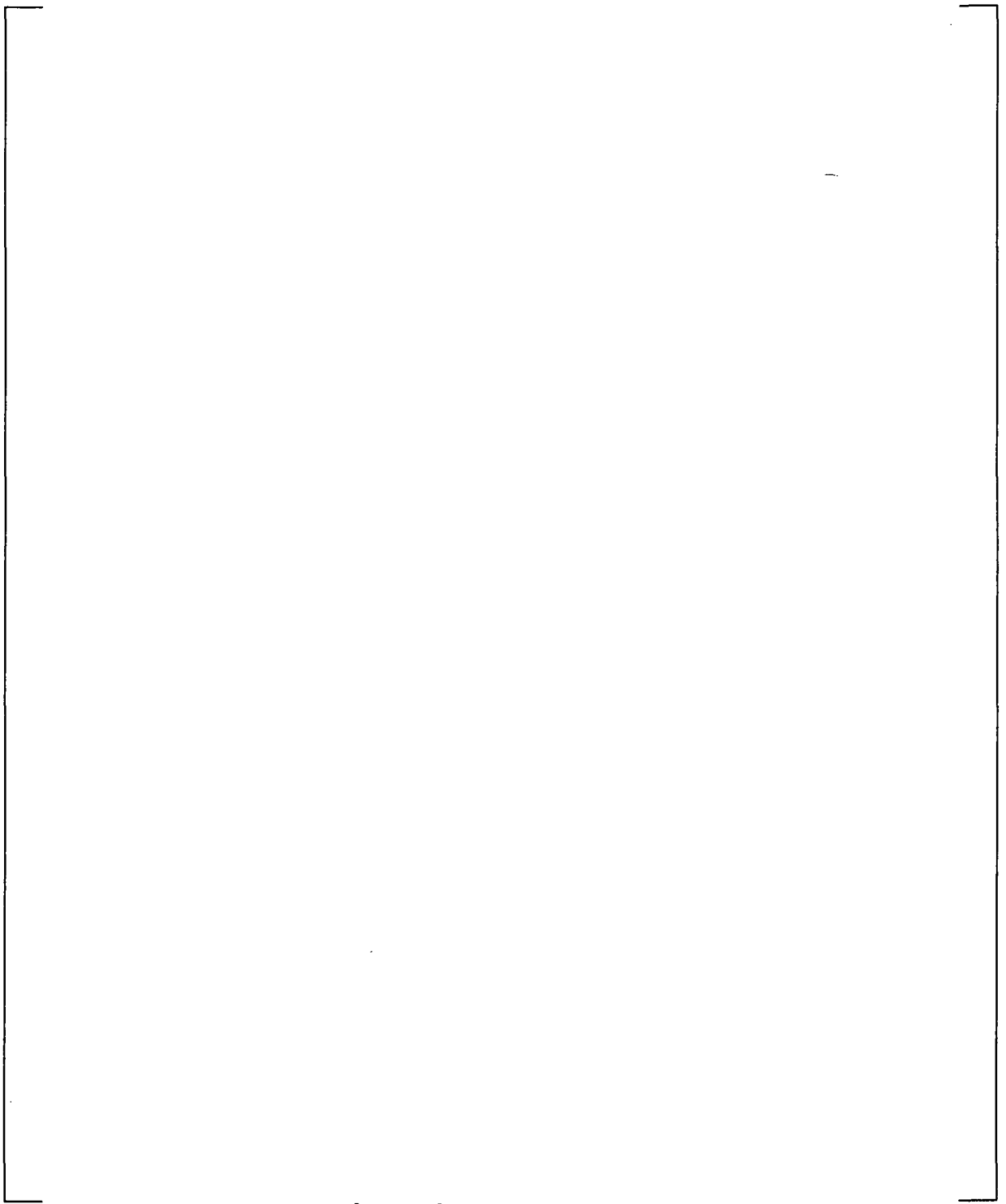

Figure 6-23 Specimen temperature decreased during the test. |

]a,b,c

a,b,c

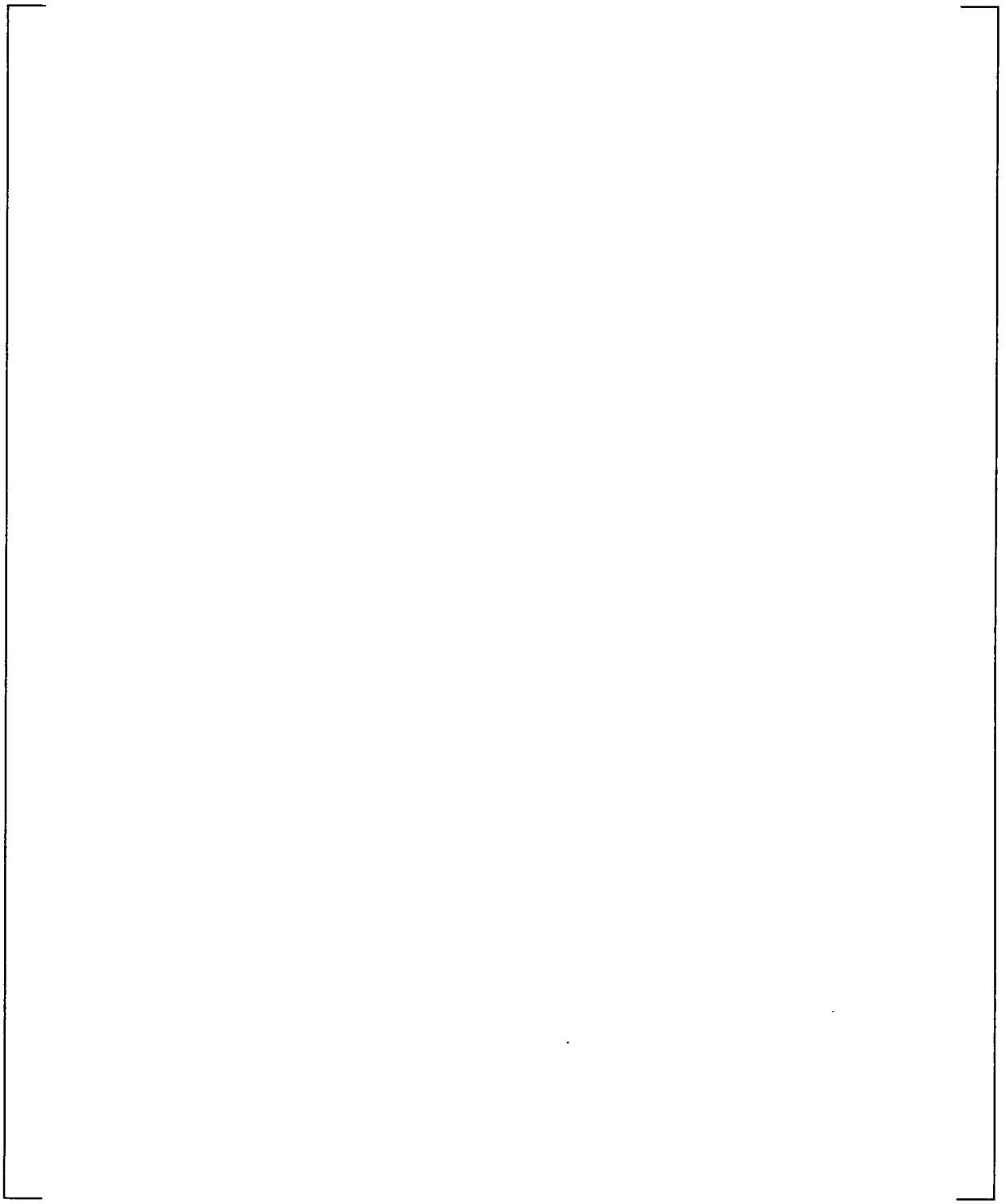

Figure 6-24 Primary pressure was increased each 10 min period. [

]^{a,b,c}

a,b,c

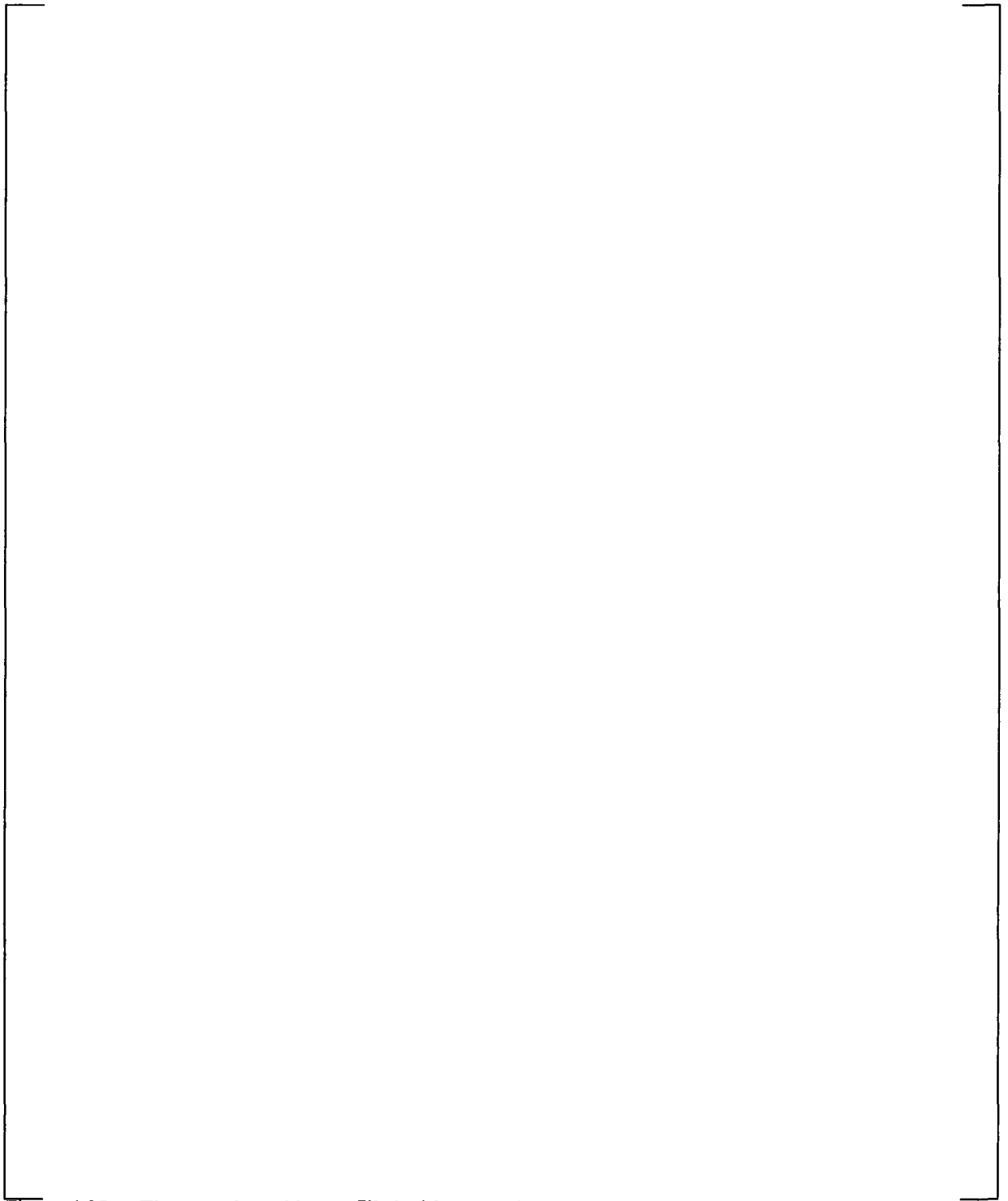

Figure 6-25 The secondary side was filled with water. [

]^{a,b,c}

a,b,c

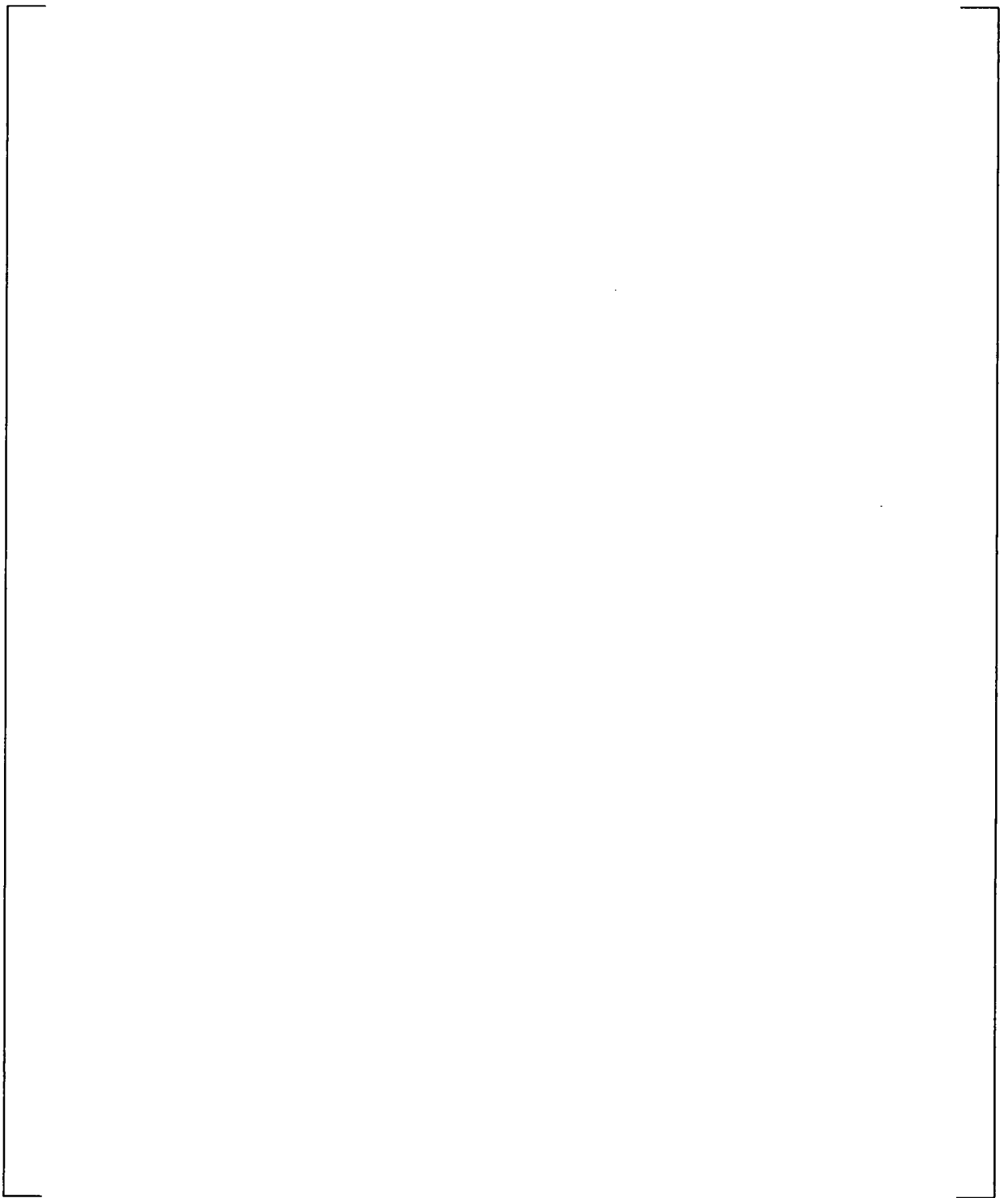

Figure 6-26 Primary pressure was increased each 10 minute period up to 2567 psia. [

]^{a,b,c}

a,b,c

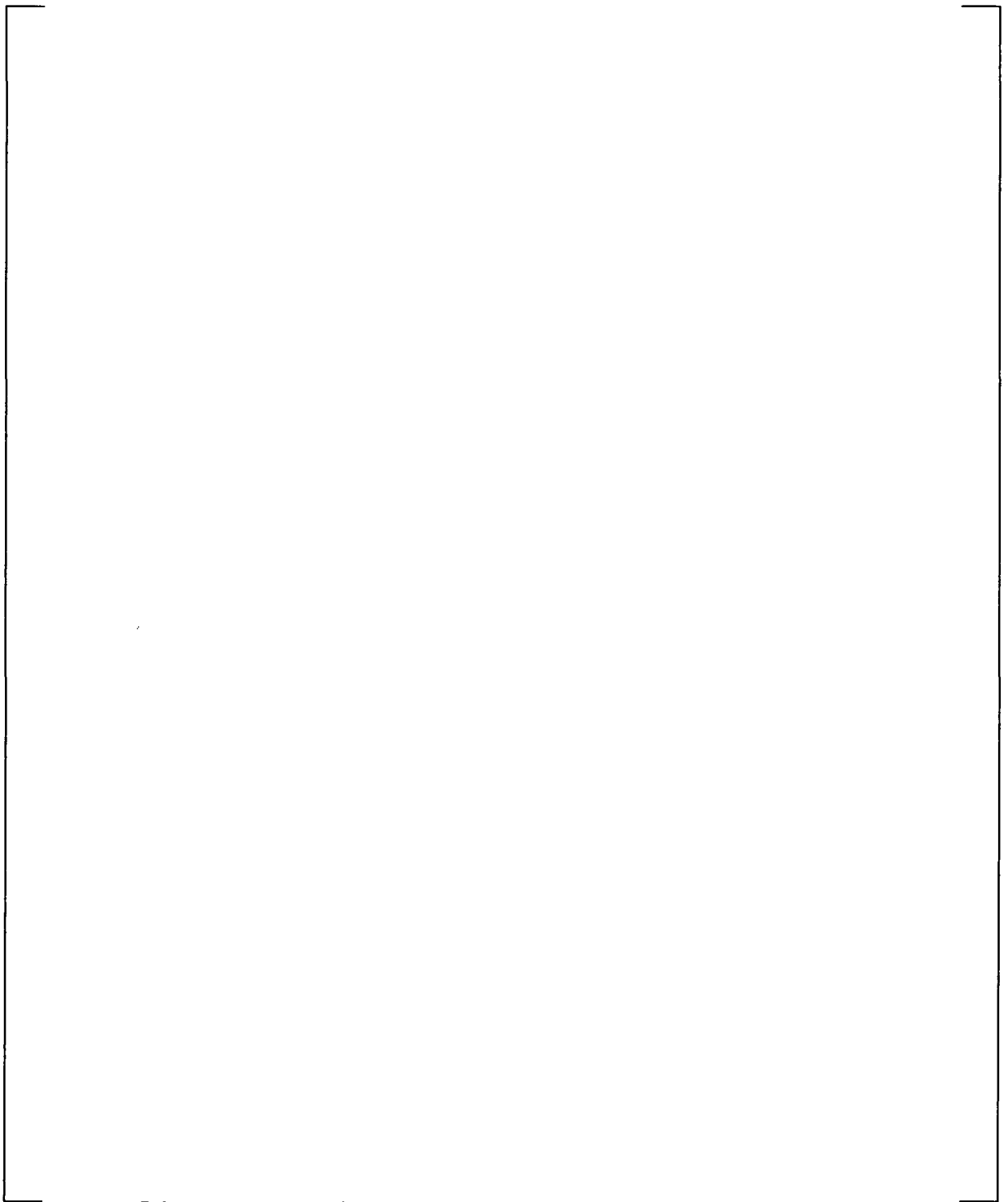

Figure 6-27 Primary pressure was increased each 10 minute period up to 2834 psia. |

]^{a,b,c}

a,b,c

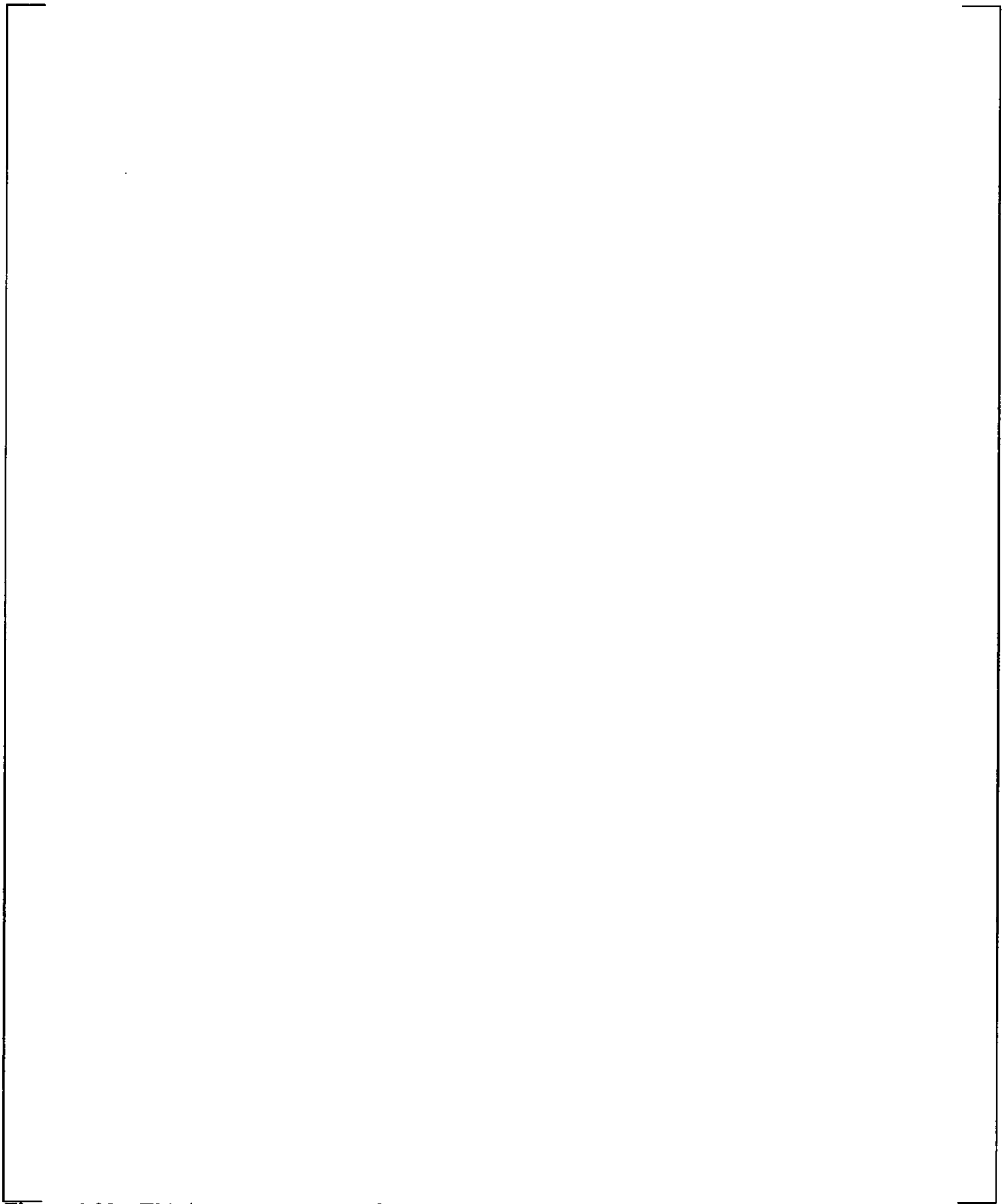

Figure 6-28 This is a water-to-water leak rate test. [

]a,b,c

7 DISCUSSION

7.1 Comparison of Leak Test Results on Specimens 7 and 8

A comparison of the leak rates observed on specimens 7 and 8 are shown in Figure 7-1 and 7-2. [

]^{a,b,c}

Figure 7-1 Comparison of Best-Estimate Leak Rates observed on specimens 7 and 8 for test conditions 1 through 6

a,b,c

Figure 7-2 Comparison of Best-Estimate Leak Rates observed on specimens 7 and 8 for test conditions 7 and 8

Evidence of these subtle differences can also be seen by comparing how the pressure drop was distributed along the crevice. Comparisons were made examining each specimen responded during comparable tests. A simple comparison can be made for the room temperature test 1d for each specimen. The table below shows how the pressure drop was distributed during one of the single phase, room temperature water tests.

Table 7-1 Comparison of the distribution of the total pressure drop observed during room temperature tests

a,b,c

[

]a,b,c

7.2 Comparison of Leak Test Results 2005 vs. 2003

These same two specimen were previously tested in 2003 and the results were reported by Pearce in Westinghouse Report STD-MCE-03-49. Comparisons were made for specimen 7 and 8 in Figures 7-3 and 7-4, respectively. Average temperatures and pressures are reported on the figures to describe small differences in experimental conditions.

a,b,c

Figure 7-3 Comparison of Leak Rates observed on Specimen 7 under similar test conditions

Note: for 2005 test 2a, [

]a,b,c

[

]a,b,c

a,b,c

Figure 7-4 Comparison of Leak Rates observed on specimen 8 under similar test conditions

[

]a,b,c

7.3 Pressure Profiles and Flow in the Tube/Tubesheet Crevice

The main reason for conducting this test program was to determine the pressure profile along the tubesheet crevice of a tube-to-tubesheet joint that was hydraulically expanded into tubesheets of Westinghouse designed steam generators. In addition to collecting this empirical, pressure profile data, an important factor was to determine for elevated temperature tests, where in the crevice did the flow change from primary water to steam.

A complete collection of pressure profiles is shown in Appendix E. [

]^{a,b,c}

a,b,c

Figure 7-5 Final Pressure Profile for Specimen 7, test condition 1-d; single phase test at room temperature

Figure 7-6 shows the final pressure profile room temperature test 7c. [

]a,b,c

a,b,c

Figure 7-6 Final Pressure Profile for Specimen 7, test condition 7-c; single phase test at 587°F

Figures 7-7 and 7-8 show the pressure profiles for two similar tests on Specimen 8. [

]a,b,c

a,b,c

Figure 7-7 Final Pressure Profile for Specimen 8, test condition 1-d; single phase test at 68°F

a.b.c

Figure 7-8 Final Pressure Profile for Specimen 8, test condition 7-c; [ ]^{a,b,c}

The pressure profiles observed during accident condition tests were [

]^{a,b,c}

For all the examples shown, most of the crevice remains [

]^{a,b,c}

a,b,c

Figure 7-9 Final Pressure Profile for Specimen 7, test condition 3-a; accident test at 624°F

a,b,c

Figure 7-10 Final Pressure Profile for Specimen 7, test condition 5-a; accident test at 467°F

a,b,c

Figure 7-11 Final Pressure Profile for Specimen 8, test condition 3-b; accident test at 547°F

a,b,c

Figure 7-12 Final Pressure Profile for Specimen 8, test condition 5-a; accident test at 382°F

a,b,c

Figure 7-13 Location where water flashed to steam in the specimen 7 tube-to-tubesheet crevice

a,b,c

Figure 7-14 Location where water flashed to steam in the specimen 8 tube-to-tubesheet crevice

a,b,c

Figure 7-15 This graph shows a comparison of the density of water and steam over temperature range of concern for steam generator operation. Once water flashes to steam in a crevice, the fluid velocity needs to increase to allow for the density change between water and saturated steam.

8 SUMMARY

These data obtained in this test series provided a unique insight into the phenomena associated with leakage through a crevice between a hydraulically expanded steam generator tube and the tubesheet. These results indicate that the fluid in the crevice is [

]a,b,c

a,b,c

Figure 8-1 Distribution of leak rates measured in this test series.

9 CONCLUSIONS

1. The ability to monitor pressure at various locations along the steam generator tube to tubesheet crevice provided key information to understand the factors that affect leak rates under normal operation and accident conditions. A key finding of this test series was that for the majority of the cases considered, the crevice between the steam generator tube and the tubesheet material is [

]^{a,b,c}

2. The flow rates measured in these tests appeared to be modest. Review of the entire hydraulic expansion database may support arguments for obtaining inspection relief for interested utilities. The point would be that even if a through-wall leak existed near the bottom of a hydraulically expanded steam generator tubesheet joint, the potential for measuring significant leakage is not high.

3. Subtle differences in the pressure profiles were observed between the two specimens tested in the resistance to flow along the hydraulic expansion region. [

]^{a,b,c}

4. For the cases where the average test temperatures were less than 500°F which may be typical of the times following a loss-of-coolant accident, [

]^{a,b,c}

10 APPENDICES

APPENDIX A – CALIBRATION RECORDS

APPENDIX B – TEST CONDITIONS MATRIX

APPENDIX C – SPECIMEN FABRICATION RECORDS

APPENDIX D – SUMMARY OF LEAK TEST RESULTS

APPENDIX E – FINAL PRESSURE PROFILES

APPENDIX F – DEVIATIONS AND/OR UNSATISFACTORY RESULTS

APPENDIX G – CERTIFICATION OF TEST RESULTS

APPENDIX A - CALIBRATION RECORDS

a,c,e

[ ]

APPENDIX B - TEST CONDITIONS MATRIX

a,c,e

APPENDIX C - SPECIMEN FABRICATION RECORDS

Welding Sign-off Sheet – Project SAP 113806 Specimen 7

[

]^{a,b,c}

Welding Sign-off Sheet – Project SAP 113806 Specimen 8

[

]^{a,b,c}

APPENDIX D – Specimen Results

APPENDIX D-1 SPECIMEN 7 RESULTS

a,b,c

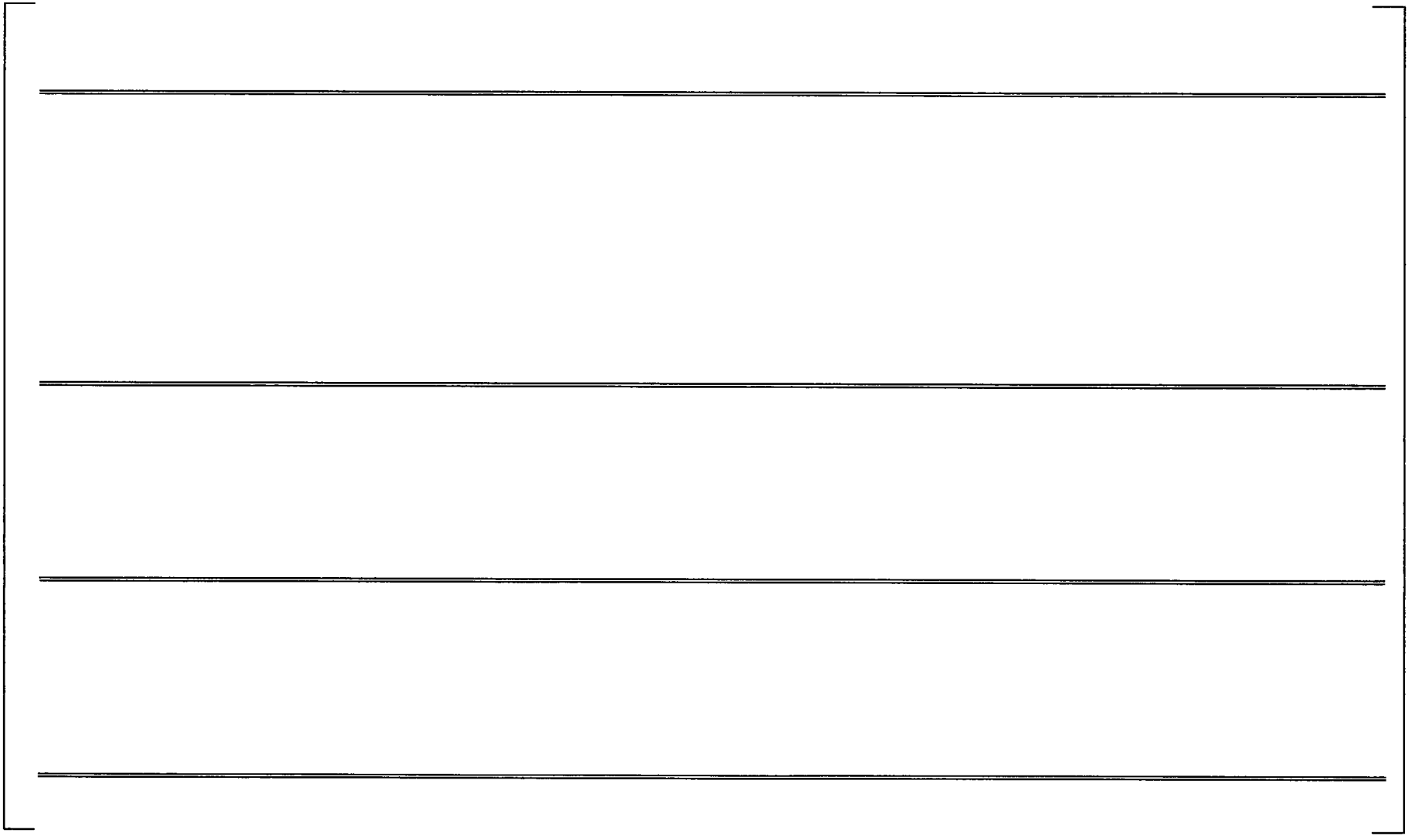

APPENDIX D-1 SPECIMEN 7 RESULTS (Continued)

a,b,c

APPENDIX D-1 SPECIMEN 7 RESULTS (Continued)

a.b,c

APPENDIX D-1 SPECIMEN 7 RESULTS (Continued)

a,b,c

APPENDIX D-1 SPECIMEN 7 RESULTS (Continued)

a,b,c

APPENDIX D-1 SPECIMEN 7 RESULTS (Continued)

a,b,c

APPENDIX D-1 SPECIMEN 7 RESULTS (Continued) a,b,c

APPENDIX D-2 SPECIMEN 8 RESULTS

a,b,c

a,b,c

a,b,c

a,b,c

a,b,c

APPENDIX D-2 SPECIMEN 8 RESULTS (Continued)

a,b,c

a,b,c

APPENDIX E- FINAL PRESSURE PROFILES

a,b,c

a,b,c

a,b,c

[ ]

a,b,c

[ ]

a,b,c

[redacted]

a,b,c

[redacted]

a,b,c

[redacted]

a,b,c

[redacted]

a,b,c

[ ]

a,b,c

[ ]

a,b,c

[ ]

a,b,c

[ ]

a,b,c

a,b,c

a,b,c

[ ]

a,b,c

[ ]

a,b,c

[ ]

a,b,c

[ ]

a,b,c

[redacted]

a,b,c

[redacted]

a,b,c

[redacted]

a,b,c

[redacted]

a,b,c

[ ]

a,b,c

[ ]

a,b,c

[ ]

a,b,c

[ ]

a,b,c

[ ]

a,b,c

[ ]

APPENDIX F - DEVIATIONS AND/OR UNSATISFACTORY RESULTS

DEVIATIONS AND/OR UNSATISFACTORY RESULTS

Sheet 1 of 2

a,b,c

Deviation or Unsatisfactory Results or Comments: total number - 9

Resolutions/Necessary Actions: number of actions 9 a,b,c

DEVIATIONS AND/OR UNSATISFACTORY RESULTS

Sheet 2 of 2

Deviation or Unsatisfactory Results or Comments: total number - 9 a,b,c

Resolutions/Necessary Actions: number of actions 9 a,b,c

APPENDIX G - CERTIFICATION OF TEST RESULTS

1.0 This test has been performed in accordance with test procedure ***RJ Jacko***

2.0 Computer software application and version Not applicable

Equipment drawing number and revision SK1B81517

3.0 Test data and results have been reviewed against the requirements and acceptance criteria of the test procedure and are accepted.

4.0 Any deviations to this procedure and/or any unsatisfactory results are resolved and documented.

5.0 List any actions not affecting equipment/process acceptability:

N/A

6.0 This test completes all testing required by the following Design Review Action Items:

Test Data Package Reviewers:

Project Manager	Richard J. Jacko	Date	5-Jul-2006
System Eng.		Date	
Quality		Date	

7.0 The results of this test, including any deviations and unsatisfactory results with their resolutions, have been reviewed and are acceptable. The equipment/process/computer software are hereby deemed acceptable for field service application.

* Cognizant Managers:

Product		Date	
Engineering		Date	
Quality		Date	

APPENDIX G - CERTIFICATE OF TEST COMPLETION (Continued)

EQUIPMENT/PROCESS: _____

8.0 The test acceptance criteria have been partially satisfied. Limited field use is certified as follows:

_____

_____

_____

The functional specification has been revised consistent with the above limitations.

Westinghouse

STD Final Report Verification Checklist

Note: If completing form electronically, highlight the checkbox and type an "x" to fill in the checkbox.

Document Title: Pressure Profile Measurements During Tube-to-Tubesheet Leakage Tests of Hydraulically Expanded Steam Generator Tubing

STD Letter Number: STD-MC-06-11 **Date 7/05/06**

Test Prospectus Verifier: L. A Nelson (NS) **Revision 0**

Checklist		Yes	No
1.0	Is the approved test prospectus provided?	☒	☐
2.0	Are the STD procedures identified?	☒	☐
3.0	Were the calculations correctly performed?	☒	☐
4.0	Were data properly transcribed?	☒	☐
5.0	Were test samples correctly identified with respect to lot number, fabrication history, etc.?	☒	☐
6.0	Were test deviations identified?	☒	☐
If yes to 6.0, were there any possible effects to the test results? If so, please list		☒	☐

Verifier Statement – List steps and techniques used in verification

Reviewed final report for accuracy and completeness

Checked calculations using steam tables

Verified conclusions

Verification Signature Rachel L Levito Date 7/05/06

Westinghouse

To: H. O. Lagally **Date:** September 24, 2007

cc: P. R. Nelson, G. W. Whiteman, J. G. Thakkar, E. P. Morgan, B. A. Bell, W. K. Cullen

From: C. D. Cassino
Ext: 724 722-6018
Fax: 724 722-5889

Your ref:
Our ref: LTR-SGDA-07-4-NP, Rev. 3

Subject: **Letter Summary of Changes to B* and H* Analysis due to New Crevice Pressure and Divider Plate Data**

The technical basis for H* and B* as documented in the Alternate Repair Criteria (ARC) WCAPs and Calc Notes (see Reference 1 for an example) is based, in part, on of the fundamental assumption that leakage through a postulated crack below H* flashes to steam in the crevice. This establishes the pressure in the crevice as the saturation pressure. Test data show that leakage through a crack below H* does not flash to steam and remains a single-phase fluid; therefore, the original assumption is not justified and changes must be made to the B* and H* analysis inputs to reflect the new test results.

The purpose of the test was to determine the pressure in the crevice between the tube and the tubesheet. The tests show that there is a distribution of pressure in the tubesheet crevice that is [ ]^{a,c,e} The results showed that the fluid in the crevice remained single phase to very near the top (secondary side face) of the [long test specimens. Therefore, the crevice pressure is [ ]^{a,c,e} An increased pressure in the crevice will result in:

1. The driving potential on the leaked fluid from the primary side to the crevice has been reduced.
2. The driving potential on the leaked fluid from the crevice to the secondary side is increased at the bottom of the tubesheet and decreased at the top of the tubesheet.
3. The resistance to flow from viscous effects has increased.
4. The tube expansion component of the contact pressure analysis has been reduced.
5. The tube expansion component of the leakage resistance analysis has been reduced.

A discussion of the impact of the test results documented in Reference 1 on H*/B* analyses from a generic perspective is provided. The effects of varying the divider plate factor on a generic H*/B* analysis are also discussed. Note that the flaw in the test specimens discussed in this document was specifically [
]^{a,c,e}. It is possible to maintain a large pressure drop across the tube wall in smaller crack geometries. [
]^{a,c,e} Therefore, the results described in this letter are bounding for the worst case scenario [
]^{a,c,e} exists in the tube portion within the tubesheet.

If there are any questions regarding the contents of this letter please contact either Chris Cassino or Herm Lagally.

Author:

C.D. Cassino

Chemistry, Diagnostics and Materials Engineering

Reviewer:

H.O. Lagally

Chemistry, Diagnostics and Materials Engineering

References

1. STD-MC-06-11, Rev.1.
2. LTR-CDME-05-32-P, Rev. 2.
3. http://www.cee.vt.edu/ewr/environmental/teach/smprimer/outlier/outlier.html, 07/01/2007, 11:34:07 AM EST.
4. M.R. Chernick, "A Note on the Robustness of Dixon's Ratio Test in Small Samples", *American Statistician*, Vol. 36, No. 2 (May, 1982), p. 140.
5. W.B. Middlebrooks, D.L. Harrod, R.E. Gold, "Residual Stresses Associated with the Hydraulic Expansion of Steam Generator Tubing into Tubesheets," Nuclear Engineering and Design 143 (1993) 159-169 North-Holland.
6. LTR-SGDA-06-156.
7. LTR-SGDA-06-157.
8. CN-SGDA-07-6.
9. Terakawa, T., Imai, A., Yagi, Kazushige, Fukada, Y., Okada, K., "Stiffening Effects of Tubes in Heat Exchanger Tube Sheet", Journal of Pressure Vessel Technology Transactions, ASME Vol. 106, No.3, August 1984.
10. LTR-SGDA-06-160.
11. LTR-SGDA-07-3.
12. TP-SGDA-03-2, Rev.1.
13. *Divider Plate Cracking in Steam Generators: Results of Phase 1: Analysis of Primary Water Stress Corrosion Cracking and Mechanical Fatigue in the Alloy 600 Stub Runner to Divider Plate Weld Material.* EPRI, Palo Alto, CA: 2007. 1014982.
14. Stress Report: 51 Series Steam Generator Calculated and Measured Strains and Deflections for Steam Generator Tubesheet Channel Head Model Under Limit Conditions, Volume 1, MPR Associates, November 1969.
15. WCAP-16820-P.
16. WCAP-16053-P.
17. LTR-SGDA-07-201.

1.0 Discussion of Crevice Pressure Test Results

The tests documented in Reference 1 were performed to determine the pressure distribution in the crevice of a hydraulically expanded tubesheet region with a postulated through wall flaw near the bottom of the expansion. [

]^{a,c,e} The data from the NOP and SLB tests from both specimens [1], taken after the pressure in the crevice reached steady state conditions, are shown in Table 1and Table 2 below.

Table 1 Crevice Pressure Specimen Data from Steady State NOP Conditions

a,c,e

[

]

Table 2 Crevice Pressure Specimen Data from Steady State SLB Conditions

a,c,e

[

]

a,c,e

Figure 1 Picture of Typical Test Specimens Used in Crevice Pressure Experiments.

[

]a,c,e

a,c,e

Figure 2 Plot of Crevice Pressure Ratio as a Function of Depth Ratio into the Test Specimen for Simulated NOP conditions.

a,c,e

Figure 3 Plot of Crevice Pressure Ratio as a Function of Depth Ratio into the Test Specimen for Simulated SLB conditions.

[

]a,c,e

2.0 Discussion of Increased Crevice Pressures relative to an H*/B* Analysis

[

]a,c,e

1. [
]a,c,e
2. [
]a,c,e
3. [ ]a,c,e
4. [
]a,c,e
5. [
]a,c,e

[

]a,c,e

The contact pressure between the tube wall and the tubesheet hole is calculated in the H* and B* analysis for two reasons:

1. [ ]a,c,e
2. [
]a,c,e

The components that contribute to the contact pressure between the tube material and the tubesheet crevice are:

- [
]a,c,e

- [ ]a,c,e
- [ ]a,c,e
- [ ]a,c,e

Of these, only the contribution of the [ ]a,c,e The contribution of the thermal growth in each material will not be affected by an [ ]a,c,e Similarly, [ ]a,c,e

The unrestrained radial expansion of a tube OD due to a pressure differential across the tube wall is

a,c,e

[ ]

In the original analysis, P_o was assumed to be equal to the secondary side pressure. If the value of P_o is increased, the value will ΔR_{to}^{pr} decrease. For example, [ ]a,c,e

An interesting observation from Figures 2 and 3 is [ ]a,c,e

[

]a,c,e

3.0 Calculation of the Limiting Crevice Pressure Ratio

[

]^{a,c,e}

Figure 4 Plot of Crevice Pressure Model Comparisons using average test data results for the normal operating condition.

[a,c,e

]

Figure 5 Plot of Crevice Pressure Model Comparisons using average test data results for the SLB accident condition.

[

]a,c,e

There are many sources available for detailed discussions of the application of the mean and the median in statistics. The discussion in the paragraph below is paraphrased from a discussion board hosted by Purdue University (http://www.cyto.purdue.edu/hmarchiv/1998/0824.htm) and several text books. Similar comments can be found in reliability engineering text books (e.g. Statistics, Probability and Reliability for Civil and Environmental Engineers, McGraw-Hill, © 1997).

The median, or 50th centile, is the value that corresponds to the middle item in a ranked list (e.g., sorted by magnitude) of all recorded measurements in a data set. The median is a robust statistical measure in that it doesn't necessarily change in response to small numbers of outliers, or to skewing of the tails of a distribution, whereas the mean is tugged by both. This is why the median is typically described as a "resistant" measure. One situation where the median is perhaps the only valid measure is when data congregate at one or both extremes. However, as long as more than 50% of the data are clear of the

extremes a valid median is obtained, but any type of mean (geometric or arithmetic) will be less accurate.

A commonly used statistical tool to determine outliers in a limited population of data is the Dixon Ratio test. The Dixon Ratio test is used to assess the character (i.e., mostly average values, a small number of outliers, entirely composed of outlier values, etc.) of the data set and limit the inlfuence of potential outliers that could affect the limiting crevice pressure ratio result. The following text is adapted from the tutorial on the detection and accommodation of outliers from the web library of Virginia Polytechnic Institute and State University department of Civil and Environmental Engineering [3]. Dixon's test is generally used for detecting a small number of outliers. This test can be used when the sample size is between 3 and 25 observations [4], but is typically employed whenever a sample set is less than an ideal population to apply standard statistical tools. In a smaller data set, it is less likely to obtain a significant portion of outliers, but the presence of outliers can make a drastic change to statistical interpretations of a small data set. The data is ranked in ascending order and then sorted on the sample size. The τ statistic for the highest value or lowest value is computed. [

]^{a,c,e} The chart below gives a list of how to calculate the appropriate Dixon Ratio values.

Observations	Highest value suspect	Lowest value suspect
3 to 7	$\tau = \frac{X_n - X_{n-1}}{X_n - X_1}$	$\tau = \frac{X_2 - X_1}{X_n - X_1}$
8 to 10	$\tau = \frac{X_n - X_{n-1}}{X_n - X_2}$	$\tau = \frac{X_2 - X_1}{X_{n-1} - X_1}$
11 to 13	$\tau = \frac{X_n - X_{n-2}}{X_n - X_2}$	$\tau = \frac{X_3 - X_1}{X_{n-1} - X_1}$
14 to 20-30	$\tau = \frac{X_n - X_{n-2}}{X_n - X_3}$	$\tau = \frac{X_3 - X_1}{X_{n-2} - X_1}$

The τ statistic is compared to a critical value at a chosen value of α. If the τ statistic is less than the critical value, the null hypothesis is not rejected, and the conclusion is that no outliers are present. If the τ statistic is greater than the critical value, the null hypothesis is rejected, and the conclusion is that the most extreme value is an outlier. To check for other outliers, the Dixon test can be repeated, however, the power of this test decreases as the number of repetitions increases. .]^{a,c,e}

[

]a,c,e

Table 3 Data Set for Calculating the Dixon Ratio Test NOP results using Model 1

[ ]a,c,e

Table 4 Data Set for Calculating the Dixon Ratio Test NOP results using Model 2

[ ]a,c,e

Table 5 Data Set for Calculating the Dixon Ratio Test NOP results using Model 3

[ ]a,c,e

Table 6 Data Set for Calculating the Dixon Ratio Test SLB results using Model 1 a,c,e

[

]

Table 7 Data Set for Calculating the Dixon Ratio Test SLB results using Model 2 a,c,e

[

]

Table 8 Data Set for Calculating the Dixon Ratio Test SLB results using Model 3 a,c,e

[

]

[

]a,c,e

Table 9 Rank Ordered Data Set for NOP Condition a,c,e

[

]

Table 10 Rank Ordered Data Set for SLB Condition

a,c,e

[

]

The equation used to calculate the Dixon Ratio test value for a data set changes based on the size of the data population and whether the higher or lower values are suspect. [

]a,c,e The a,c,e
equation for determining the Dixon ratio test value for the NOP case is:

[

]

Where τ is the Dixon ratio test value, x_n refers to the largest value in the data set, x_2 refers to the second lowest value in the data set and x_1 refers to the lowest value in the data set. The equation for determining the Dixon ratio test value for the SLB case is: a,c,e

[

]

Where x_3 refers to the third lowest ranked value in the data set and x_{n-1} refers to the second largest value in the data set. Calculating the Dixon ratio test values yield the results shown in Table 11 and Table 12 below.

Table 11 Comparison of Dixon Ratio test values for NOP

a,c,e

[

]

Table 12 Comparison of Dixon Ratio test values for SLB a,c,e

[

]

[

]a,c,e The summary of the calculations is provided in Table 13. The effect of the limiting crevice pressure ratio on the H* and B* inspection distances are evaluated in section 6.0.

4.0 The Crevice Pressure Effects on the Loss Coefficient Data

The effective contact pressure between the tube and the tubesheet is a function of four phenomena:

1. thermal growth/mismatch between the tube and the tubesheet,
2. tubesheet displacement resulting in hole dilation,
3. tube expansion due to the pressure differential, and
4. residual mechanical joint strength due to the tube expansion process during installation.

[

]^{a,c,e}

See Appendix C, response to RAI No. 11, in Reference 15 for a discussion of the results of incorporating different crevice pressure assumptions into the loss coefficient versus contact pressure regression analysis. See Reference 16 for the development of the theory of elasticity model used to calculate the contact pressure associated with a primary to secondary pressure differential during a leak rate experiment. See Reference 1 for the data used to calculate the crevice pressure ratios used in the contact pressure analysis.

[

]^{a,c,e}

The crevice pressure ratios used with each applied ΔP are summarized in Table 13. The results of the varied crevice pressure with applied ΔP are summarized in Table 14. The spreadsheets and calculation tools used in the analysis are captured in the attachments to Reference 17.

Table 13 Crevice Pressure Ratio Summary for Leak Rate Analysis a,c,e

[ ]

Table 14 Summary of Contact Pressure Results for Loss Coefficient Analysis

a,c,e

SG Type	Primary Side Test Pressure (PSI)	Test Temperature (°F)	Contact Pressure (PSI)	Crevice Pressure Differential (PSI)

5.0 The Effect of the Divider Plate Factor on B* and H* Analysis

Indications of cracks in the divider plates have been reported in several steam generators located in France. These indications have been observed in steam generators located at the Chinon, Saint-Laurent, Blayais, Dampierre and Gravelines nuclear power stations. The cracks were observed on the hot leg side of the divider plate in the stub runner divider plate weld, stub runner base metal and also at or in the divider plate itself. See Figure 6 for a sketch of the region where cracking has been observed to occur.

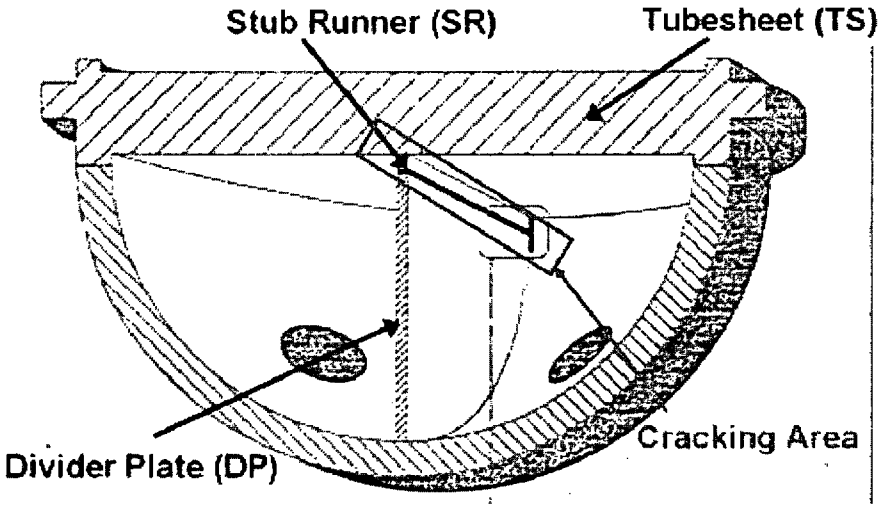

Figure 6 Sketch of Divider Plate, Channel Head and Tubesheet with potential cracking areas highlighted.

The network of cracks has been reported to extend along most of the divider plate (~6 feet) and have also been reported to be relatively shallow with depth, typically less than 2 mm (~75 mils deep).

The French utilities inspected this location to determine if any indications of cracking could be found during a visual inspection because these steam generators used an Alloy 600 material in the divider plate to stub runner weld. During the initial visual inspection it was reported that indications of cracks were observed but that they appeared to be shallow in depth. Various other methods were used in subsequent refueling outages to determine the extent of cracking and to determine the crack growth rate. Available information indicates that these inspections have been performed since 1993 using a combination of liquid penetrant examination (PT) and visual examination (VT) methods with indications of cracking observed in some of these plants. Through the winter of 2005, a total of thirty five inspections using VT and PT were performed in the French 900 megawatt (MW) and 1300 MW units with indications of cracking being found in at least four of the plants as noted above.

Primary water stress corrosion cracking (PWSCC) is a know mechanism of cracking in Alloy 600 and it is likely this is the primary contributor to cracking at this location. However, other potential contributors to cracking have been reported to be defects in the weld or base material, along with deformations associated with loose part impingement and these may be contributing factors. See Reference 13.

The maximum depth of the majority of the cracks observed in the French units has been reported to be about 2 mm (~75 mils). The maximum crack depth indication that has been observed is 7 mm (~0.28 inch) however this indication is the likely result of loose part damage on the hot leg side of the divider plate in the affected generator. Various inspection methods (VT, PT, and then UT) have been used in plants with indications of divider plate cracking. It has been reported that consecutive inspections using identical methods have not been performed to date; therefore, it is not possible to develop an accurate growth rate from the French inspection data. From the available information it can be inferred that the cycle-to-cycle growth rate of the cracks is small based on the following: The difficulty in obtaining an accurate measure of the depth of the crack due to the shallowness of the crack (smaller cracks are harder to detect than larger cracks), the continued reports of finding only shallow depth cracks, and the relatively long period of time that these cracks have been known to exist.

The majority of the cracks included by the French experience are small with a relatively small cycle-to-cycle growth rate; therefore, the effect on the divider plate function is also expected to be small. It would be expected that cracks of the size reported would not affect the general displacement response of the tubesheet since only a very small change in divider plate stiffness would be expected. In addition, it would not be expected that cracks of the size reported would rapidly grow due to mechanically induced loadings resulting from normal/upset events or during a faulted event. However, there may be a potential for long term growth of these cracks which could eventually affect tubesheet displacements and result in an increased rate of crack propagation. See Reference 13 for a conservative analysis estimate of crack growth in the divider plate.

Tubesheet displacements can directly affect multiple regions in the SG that include such areas as:

a. Stress in the tubesheet/shell and tubesheet/channelhead connections

b. Tube stresses and field repairs

c. Plug retention/acceptability issues.

The divider plate is accounted for in B* and H* analyses via a divider plate factor, which is the ratio of the maximum vertical tubesheet displacements with an intact divider plate compared to the maximum vertical displacements of a tubesheet with no divider plate present. The factor is based on the ASME stress report

provided for the SGs, which considered both to conservatively calculate stresses in the tubesheet and in the components attached to the tubesheet. The ratio of the maximum tubesheet displacement with and without the benefit of the divider plate is [ ]^{a,c,e}, which means that the maximum vertical displacement of the tubesheet with an intact divider plate is [ ]^{a,c,e} less than the maximum vertical displacement of a tubesheet without a divider plate based on the ASME Code Stress Report for the SGs. This value [ ]^{a,c,e} is used for the divider plate factor in the B* and H* analyses prior to 2007. A value of [ ]^{a,c,e} for the divider plate factor is used in the H* and B* analyses to evaluate the condition where the divider plate does not restrain the vertical tubesheet displacements of the tubesheet.

[

]^{a,c,e}

[

]^{a,c,e}

by an order of magnitude. There have been no cracking indications observed in the divider plate to channelhead welds. This is likely because the divider plate to

channelhead connections are heat treated prior to the divider plate to stub runner weld being made. Therefore, it is possible to conclude that the majority of the stiffening effect of the divider plate comes from the divider plate to channelhead connection, not the divider plate to tubesheet connection, and that this connection is not subject to the same cracking risks as the stub runner weld.

The change in divider plate factor for the case of only the channelhead to divider plate connections being intact is equal to [

]^{a,c,e}

The effect of a reduced divider plate factor with a non-degraded divider plate will [

]^{a,c,e}

To evaluate the effect of a degraded divider plate, a bounding analysis was performed which assumed that the divider plate provides [

]^{a,c,e}

Evaluation of divider plate degradation is continuing under EPRI sponsorship. The effects of long term operation with postulated larger cracks in the divider plate must be evaluated to determine if the cracks could grow to a point where either rapid crack growth could occur during operation of the SG or if increased tubesheet displacements could affect other aspects of the steam generator, such as tubesheet stress, secondary side shell stress, channel head stress, tube stress, plug retention/acceptability issues and the ARCs [6, 13].

The following conclusions are reached based on the current evaluation of divider plate degradation:

1. The original divider plate factor from the ASME Code stress report, the ratio of the maximum tubesheet displacement assuming a fully effective divider plate to that assuming no contribution from the divider plate, is [ ]^{a,c,e}

2. Based on a more detailed finite element model of the tubesheet/divider plate assembly, the revised divider plate factor is [ ]^{a,c,e}

3. The divider plate factor obtained by comparing the displacements of the tubesheet with and without the contribution of the potentially cracked region of the divider plate is [ ]^{a,c,e}

4. The preliminary conservative estimate of H* and B* assuming no structural contribution from the cracked region of the divider plate is bounded by [ ]^{a,c,e}

5. The presence or absence of the cracked region of the divider plate does not impact a 17 inch inspection depth, since sufficient margin exists between [ ]^{a,c,e} The structural model used for this assessment is the refined finite element model of the tubesheet/divider plate assembly.

6.0 Results from Implementing Changes in H* and B* Analysis

Table 15 below summarizes the limiting crevice pressure ratios [

]^{a,c,e}

Table 15 Limiting Crevice Pressure Ratios from 3 Models

a,c,e

[

]

From Section 1, the pressure ratio [

]^{a,c,e}

Therefore, the smallest pressure drop [

]^{a,c,e}

Table 16 H* and B* Prediction for Different Models of Crevice Pressure

(Data based on improved tubesheet/divider plate structural model) a,c,e

[

]

(H* and B* are referenced to the bottom of the expansion transition)

The results [

]a,c,e

The following figures show [

]a,c,e

Figure 7 shows [

]a,c,e

a,c,e

Figure 7 Unaltered Data and Methods for B* and H*. Crevice Pressure = $P_{Pri} - P_{Sec}$, DP = 0.76.

[

]a,c,e

a,c,e

Figure 8 Updated Input Data and Methods for B* and H*. Crevice Pressure = $CP*P_{Pri}$, DP = 0.399.

The results for the updated analysis input with a divider plate factor of [ ]^{a,c,e} (i.e., no structural restraint provided by the potentially cracked region of the divider plate) are shown in Figure 9

[ ]^{a,c,e}

Figure 9 Updated Input Data and Methods for B* and H*. Crevice Pressure = CP^*P_{Pri}, DP = 0.64.

Comparing the results shown in Figure 7 and Figure 9 proves that the changes in the B* and H* inputs due to the increased crevice pressure and divider plate effects are reasonable and follow similar trends compared to the prior results. The results shown in Figure 9 prove that the generic bounding analysis conditions (using mean ASME material properties and design inputs) in the event that the divider plate to stub runner is fully degraded are still below the previously reported bounding value of 12.50 inches. [

]^{a,c,e}

The choice of crevice pressure model maximizes the B* and H* depths by minimizing the structural and leakage resistance of the tube to tubesheet crevice joint. An alternative method to using a limiting constant crevice pressure ratio is to use a depth based approach. That is, to vary the crevice pressure ratio at each depth based on the available test data so that the pressure difference across the tube varies as a function of tubesheet elevation. The depth based crevice

pressure approach [

]^{a,c,e}

1. [

]^{a,c,e}

2. [

]^{a,c,e}

3. [

]^{a,c,e}

The constant crevice pressure approach does yield different results from the depth based approach during accident conditions. [

]^{a,c,e}

In conclusion, [

]^{a,c,e}

7.0 Summary and Conclusions

The following summarizes this "White Paper" regarding the effects of new test data and updated analysis methods on the H*/B* technical justifications:

1. Recently obtained test data indicate that postulated leakage through a tube crack in the tubesheet expansion region [

   ]^{a,c,e}

2. Updated finite element analysis of the tubesheet/divider plate assembly shows that the ratio of the maximum deflection of the tubesheet with an un-degraded divider plate to the maximum deflection with no structural restraint from the divider plate is much [ ]^{a,c,e} than the factor derived from the original ASME Code Stress Report.

3. Analysis using the updated divider plate factor shows that the bounding value for H*/B* is about [ ]^{a,c,e} (using mean ASME code material properties and design inputs). Only the "true" B* value will be affected if the divider plate is assumed to be non-functional. Significant margin exists for [ ]^{a,c,e} inch inspection depth.

4. Several models were developed to represent the new crevice pressure test data. The most conservative model, that minimizes the pressure drop from the primary side to the crevice, was identified.

5. Integrated analysis accounting for both the divider plate degradation and revised crevice pressure show that the justification for H* and B* is still valid when the most conservative crevice pressure model and the refined structural model for the tubesheet/divider plate assembly are used.

APPENDIX C

Hot and Cold Leg H* and B* Results

September 24, 2007

HOT LEG RESULTS

Table 7-6 Cumulative Forces Resisting Pull Out from the TTS Wolf Creek Hot Leg Normal Conditions – Reduced T_{hot}, P_{sec} = 792 psig

a,c,e

[

]

Table 7-7 Cumulative Forces Resisting Pull Out from the TTS Wolf Creek Hot Leg Normal Conditions – T_{hot} = 620°F, P_{sec} = 935 psig

a,c,e

Table 7-8 Cumulative Forces Resisting Pull Out from the TTS Wolf Creek Faulted (SLB) Conditions, Psec = 0 psig

a,c,e

C-4

Table 7-9 Cumulative Forces Resisting Pull Out from the TTS Wolf Creek FLB Conditions, Reduced T_{hot}

a,c,e

Table 7-10 Cumulative Forces Resisting Pull Out from the TTS Wolf Creek FLB Conditions, T_{hot} = 620°F

a,c,e

[ ]

Table 7-11 Summary of H* Calculations for Wolf Creek a,c,e

[

]

Table 7-12 H* Summary Table
Structural Criteria Required Engagement

Zone	Limiting Loading Condition	Engagement from TTS (inches)[3,4]
		Hot Leg

a,c,e

a,c,e

Figure 7-3 Contact Pressures for NOp at Wolf Creek, Reduced T_{hot}, P_{sec} = 792 psig

a,c,e

Figure 7-4 Contact Pressures for NOp at Wolf Creek, T_{hot} = 620°F, P_{sec} = 935 psig

a,c,e

Figure 7-5 Contact Pressures for SLB Faulted Condition at Wolf Creek

a,c,e

Figure 7-6 Contact Pressures for FLB Condition at Wolf Creek, Reduced T_{hot}

a,c,e

Figure 7-7 Contact Pressures for FLB Condition at Wolf Creek, T_{hot} = 620 F

a,c,e

Figure 8-1 Change in Contact Pressure at 20.0 Inches Below the TTS

a,c,e

Figure 8-2 Change in Contact Pressure at 16.9 Inches Below the TTS

a,c,e

Figure 8-3 Change in Contact Pressure at 12.6 Inches Below the TTS

a,c,e

Figure 8-4 Change in Contact Pressure at 10.5 Inches Below the TTS

a,c,e

Figure 8-5 Change in Contact Pressure at 8.25 Inches Below the TTS

a,c,e

Figure 8-6 Change in Contact Pressure at 6.0 Inches Below the TTS

Table 11-1 Calculated H* and B* Depths (Hot Leg)

a,c,e

Tubesheet Radius	Hot Leg	
	H* [2] (in. from TTS)	B* (in. from TTS)

a,c,e

Figure 11-1 Comparison of H* and B* Hot Leg Results

COLD LEG RESULTS

Table 7-6a Cumulative Forces Resisting Pull Out from the TTS Wolf Creek Cold Leg Normal Conditions – Reduced T_{hot}, P_{sec} = 792 psig

a.c.e.

Table 7-7a Cumulative Forces Resisting Pull Out from the TTS Wolf Creek Cold Leg Normal Conditions – T_{hot} = 620°F, P_{scc} = 935 psig

a.c.e.

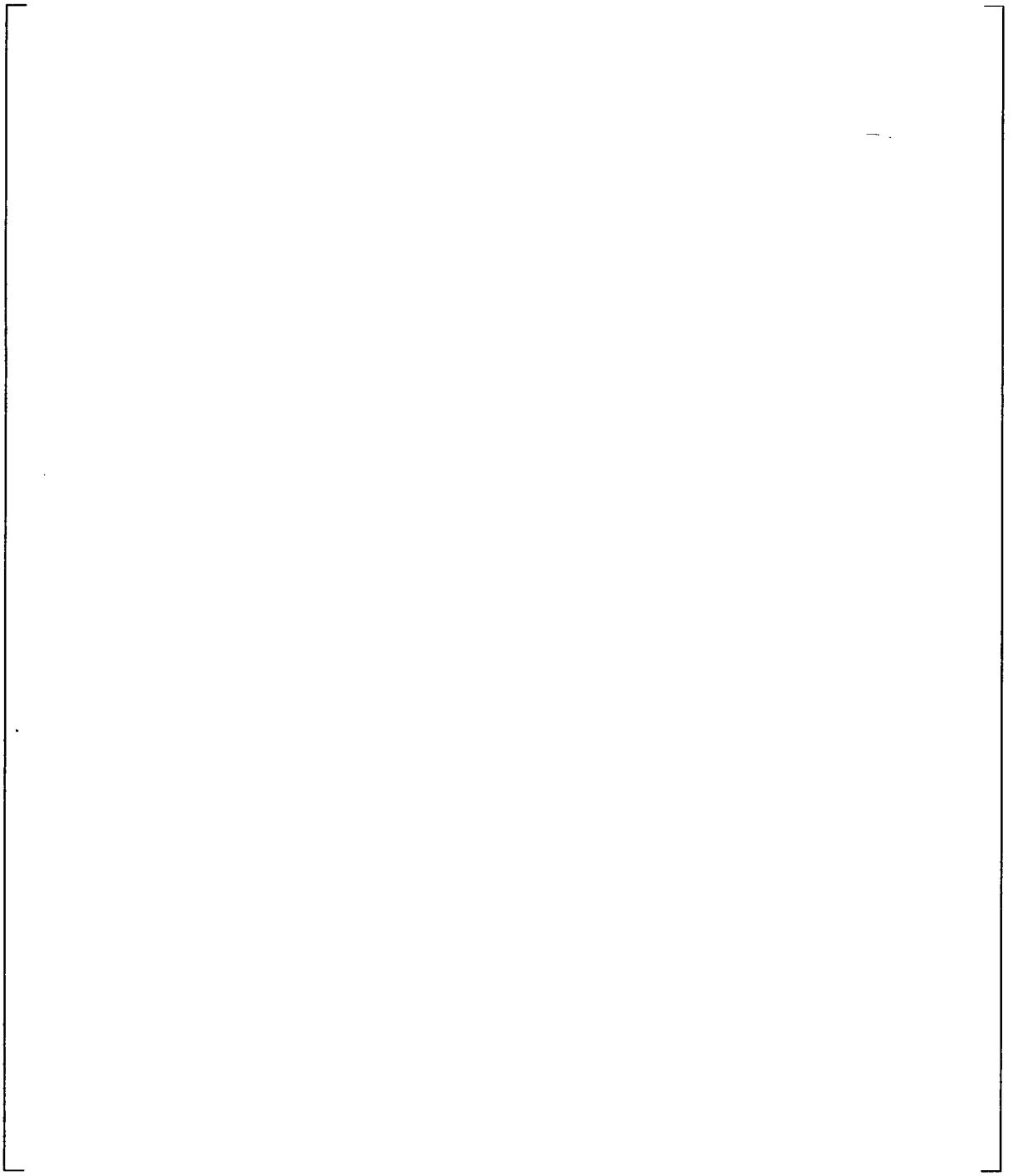

Table 7-8a Cumulative Forces Resisting Pull Out from the TTS Wolf Creek Faulted (SLB) Conditions, Psec = 0 psig

a.c.e.

Table 7-9a Cumulative Forces Resisting Pull Out from the TTS Wolf Creek Cold Leg FLB Conditions, Reduced T_{hot}

a.c.e.

Table 7-10a Cumulative Forces Resisting Pull Out from the TTS Wolf Creek Cold Leg FLB Conditions, T_{hot} = 620°F

a.c.e.

Table 7-11a Summary of H* Calculations for Wolf Creek

a,c,e,

[

]

Table 7-12a H* Summary Table
Structural Criteria Required Engagement

a,c,e

Figure 7-3a Contact Pressures for Nop at Wolf Creek, Reduced T_{hot}, P_{sec} = 792 psig

a,c,e

Figure 7-4a Contact Pressures for Nop at Wolf Creek, T_{hot} = 620°F, P_{sec} = 935 psig

a,c,e

Figure 7-5a Contact Pressures for SLB Faulted Condition at Wolf Creek

a,c,e

Figure 7-6a Contact Pressures for FLB Condition at Wolf Creek, Reduced T_{hot}

a,c,e

7-7a Contact Pressures for FLB Condition at Wolf Creek, T_{hot} = 620 F

a,c,e

Figure 8-1a Change in Contact Pressure at 20.0 Inches Below the TTS

a,c,e

Figure 8-2a Change in Contact Pressure at 16.9 Inches Below the TTS

a,c,e

Figure 8-3a Change in Contact Pressure at 12.6 Inches Below the TTS

a,c,e

Figure 8-4a Change in Contact Pressure at 10.5 Inches Below the TTS

a,c,e

Figure 8-5a Change in Contact Pressure at 8.25 Inches Below the TTS

a,c,e

Figure 8-6a Change in Contact Pressure at 6.0 Inches Below the TTS

a,c,e

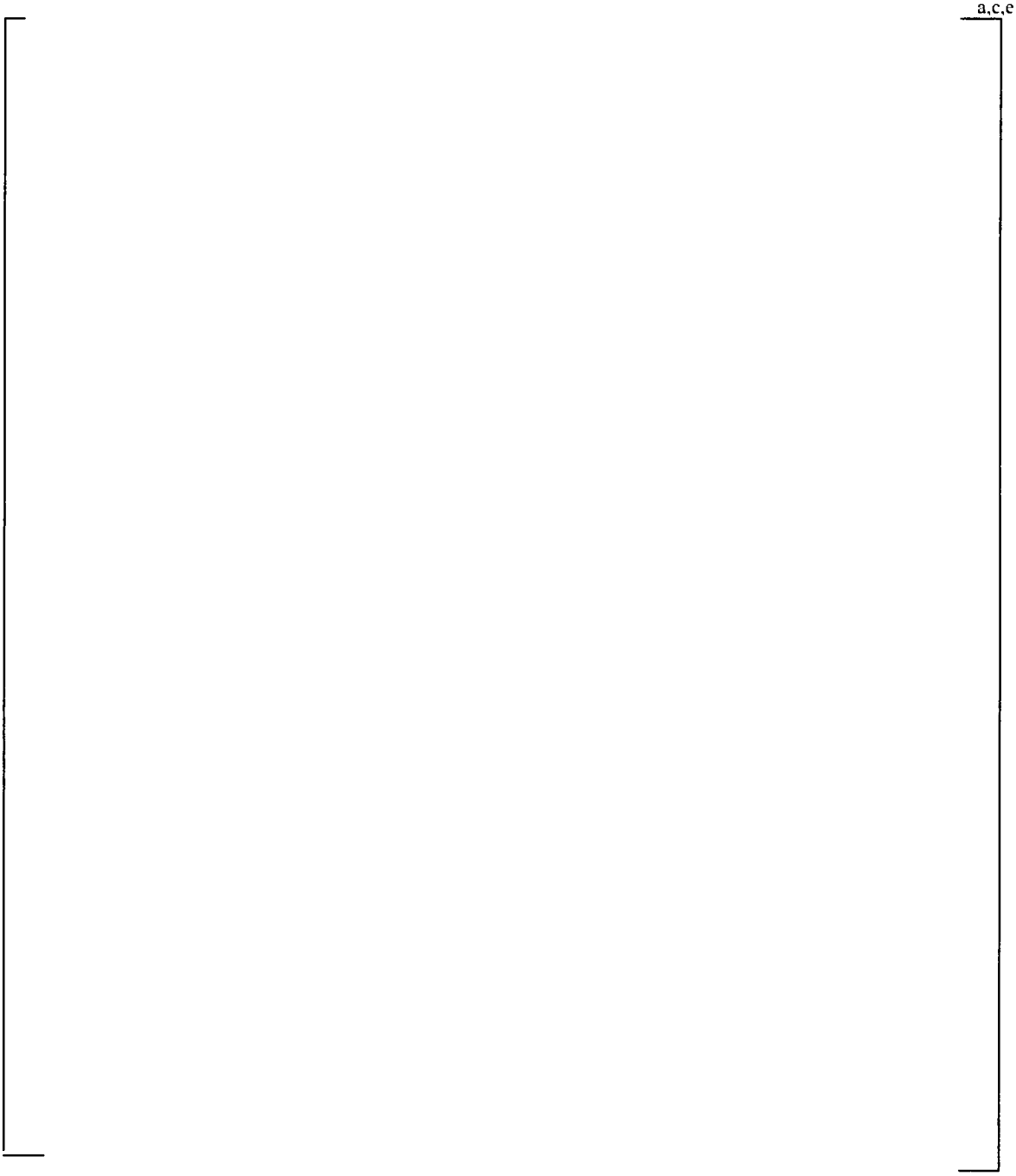

a,c,e

Figure 11-2 Comparison of H* and B* Cold Leg Results

Table 11-2 Inspection Program for H*/B*

a.c.e

a,c,e

Figure 11-3 Wolf Creek Hot Leg Inspection Depth Profile

a,c,e

Figure 11-4 Wolf Creek Cold Leg Inspection Depth Profile

a,c,e

Figure 11-5 Wolf Creek Hot Leg Inspection Depth Zones

a,c,e

Figure 11-6 Wolf Creek Cold Leg Inspection Depth Zones

Enclosure III to ET 07-0043

Westinghouse Electric Company LLC LTR CAW-07-2335, "Application for Withholding Proprietary Information from Public Disclosure"

Westinghouse Electric Company
Nuclear Services
P.O. Box 355
Pittsburgh, Pennsylvania 15230-0355
USA

U.S. Nuclear Regulatory Commission
Document Control Desk
Washington, DC 20555-0001

Direct tel: (412) 374-4643
Direct fax: (412) 374-4011
e-mail: greshaja@westinghouse.com

Our ref: CAW-07-2335

September 25, 2007

APPLICATION FOR WITHHOLDING PROPRIETARY INFORMATION FROM PUBLIC DISCLOSURE

Subject: LTR-CDME-07-198 P-Attachment, "Response to NRC Request for Additional Information Relating to LTR-CDME-07-72 P-Attachment and LTR-CDME-05-209-P of the Wolf Creek Generating Station (WCGS) Permanent B* License Amendment Request," dated September 24, 2007 (Proprietary)

The proprietary information for which withholding is being requested in the above-referenced report is further identified in Affidavit CAW-07-2335 signed by the owner of the proprietary information, Westinghouse Electric Company LLC. The affidavit, which accompanies this letter, sets forth the basis on which the information may be withheld from public disclosure by the Commission and addresses with specificity the considerations listed in paragraph (b)(4) of 10 CFR Section 2.390 of the Commission's regulations.

Accordingly, this letter authorizes the utilization of the accompanying affidavit by Wolf Creek Nuclear Operating Corporation (WCNOC).

Correspondence with respect to the proprietary aspects of the application for withholding or the Westinghouse affidavit should reference this letter, CAW-07-2335, and should be addressed to J. A. Gresham, Manager, Regulatory Compliance and Plant Licensing, Westinghouse Electric Company LLC, P.O. Box 355, Pittsburgh, Pennsylvania 15230-0355.

Very truly yours,

J.A. Gresham, Manager
Regulatory Compliance and Plant Licensing

Enclosures

cc: Jon Thompson (NRC O-7E1A)

bcc: J. A. Gresham (ECE 4-7A) 1L
R. Bastien, 1L (Nivelles, Belgium)
C. Brinkman, 1L (Westinghouse Electric Co., 12300 Twinbrook Parkway, Suite 330, Rockville, MD 20852)
RCPL Administrative Aide (ECE 4-7A) 1L (letter and affidavit only)
G. W. Whiteman, Waltz Mill
H. O. Lagally, Waltz Mill
C. D. Cassino, Waltz Mill
P. J. McDonough, EC 561 C

CAW-07-2335

AFFIDAVIT

COMMONWEALTH OF PENNSYLVANIA:

ss

COUNTY OF ALLEGHENY:

Before me, the undersigned authority, personally appeared J. A. Gresham, who, being by me duly sworn according to law, deposes and says that he is authorized to execute this Affidavit on behalf of Westinghouse Electric Company LLC (Westinghouse), and that the averments of fact set forth in this Affidavit are true and correct to the best of his knowledge, information, and belief:

J. A. Gresham, Manager
Regulatory Compliance and Plant Licensing

Sworn to and subscribed before me
this 25th day of September, 2007

Notary Public

COMMONWEALTH OF PENNSYLVANIA
Notarial Seal
Sharon L. Markle, Notary Public
Monroeville Boro, Allegheny County
My Commission Expires Jan. 29, 2011
Member, Pennsylvania Association of Notaries

(1) I am Manager, Regulatory Compliance and Plant Licensing, in Nuclear Services, Westinghouse Electric Company LLC (Westinghouse), and as such, I have been specifically delegated the function of reviewing the proprietary information sought to be withheld from public disclosure in connection with nuclear power plant licensing and rule making proceedings, and am authorized to apply for its withholding on behalf of Westinghouse.

(2) I am making this Affidavit in conformance with the provisions of 10 CFR Section 2.390 of the Commission's regulations and in conjunction with the Westinghouse "Application for Withholding" accompanying this Affidavit.

(3) I have personal knowledge of the criteria and procedures utilized by Westinghouse in designating information as a trade secret, privileged or as confidential commercial or financial information.

(4) Pursuant to the provisions of paragraph (b)(4) of Section 2.390 of the Commission's regulations, the following is furnished for consideration by the Commission in determining whether the information sought to be withheld from public disclosure should be withheld.

(i) The information sought to be withheld from public disclosure is owned and has been held in confidence by Westinghouse.

(ii) The information is of a type customarily held in confidence by Westinghouse and not customarily disclosed to the public. Westinghouse has a rational basis for determining the types of information customarily held in confidence by it and, in that connection, utilizes a system to determine when and whether to hold certain types of information in confidence. The application of that system and the substance of that system constitutes Westinghouse policy and provides the rational basis required.

Under that system, information is held in confidence if it falls in one or more of several types, the release of which might result in the loss of an existing or potential competitive advantage, as follows:

(a) The information reveals the distinguishing aspects of a process (or component, structure, tool, method, etc.) where prevention of its use by any of Westinghouse's competitors without license from Westinghouse constitutes a competitive economic advantage over other companies.

(b) It consists of supporting data, including test data, relative to a process (or component, structure, tool, method, etc.), the application of which data secures a competitive economic advantage, e.g., by optimization or improved marketability.

(c) Its use by a competitor would reduce his expenditure of resources or improve his competitive position in the design, manufacture, shipment, installation, assurance of quality, or licensing a similar product.

(d) It reveals cost or price information, production capacities, budget levels, or commercial strategies of Westinghouse, its customers or suppliers.

(e) It reveals aspects of past, present, or future Westinghouse or customer funded development plans and programs of potential commercial value to Westinghouse.

(f) It contains patentable ideas, for which patent protection may be desirable.

There are sound policy reasons behind the Westinghouse system which include the following:

(a) The use of such information by Westinghouse gives Westinghouse a competitive advantage over its competitors. It is, therefore, withheld from disclosure to protect the Westinghouse competitive position.

(b) It is information that is marketable in many ways. The extent to which such information is available to competitors diminishes the Westinghouse ability to sell products and services involving the use of the information.

(c) Use by our competitor would put Westinghouse at a competitive disadvantage by reducing his expenditure of resources at our expense.

(d) Each component of proprietary information pertinent to a particular competitive advantage is potentially as valuable as the total competitive advantage. If competitors acquire components of proprietary information, any one component may be the key to the entire puzzle, thereby depriving Westinghouse of a competitive advantage.

(e) Unrestricted disclosure would jeopardize the position of prominence of Westinghouse in the world market, and thereby give a market advantage to the competition of those countries.

(f) The Westinghouse capacity to invest corporate assets in research and development depends upon the success in obtaining and maintaining a competitive advantage.

(iii) The information is being transmitted to the Commission in confidence and, under the provisions of 10 CFR Section 2.390, it is to be received in confidence by the Commission.

(iv) The information sought to be protected is not available in public sources or available information has not been previously employed in the same original manner or method to the best of our knowledge and belief.

(v) The proprietary information sought to be withheld in this submittal is that which is appropriately marked in LTR-CDME-07-198 P-Attachment, "Response to NRC Request for Additional Information Relating to LTR-CDME-07-72 P-Attachment and LTR-CDME-05-209-P of the Wolf Creek Generating Station (WCGS) Permanent B* License Amendment Request," dated September 24, 2007 (Proprietary), for submittal to the Commission, being transmitted by Wolf Creek Nuclear Operating Corporation (WCNOC) Application for Withholding Proprietary Information from Public Disclosure to the Document Control Desk. The proprietary information as submitted for use by Westinghouse for the Wolf Creek Generating Station is expected to be applicable to other licensee submittals in support of implementing a limited inspection of the tube joint within the tubesheet region of the steam generators and is provided in response to a NRC request for additional information on both LTR-CDME-07-72 P-Attachment, "Response to NRC Request for Additional Information Relating to LTR-CDME-05-209-P of the Wolf Creek Generating Station (WCGS) Permanent B* License Amendment Request," and LTR-CDME-05-209-P, "Steam Generator Tube Alternate Repair Criteria for the Portion of the Tube Within the Tubesheet at Wolf Creek Generating Station," dated July 2007.

This information is part of that which will enable Westinghouse to:

(a) Provide documentation of the analyses, methods, and testing for the implementation of an alternate repair criteria for the portion if the tubes within the tubesheet of the Wolf Creek Generating Station steam generators.

(b) Assist the customer in obtaining NRC approval of the Technical Specification changes associated with the alternate repair criteria.

Further this information has substantial commercial value as follows:

(a) Westinghouse plans to sell the use of similar information to its customers for the purposes of meeting NRC requirements for licensing documentation.

(b) Westinghouse can sell support and defense of the technology to its customers in the licensing process.

Public disclosure of this proprietary information is likely to cause substantial harm to the competitive position of Westinghouse because it would enhance the ability of competitors to provide similar calculation, evaluation and licensing defense services for commercial power reactors without commensurate expenses. Also, public disclosure of the information would enable others to use the information to meet NRC requirements for licensing documentation without purchasing the right to use the information.

The development of the technology described in part by the information is the result of applying the results of many years of experience in an intensive Westinghouse effort and the expenditure of a considerable sum of money.

In order for competitors of Westinghouse to duplicate this information, similar technical programs would have to be performed and a significant manpower effort, having the requisite talent and experience, would have to be expended.

Further the deponent sayeth not.

PROPRIETARY INFORMATION NOTICE

Transmitted herewith are proprietary and/or non-proprietary versions of documents furnished to the NRC in connection with requests for generic and/or plant-specific review and approval.

In order to conform to the requirements of 10 CFR 2.390 of the Commission's regulations concerning the protection of proprietary information so submitted to the NRC, the information which is proprietary in the proprietary versions is contained within brackets, and where the proprietary information has been deleted in the non-proprietary versions, only the brackets remain (the information that was contained within the brackets in the proprietary versions having been deleted). The justification for claiming the information so designated as proprietary is indicated in both versions by means of lower case letters (a) through (f) located as a superscript immediately following the brackets enclosing each item of information being identified as proprietary or in the margin opposite such information. These lower case letters refer to the types of information Westinghouse customarily holds in confidence identified in Sections (4)(ii)(a) through (4)(ii)(f) of the affidavit accompanying this transmittal pursuant to 10 CFR 2.390(b)(1).

COPYRIGHT NOTICE

Enclosure IV to ET 07-0043

Detection and Accommodation of Outliers in Normally Distributed Data Sets

Environmental Sampling & Monitoring Primer

Detection and Accommodation of Outliers in Normally Distributed Data Sets

by Agata Fallon and Christine Spada

Table of contents

Introduction

Anyone, who has heard the statement: □You can not just throw data away without an explanation or a reason□, is familiar with the headaches caused by outliers. Outliers are the observations that appear to be inconsistent with the reminder of the collected data (Iglewicz, 1993). The term outlier is used collectively for discordant observations and for contaminants. A discordant observation is defined as an observation that appears surprising or discrepant to the investigator (Iglewicz, 1983). A contaminant is defined as an observation from a different distribution then the rest of the data. Contaminants may or may not be noted by the investigator (Barnett, 1984). Figure 1 shows some examples of outliers.

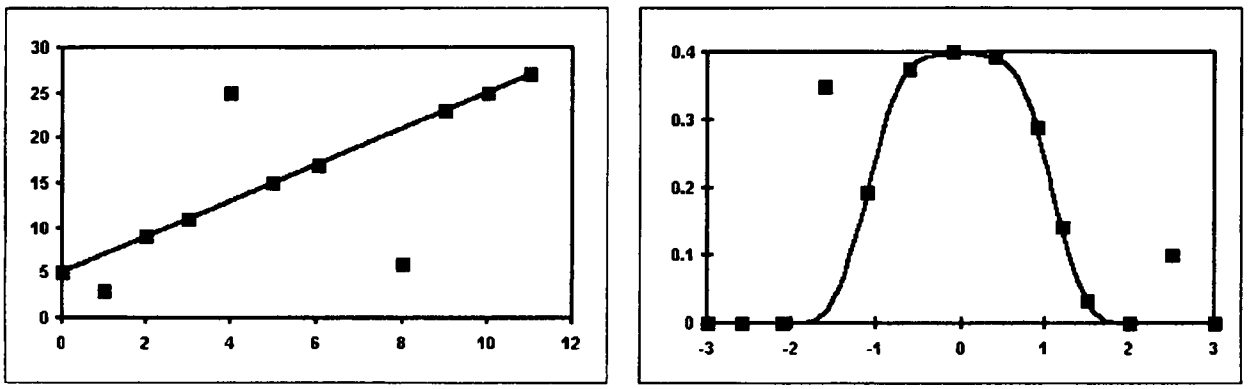

Figure 1. Examples of outliers Note: Outliers are indicated in red

Sources of outliers

Possible sources of outliers are: recording and measurement errors, incorrect distribution assumption, unknown data structure, or novel phenomenon (Iglewicz, 1993). Recording and measurement errors are often the first suspected source of outliers. Incorrect assumption about the data distribution can lead to mislabeling data as outliers. The data which does not fit well into the assumed distribution may fit well into a different distribution, as shown in Figure 2.

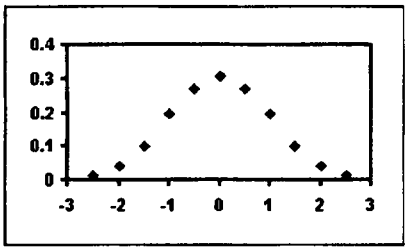

Figure 2. The effect of assumed data distribution on the presence of apparent outliers.

Unknown data structure and correlations can cause apparent outliers. A data set could be made up of subsets, which are subject to different mechanisms and should be analyzed independently of each other, as shown in Figure 3.

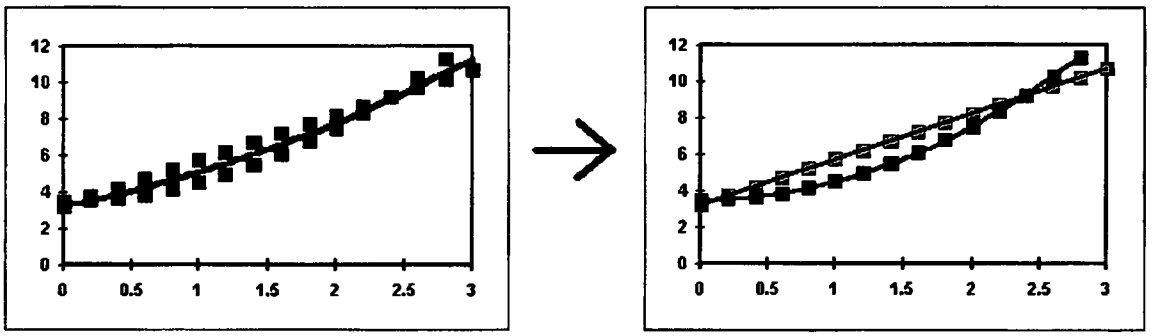

Figure 3. Effect of data subsets on the presence of apparent outliers

A data set indicative of a novel phenomenon can be often labeled as an outlier. For example, the measurements indicating existence of the hole in the ozone layer were initially thought to be outliers and they were automatically discarded. This oversight delayed the discovery of the phenomenon by several years (Berthouex, 1994)

Managing outliers

There are two ways of managing data outliers. In the laboratory, good record keeping for each experiment is recommended. All data should be recorded with any possible explanation or additional information. In the data analysis, robust statistical methods are recommended. These methods are minimally effected by outliers and will be introduced in a later part of this report.

Labeling outliers

The first step in data analysis is to label suspected outliers for further study. Three different methods are available to the investigator for normally distributed data: z-score method, modified z-score method, and boxplot method (Iglewicz, 1993, Barnett, 1984). These techniques are based on a robust regresion methods. All of the experimental observations are standardized and the standardized values outside a predetermined bound are labeled as outliers (Rousseeuw, 1987).

In a z-score test, the mean and standard deviation of the entire data set are used to obtain a z-score for each data point, according to following formula:

$$z_i = \frac{(x_i - \bar{x})}{s}$$

where

$$s = \sqrt{\frac{\sum_{i=1}^{n}(x_i - \bar{x})^2}{n-1}}$$

A test heuristic states that an observation with a z-score greater than three should be labeled as an outlier. This method is not a reliable way of labeling outliers since both the mean and standard deviation are effected by the outliers.

In a modified z-score test the z-score is determined based on outlier resistant estimators. The median of absolute deviation about the median (MAD) is such an estimator.

$$MAD = median\{|x_i - \bar{x}|\}$$

MAD is calculated and used in place of standard deviation in z-score calculations, as shown below in Figure 4.

Data (xi)		
3.2		
3.3		
8.1		
3.2		
2.9		
3.7		
3.1		
3.5		
3.3		
9.2		

Figure 4. Modified z-score calculation.

The test heuristic states that an observation with a modified z-score greater than three and a half should be labeled as an outlier. This is a reliable test since the parameters used to calculate the modified z-score are minimally effected by the outliers.

In a boxplot test the graphical representation of data is used to label an observation as an outlier as shown in Figure 5. A box in drawn around the interquartile range. A line inside the box indicates the median value. Error bars are drawn at the 5% and the 95% confidence intervals. Any data outside the error bars are plotted as single points and labeled as possible ouliers.

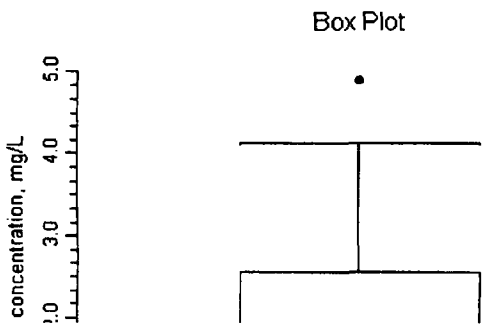

Figure 5. Example of a boxplot.

Accommodating outliers

Outliers can sometimes be accommodated in the data analysis. This process prevents the outliers from biasing the estimated population parameters. Some ways of accommodating outliers are the use of trimmed means, scale estimators, or confidence intervals. In calculations of a trimmed mean a fixed percentage of data is dropped from each end of an ordered data. The mean value is calculated for the remaining data. This trimming will drop the outliers from the data and it will often increase the efficiency of estimating the population mean. In calculations of scale estimators the median of the absolute deviation about the sample median (MAD) is used to calculate a measure of variability in the sample. This measure of variability is resistant to outliers and can be used in place of standard deviation, as it was done in the modified z-score test, for example:

$$S_{bi} = \frac{\sqrt{n\sum(x_i - \bar{x})^2(1-u_i^2)^4}}{\left|(1-u_i^2)(1-5u_i^2)\right|}$$

where

$$u = \frac{x_i - \bar{x}}{9\,MAD}$$

The confidence interval can be adjusted using the Winsorized variance to minimize the effect of the outliers. This type of variance utilizes the trimmed mean in place of the population mean.

Detecting outliers

There are numerous tests for identifying outliers. Four common outlier tests for normal distributions are the Rosner test, Dixon test, Grubbs test, and the box plot rule. These techniques are based on hypothesis testing rather the regression methods.

Rosner's Test

Rosner□s Test for detecting up to k outliers can be used when the number of data points is 25 or more. This test identifies outliers that are both high and low, it is therefore always two-tailed (Gibbons, 1994). The data are ranked in ascending order and the mean and standard deviation are determined. The procedure entails removing from the data set the observation, x, that is farthest from the mean. Then a test statistic, R, is calculated:

$$R_{i+1} = \frac{\left|x^{(i)} - \bar{x}^{(i)}\right|}{s^{(i)}}$$

The R statistic is then compared with a critical value (Gilbert, 1987). The null hypothesis, stating that the data fits a normal distribution, is then tested. If R is less than the critical value, the null hypothesis cannot be rejected, and therefore there are no outliers. If R is greater than the critical value, the null hypothesis is rejected and the presence of k outliers is accepted. This test can also be used with log-normally distributed data, when the logarithms of the data are used for computation.

Dixon's Test

Dixon□s test is generally used for detecting a small number of outliers (Gibbons, 1994). This test can be used when the sample size is between 3 and 25 observations. The data is ranked in ascending order, then based on the sample size, the tau statistic for the highest value or lowest value is computed.

Observations	Highest value suspect	Lowest value suspect
3 to 7	$\tau = \frac{x_n - x_{n-1}}{x_n - x_1}$	$\tau = \frac{x_2 - x_1}{x_n - x_1}$
8 to 10	$\tau = \frac{x_n - x_{n-1}}{x_n - x_2}$	$\tau = \frac{x_2 - x_1}{x_{n-1} - x_1}$
11 to 13	$\tau = \frac{x_n - x_{n-2}}{x_n - x_2}$	$\tau = \frac{x_3 - x_1}{x_{n-1} - x_1}$
14 to 20-30	$\tau = \frac{x_n - x_{n-2}}{x_n - x_3}$	$\tau = \frac{x_3 - x_1}{x_{n-2} - x_1}$

The tau statistic is compared to a critical value at a chosen value of alpha (Gibbons, 1994). If the tau statistic is less than the critical value, the null hypothesis is not rejected, and the conclusion is that no outliers are present. If the tau statistic is greater than the critical value, the null hypothesis is rejected, and the conclusion is the most extreme value is an outlier. To check for other outliers, the Dixon test can be repeated, however, the power of this test decreases as the number of repetitions increases.

Boxplot Rule

The boxplot rule is a visual test to inspect for outliers, see Figure 5 for example of a boxplot. The interquartile range is included into a box and the 5% and 95% confidence intervals are indicated with error bars outside of the box. Values that lie outside of the confidence interval are possible outliers (Iglewicz, 1993).

95% confidence interval limit: $\frac{x - Q_3}{Q_3 - Q_1} > k$ and 5% confidence interval limit: $\frac{Q_1 - x}{Q_3 - Q_1} > k$

Grubbs' Test

Grubbs□ test is recommended by the EPA as a statistical test for outliers (US EPA, 1992). The EPA suggests taking the logarithms of environmental data, which are often log-normally distributed. The data are ranked in ascending order and the mean and standard deviation are calculated. The lowest or highest data point can be tested as an outlier.

The tau statistic for the smallest value is: $T = \frac{\bar{X} - X_1}{s}$. The tau statistic for the largest value is: $T = \frac{X_n - \bar{X}}{s}$

The tau statistic is compared with a critical tau value for the sample size and selected alpha (Taylor, 1987). If the tau statistic is greater than the tau critical, the null hypothesis is rejected and the conclusion is that the datum under consideration is an outlier. Figure 6 shows an example of a Grubbs' test

Data		
2.15		
11.76		
5.08		
3.12		
12.87		
32.13		
219		
19.69		
179		
9609		
327		
74.2		
102		
47.8		
8.97		

Figure 6. Grubbs' test calculation.

Conclusions

All of the above discussed statistical tests are used to determine if experimental observations are statistical outliers in normally distributed data sets. If an observation is statistically determined to be an outlier, the EPA suggests determining an explanation for this outlier before its exclusion from further analysis (US EPA, 1992). If an explanation cannot be found, then the observation should be treated as an extreme but valid measurement and it should be in further analysis (US EPA, 1992).

The tests for normal data set are easy to use and powerful, however, the tests for non-normal data more difficult and not as powerful (Iglewicz, 1993). Some of these tests are included in Barnett and Lewis (1984). In many situations the data can be transformed to approximate a normal distribution and it can be analyzed using the techniques presented above (Iglewicz, 1993).

Variables

- alpha = the probability of false positive conclusion for a statistical test
- i = rank of the observation
- k = critical value in the boxplot rule
- MAD = median of the absolute deviation about the median
- n = number of observations in a data set
- R_{i+1} = Rosner's test statistic for determining if i+1 most extreme values are outliers
- s = standard deviation
- $s^{(i)}$ = standard deviation of n-i data points after the i most extreme have been deleted
- S_{bi} = bi-weight estimator of location
- tau = the test statistic ratio for Dixon's test
- u_i = quotient of the deviation about the mean and MAD
- x = the farthest data point from the mean in Rosner's test or a data point outside the upper or lower cutoff in the boxplot rule
- x_i = ith observation in the data set when data ranked in ascending order
- $x^{(i)}$ = the most outlying data point after the i most exterme have been deleted
- $xbar^{(i)}$ = the mean of n-i data points after i most estreme have been deleted
- x_m, x = median
- x_n = the highest data point when data ranked in ascending order
- x_{n-1} = the second highest data point when data ranked in ascending order

- z_i = z-score of the ith observation

Links to related topics at other Web pages

1. Outliers from Multivariate Statistics: a Practical Guide
2. Outliers and Data Having Undue Influence
3. Outliers and Influence
4. Novel Graphical Model for Identification of Outliers in a Time Series
5. Q-Test

References

1. Barnett, V. and Lewis, T.: 1984, *Outliers in Statistical Data*, John Wiley & Sons, New York.
2. Berthouex, P.M. and Brown L.C.:1994, *Statistics for Environmental Engineers*, CRC Press, London.
3. Environmental Protection Agency.: 1992, *Statistical Training Course for Ground-Water Monitoring Data Analysis*, EPA/530-R-93-003, Office of Solid Waste, Washington, DC.
4. Gilbert, R. O.: 1987, *Statistical Methods for Environmental Pollution Monitoring*, Van Nostrand Reinhold, New York.
5. Gibbons, R. D.: 1994, *Statistical Methods for Groundwater Monitoring*, John Wiley & Sons, New York.
6. Iglewicz, B. and Hoaglin, D. C.: 1993 *How to Detect and Handle Outliers*, American Society for Quality Control, Milwaukee, WI.
7. Rousseeuw, P.J. and Leroy, A.M.:1987 *Robust Regression and Outlier Detection*, John Wiley & Sons, New York.
8. Taylor, J. K.: 1987, *Quality Assurance of Chemical Measurements*, Lewis Publishers, Chelsea, MI.


Sampling & Monitoring Primer Table of Contents


Previous Topic


Next Topic

Send comments or suggestions to:
Student Authors: Agata Fallon, afallon@vt.edu, and Christine Spada, cspada@vt.edu
Faculty Advisor: Daniel Gallagher, dang@vt.edu

Last Modified: 09-10-1997

A Note on the Robustness of Dixon's Ratio Test in Small Samples
[COPYRIGHT INFORMATION]

A Note on the Robustness of Dixon's Ratio Test in Small Samples

Michael R. Chernick

The American Statistician, Vol. 36, No. 2. (May, 1982), p. 140.

A Note on the Robustness of Dixon's Ratio Test in Small Samples

MICHAEL R. CHERNICK*

Dixon (1950) introduced his ratio statistic $r_{10} = (X_{(n)} - X_{(n-1)})/(X_{(n)} - X_{(1)})$ to test for outlying observations, where $X_{(1)}, X_{(2)}, X_{(3)}, \ldots, X_{(n)}$ are the order statistics from a sample of size n. That article illustrates the effectiveness of r_{10} and similar ratios for testing a null hypothesis that all the data come from a single normal population versus the alternative that at least one observation comes from a normal distribution with a shift in mean (contamination model A) or with a larger variance (contamination model B). Dixon (1951) derives the exact density of r_{10} under the null hypothesis for $n = 3$, 4, and 5 and gives tables for larger values of n. Likes (1966) gives tables of Dixon's ratio when the data are assumed to come from an exponential distribution. See the text of Barnett and Lewis (1978) for applications of Dixon's test under various null distributions.

In moderate sample sizes (15 to 30) two or more outliers may be present and r_{10} would not be very useful. Dixon proposed other ratio tests to avoid this problem, known as masking.

Naus (1975) recommends the use of Dixon's ratio test to detect gross outliers. He calls the method of applying the test to small groups of data the gross error control method; he attributes this application to Nordbotten (1963). The technique is recommended for use in groups as small as three and for situations where the data are normally distributed but the mean or variance change slowly over time.

In this note we show that Dixon's test is robust to departures from normality when the sample size $n = 3$. Naus was apparently unaware of this robustness property, for he writes "The main limitation of this method is that it requires the assumption of normality; it is most useful for spotting individual outliers rather than group outliers."

Thomas (1969) did a Monte Carlo investigation of the robustness of Dixon's test by comparing the critical values given by Dixon for the normal case with Monte Carlo estimates for gamma- and beta-distributed data when $n = 6$, 10, and 15. His study showed that for symmetric beta-distributions the critical values were nearly the same as for the normal case. However, for skewed distributions the critical values varied markedly.

In Table 1, we compare the critical values at the five percent level for the uniform, normal, and exponential distributions when $n = 3$, 4, and 5. Also included is a Monte Carlo estimate of the critical value for Cauchy observations. We see that for $n = 3$ the critical value is not sensitive to departures from normality. For $n = 4$ or 5, we see the sensitivity to skewness (the exponential case) and kurtosis (the Cauchy case).

Table 1. Comparison of Critical Values of Dixon's Ratio Test at the Five Percent Level

Sample Size	Normal	Uniform	Cauchy*	Exponential
3	.941	.950	.957	.974
4	.765	.776	.928	.894
5	.642	.632	.892	.830

*For the Cauchy case the estimate can be off by roughly ±.02 due to sampling variation.

For many data sets, Dixon's ratio test can be an effective tool for identifying gross errors in an automated procedure. The data can be grouped in samples of size three and the method can be applied to each group. It has the advantage that the procedure is robust to the assumed underlying distribution, it can be used in cases where the mean or variance vary slowly with time, and the masking problem does not exist when n is only three. In a data validation study of power plant data, Dixon's test was applied with the data grouped by seasons of three months with the test applied to groups of three. For a discussion of this application see Chernick (1980).

*Michael R. Chernick is a member of the technical staff, The Aerospace Corporation, Los Angeles, CA 90009.

REFERENCES

BARNETT, V., and LEWIS, T. (1978), *Outliers in Statistical Data*, New York: John Wiley.

CHERNICK, M.R. (1980), "A Note on the Robustness of Dixon's Ratio Test in Small Samples," ORNL/TM-7625.

DIXON, W.J. (1950), "Analysis of Extreme Values," *Annals of Mathematical Statistics*, 21, 488–506.

——— (1951), "Ratios Involving Extreme Values," *Annals of Mathematical Statistics*, 22, 68–78.

LIKES, J. (1966), "Distribution of Dixon's Statistics in the Case of an Exponential Population," *Metrika*, 11, 46–54.

NAUS, J.I. (1975), *Data Quality Control and Editing*, New York: Marcel Dekker.

NORDBOTTEN, S. (1963), "Automatic Editing of Individual Observations," in *Conference of European Statisticians, Statistical Standards and Studies No. 2*, New York: United Nations, p. 55.

THOMAS, J. (1969), "Monte Carlo Investigation of the Robustness of Dixon's Criteria for Testing Outlying Observations," in *Proceedings of the Fourteenth Conference on the Design of Experiments in Army Research, Development, and Testing*, 437–483.